Modelling trade-offs in mutation-selection dynamics of trait-structured populations

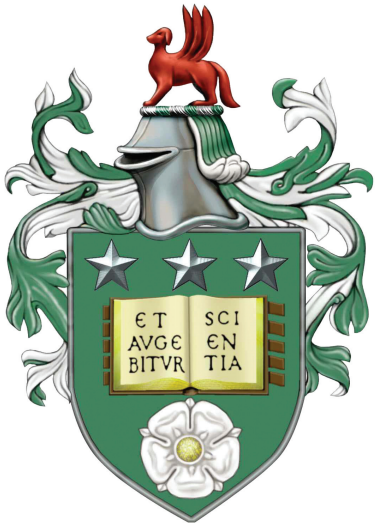

Leonardo Miele

The University of Leeds
School of Mathematics

Submitted in accordance with the requirements
for the degree of Doctor of Philosophy

July 2021

Intellectual Property Statement

The candidate confirms that the work submitted is his own, except where work which has formed part of jointly authored publications has been included. The contribution of the candidate and the other authors to this work has been explicitly indicated below. The candidate confirms that appropriate credit has been given within the thesis where reference has been made to the work of others. Chapter 3 is based on work from a jointly authored paper, titled 'Redundancy-selection trade-off in phenotype-structured populations', by L. Miele, RML Evans and S. Azaele (Miele et al., 2021a). Chapter 4 is based on work from a jointly authored pre-print, titled 'Control strategies for heterogeneous plant pathogens: evolutionary and agricultural consequences', by L. Miele, RML Evans, N. J. Cunniffe and D. Bevacqua. The manuscript is deposited on the bioRxiv server (doi: https://doi.org/10.1101/2021.06.08.447562). All co-authors contributed to designing the models and the analysis to perform, and to revising the manuscripts' drafts. The formal analysis, calculations, simulations, figures and text taken from those manuscripts and appearing in this thesis are all directly attributable to the candidate. Passages contained in Subsection 4.1.1 have been wrote by a co-author, and are therefore reported as quotations. This copy has been supplied on the understanding that it is copyright material and that no quotation from the thesis may be published without proper acknowledgement.

©2021 The University of Leeds and Leonardo Miele

Narrer des événements passés n'a de sens pour l'écrivain que si cela lui permet de découvrir les premiers germes de ce qui demain deviendra la réalité banale, de rendre publiques des valuers qui demeurent encore inaperçues.

Raymond Queneau

Applico il dubbio su tutto, spezza catene. A Nicolò.

Acknowledgements

I am grateful to RML Evans and Sandro Azaele, for their supervision, guidance and support during my time at Leeds. I am also grateful to Daniele Bevacqua, who has been brave enough to start a collaboration with an almost stranger, despite the weird times. I really hope this will be the first of a fruitful series. I am thankful to my family for their usual unconditional love and support, and to Zia Carmela for all the sfogliatelle she brings every time we meet.

What follows is a list in arbitrary order of arbitrarily ironic acknowledgements of not arbitrary people. Dear members of El Pub(e): I am aware that at least one of you would like to not be associated with my name. To fulfil this morbid wish, I have therefore replaced your real names with fictitious ones. I am bound to begin with Fab, everyone's great-grandfather and founder of this colony. Your words of wisdom have lit up my Leedsian journey. I will never forget the ambiguity of sentences like 'from rightwing, only certainties', that you have always refused to clarify despite the many requests. Diary, Rosary and Heavenly (the holy trinity): looking at you has always felt like looking at my immediate future. I could palpate the despair and frustration that are waiting for me at the doorstep. Thanks for having warned and prepared me against the sourness of academic life. Luke: well, if I've learned something after this PhD is that I will never go to Norway, and you deserve all the credit for this. Matthew: I really appreciate the multiple attempts to convince me that also Northeastern people have a heart, and that it is not entirely made of alcohol; if I am not convinced yet and still believe you are truly naughty people, it is entirely my fault. Dear members of the LucroPhascistee (ciao Digos) Bob, John, Frank and Larry: the world was not

prepared for our coming, nor were we mature enough to carry this immense burden. It has all been a matter of wrong timing, we all knew it since the beginning. May all our ideas rest undisturbed under too many layers, and let no one awake them. You have been exceptional comrades (nec recisa recedit): be it 'playing' music, cooking a midnight carbonara or making fun of Bob, anything we did together always made me feel like flying over a forest of raised arms. Home is wherever everyone agrees (on the basis of a democratico-authoritarian choice, bien entendu!) on which bottle of olive oil to buy, and I've considered you Home since the first time we gathered. A noi!

Dear all: without you, these years would have been that stereotypical, flat and pathetic experience of the Italian going abroad and hanging out only with other Italians, complaining all the time about weather and food, the lack of a decent coffee, the price of a bottle of a barely potable wine, persisting stubbornly in speaking English with that obnoxious, lazy accent typical of people who refuse to integrate. I can proudly say that I do not belong to such a filthy category, and that's all thanks to you. You have taught me that I can communicate without hand gestures, that I don't need good coffee to start the day, especially if there's bad, free one in the nearby department. You've exposed me to a different culture, and I feel invaluably enriched by this. In a sentence, thanks for being not so Italian. I hope that I haven't forgotten anyone, that would be too embarrassing. (Editor's note: we are now sure that the author instead forgot a last member of the crew, named Andrew. There is reason to believe that he did it on purpose, probably in remembrance of some old sketch or recurrence.)

Having constantly travelled these years, Home is also where old acquaintances scattered around the planet (Sisa, Simo, LoreB, Tino no perchè mi odia) can all gather together and recreate their common ecosystem: Angi you are Home. Angi, J, Flavio: I don't need to repeat the esteem I have for you, but I have to (at least) stress my gratitude for your support in these last months. GiOrto, *il maestro*: hopefully we won't live long enough to attend the 800th anniversary of the Divina Commedia. Remember: head on the subject and thanks for alLOLLOLLOLLOLLOLLOLLO. A special thanks goes to Lupone, who could have chilled for the entire summer on a

beautiful island, and instead has chosen to remain sfoaming in Florence, just to support me in these last months. True friends show up when there's 40° C outside. Lupo, thanks for keeping it alive with me (the dream is dead, long live the nightmare). A last thought goes to Stella, whose dim light beams come from a distant time and a distant space, but still happen to strike me. Your presence has been as inestimable as timeless art, I wish I could exert my droit de préemption to cancel your absence.
This thesis is dedicated to Nicolò Carnesi. You always seem to anticipate my thoughts and feelings, from that galaxy hidden in my closet to those consuming doubts breaking my chains. Your music still helps me understand myself and the world around me. It may not be the most useful gift (actually, it is one of the most useless I can think of), but this is again all I can offer you.

P.S. If anyone wonders how did I feel after finishing this thesis, the answer is here[1].

[1] https://drive.google.com/file/d/1O1w_9J7pecafnUzijuCKY1aKoCCWEzFd/view?usp=sharing, copyright of GiovanniOrtoleva.

Abstract

Understanding the factors shaping the trait distribution of a biological population is essential for a predictive theory of evolution. Mathematical modelling provides a parsimonious and rigorous means to interpret empirical data, and to investigate plausible scenarios. In this context, the Replicator-Mutator Equation is a general tool to model mutation-selection dynamics of trait-structured populations. In such populations, individuals differ in the expression of one (or more) phenotypic traits. When trade-offs occur between different traits, then the corresponding trait distributions may reveal interesting, non-trivial behaviours. In this thesis, I will focus on the modelling of two such trade-offs. First, I will introduce the degeneracy-selection trade-off, according to which fitter phenotypes are expected to be less degenerate (thus more prone to mutation disruption). In the context of trait-structured populations, this trade-off is generally treated by means of effective formulations, rather than explicitly considering degenerate fitness landscapes. Here, I compare the two approaches and discuss the limits of effective formulations in the (inevitable) presence of asymmetries between traits. In the second part, I will show an application of the Replicator-Mutator Equation in the context of evolutionary epidemiology, where pathogen display heterogeneous levels of virulence and transmission. I will frame the problem in the context of agricultural practice, where the aim is to understand how to calibrate control strategies, in order to optimise pesticide use, and show how a proper trait-dependent control strategy can harness heterogeneity in pathogen populations to our advantage. Finally, I will discuss future lines of research based on the merging of the two parts, and on the potential for a general mathematical theory of trait-dependent control strategies of heterogeneous pathogens.

Contents

List of Figures

List of Tables

Abbreviations

RME	Replicator-Mutator Equation
sRME	stationary Replicator-Mutator Equation
GP	Genotype-Phenotype
SIS	Susceptible-Infected-Susceptible
VE	Virulence-Eradication
TE	Transmission-Eradication
TVE	Transmission-Virulence-Eradication

1. Introduction

'Hardly a phenomenon in metazoan biology is more ubiquitous, yet as neglected as the inevitable heterogeneity of cell phenotypes within a population of cells of the same type.' Such is the sharp incipit of the review that the cell biologist Prof. Shi Huang dedicated to the issue of non-genetic heterogeneity of cells (Huang, 2009). Phenotypic heterogeneity refers to the diversity with which genetically identical cells living in the same environment, accomplish biological functions, such as gene expression or protein levels of activity. Despite its ubiquity, the role played by phenotype heterogeneity in biological evolution has been long overlooked, mainly for two reasons (Bonduriansky and Day, 2009, 2019): on the one hand, the modern theory of evolution has its foundation on the central dogma of molecular biology, which elected the gene as undisputed protagonist of evolutionary processes; on the other hand, the discovery (and measurement) of phenotype heterogeneity has been possible only recently, thanks to important innovations in the instruments and methods employed in laboratory single-cell analysis. The absence of tools such as flow-cytometers during the first days of evolutionary biology (from Darwin's theory of natural selection in 1895 on) inevitably biased the scientific community towards the importance of genetic (with respect to phenotypic) variations. This bias affected also the most theoretical branch of this novel, exciting discipline, inaugurated in the 1930*s* by Wright, Haldane and Fisher, under the (not coincidentally) name of population genetics. From the historical viewpoint, the genetic vs phenotypic battle for attention also reflected the ideological clash that capitalism and socialism were playing on the economic and political ground during the

20th century, and had important repercussions on the visions of society that followed (DeJong-Lambert, 2012). Fortunately for humankind, the ever-increasing amount of experimental evidence collected in the last decades (Avery, 2006; Raj and Van Oudenaarden, 2008; Balázsi et al., 2011), and the discovery of new evolutionary phenomena such as phenotypic plasticity (Callahan et al., 1997), epigenetics (Jablonka and Lamb, 2014) and non-Darwinian effects (Pisco et al., 2013; Osmanovic et al., 2018) have forced the whole scientific community into a *mise en cause* of the central dogma, with a consequent rehabilitation of phenotypic heterogeneity, whose role in the contemporary theory of biological evolution is today pivotal.

Besides experimental evidence, phenotype heterogeneity has also been validated by theoretical works, demonstrating its potential sources (McAdams and Arkin, 1997; Kaern et al., 2005), and the advantages it provides at the population level (Kaneko, 2007; Stockholm et al., 2007; Carja and Plotkin, 2017). The concept of trait-structured (also known as phenotype-structured) population has been widely employed to model mathematically cell heterogeneity. Defining a trait-structured population requires two ingredients:

i) The identification of one (or more) quantitative trait(s), which is related with some phenotypic function of the individual carrying it, and whose *value* varies across individuals due to phenotypic heterogeneity.

ii) A mechanism providing a source of heterogeneity, so that heterogeneity is an inherent feature of the entire population that is maintained over time.

Requirement *i*) is related with the *selective* nature of the trait(s), and is mathematically described by functions mapping the trait(s) into a quantitative measure of reproductive success, typically defined as *fitness*. Requirement *ii*) is related with the *mutative* nature of the trait(s), and is mathematically described by operators defining how the quantitative trait(s) mutates. Importantly, for a population to be described as trait-structured, these two requirements have to be fulfilled concomitantly: in

absence of i), there would not be any trait(s) discriminating the *structure* of the population, hence the hierarchy of the trait(s) determined by the ladder of natural selection; in absence of ii), only the trait(s) at the top of the ladder would survive, and heterogeneity would be eventually lost. Of course, the ways to implement mathematically selection and mutation are multiple, and in this thesis I have focused on a specific, though popular, set of choices.

Requirement i) will be described by means of fitness landscapes; particularly, I will consider smooth landscapes, since I will describe continuous quantitative traits. The concept of fitness landscape was first introduced in 1932 by the population genetist Sewall Wright, as a way to visually represent the trajectory performed by an evolving population in the space of possible phenotypic (or genotypic) configurations, which is pushed by natural selection towards the fitness peaks (Wright, 1932). The theory of fitness landscapes comprises a variety of models (Orr, 2005; Gavrilets, 2010; De Visser and Krug, 2014), whose overview goes beyond the purpose of this introductory chapter. For my purposes, fitness landscapes will represent simple mathematical functions mapping individuals' phenotype traits to their corresponding measure of reproductive success, that is fitness. In theoretical works, the properties of such functions are generally assumed by the modeller (though they are inspired from experimental evidence), depending on the evolutionary phenomenon of interest. This approach is deliberately descriptive and simplistic, and is needed in order to reduce the complexity of evolutionary problems to a level allowing some kind of mathematical tractability. In other, less abstract contexts, fitness landscapes may emerge as a result of the mechanistic interactions occurring between the evolving trait-structured population and the environment (Doebeli et al., 2017). In this thesis, I will investigate a problem belonging to the first (more abstract) class of models, and a problem belonging to the second (more mechanistic) class.

In both cases, requirement ii) will be fulfilled by employing a specific mathematical operator, the Laplacian, which is suited to describe mutations leading to smooth variations on the quantitative traits. This modelling choice encompasses the extreme

complexity of the mechanisms occurring at the genomic level, and aims at providing a simplified, coarse-grained description of the effects of mutations on the phenotypic trait, sometimes referred as non-genetic instability, or epimutations, *e.g.* (Chisholm et al., 2015). These two modelling choices will merge into the Replicator-Mutator Equation (RME). The RME has been widely employed to model mutation-selection dynamics of trait-structured populations in many biological (and other) research areas: population genetics (Wakano et al., 2017), pathogenic evolution (Day and Proulx, 2004; Korobeinikov and Dempsey, 2014; Bolzoni and De Leo, 2013), RNA evolution (Tsimring et al., 1996), game theory (Ruijgrok and Ruijgrok, 2015; Bomze and Burger, 1995), language evolution (Page and Nowak, 2002). Examples of biological traits to which the RME formalism has been applied include: drug tolerance to cancer treatments (Lorz et al., 2013; Lorenzi et al., 2016), pathogenic virulence (Day and Proulx, 2004; Bolzoni and De Leo, 2013) and transmission (Korobeinikov and Dempsey, 2014), antigenic types (Sasaki, 1994; Sasaki and Haraguchi, 2000), hosts' resistance to infection (Lorenzi et al., 2020). In this thesis, I will investigate the mutation-selection evolution of trait-structured populations, characterised by trade-offs entwining their phenotypic traits. In the presence of a trade-off, the quantitative value assumed by a trait has the potential to influence multiple aspects of a phenotype. Whenever such effects display contrasting effects on the individual, then the trait-structured population will evolve towards non-trivial configurations. The RME formalism provides an established mathematical tool for the qualitative investigation of such complex outcomes.

The thesis is structured as follows. In Chapter 2, I will present some basic notions of evolutionary modelling with the help of a pedagogical model. This example will allow me to introduce the distinction between monomorphic and polymorphic populations, and to frame the study of trait-structured populations within the context of the latter. Moreover, I will derive the RME employed to study the models analysed in the following chapters, and present the methodology employed to find stationary solutions of the RME. In Chapter 3, I will study trait-structured populations

evolving on abstract fitness landscapes, featuring a minimal but universal trade-off between degeneracy and selection. The consequences of such trade-off have been well documented within the field of molecular evolution. The aim of my study is to extend our understanding to trait-structured populations, and to understand the extent to which effective formulations so far employed are correct. In Chapter 4, I will study an epidemiological application, where trade-offs will occur between the phenotypic traits involved in pathogens' life cycles. The model will be framed in the context of crop pest management, with the aim of understanding how to optimise pesticide use in agricultural practices. Finally in Chapter 5, I will sum up the results, and conclude with possible future lines of research.

2. From a pedagogical example to the RME

In this Chapter, I shall introduce some fundamental concepts of evolutionary modelling by starting from a basic mutation-selection model involving two types of individuals. Starting from the microscopic description of the evolutionary interactions, I will derive both deterministic and stochastic dynamics. I will demonstrate the existence of two fundamentally different behaviours of an evolving population, that are monomorphic and polymorphic regimes. Finally, I will present the RME formalism that I will use to investigate the behaviour of trait-structured populations.

2.1. A pedagogical two-types model

2.1.1. Microscopic description of mutation-selection: the Moran process

The two most used methods to describe selection at the microscopic level are the Wright-Fisher and the Moran process. The former was introduced during the '1930s' in the context of population genetics (Wright, 1931; Fisher, 1958), to investigate gene frequency undergoing random sampling in finite populations, and is considered one of the milestones of population genetics. It is based on discrete, non-overlapping

generations, and it can be complexified in order to account for selective, mutative, migrating effects and so on (Blythe and McKane, 2007). The Moran process was introduced a few decades later (Moran, 1958), and it is based on a more 'statistical physics' description of the stochastic evolutionary events: rather than sampling the entire pool from generation after generation, individuals are chosen to mutate, die or reproduce one at a time, with a probability that depends on their features, and on the details of the dynamics. Hence, unlike the Wright-Fisher process, the Moran process has overlapping generations, and it can naturally lead to a continuous time description in terms of master equations and transition rates. For this reason, the Moran process is generally preferred when one aims at studying the evolving biological population by means of statistical physics tools (Blythe and McKane, 2007).

The Moran process describes competition for reproduction at the individual level, and it consists of three steps: *i*) *selection* of an individual; *ii*) *reproduction* of the selected individual; *iii*) *replacement* by the newborn at the expenses of another individual which is removed from the population. This process is a Birth-Death process preserving the total number of individuals, because it always replaces an individual with another one. Typically, either the *selection* or the *replacement* steps depend on fitness, so as to model Darwinian competition by natural selection in terms of fitness-dependent birth, or fitness-dependent death. Throughout the thesis, I will employ a formulation of the Moran process known as *local update rule* that does not make distinction between the two options, but still leads to the same general form of the RME (Traulsen et al., 2005, 2006).

2.1.2. Chemical reactions

The events of competition and of mutation occurring at the microscopic level of the individuals is schematised by means of the chemical reactions formalism (Gardiner et al., 1985; Van Kampen, 1992): individuals are considered as particles belonging to a chemical species; whenever particles interact, a chemical reaction may occur

leading to formation/degradation of particles, or to changes in their chemical species. For example, let X and Y be two possible chemical species, and let us consider the following chemical reaction:

$$X \xrightarrow{r} Y, \tag{2.1}$$

On the left-hand side we have the reactants, in this case a single particle of species X. On the right-hand side we have the products of the reaction, that is a single particle of species Y. The constant r is called reaction constant, and indicates the likelihood of the chemical reaction: the larger r, the more frequently the reaction will occur. This simple chemical reaction schematises the interaction for which one particle of the species X transforms into a particle of species Y. For a general chemical reaction involving $X_1, \dots X_u$ reactants and $Y_1, \dots Y_v$ products, the chemical reaction will read:

$$\alpha_1 X_1 + \alpha_2 X_2 + \cdots + \alpha_u X_u \xrightarrow{r} \beta_1 Y_1 + \beta_2 Y_2 + \cdots + \beta_v Y_v, \tag{2.2}$$

where α, β are the stoichiometric coefficients of the species in play.

The above schematism is applied to illustrate a simple microscopic evolutionary dynamics, where individuals of a population of fixed size N can be either of type A, or of type B. Individuals of type A (B) possess fitness f_A (f_B). The state of the system at a certain time is described by the numbers (N_A, N_B) of individuals of each type. The number of individuals being fixed, the system is fully described by just N_A, since $N_B = N - N_A$. The dynamics involves mutation and competition events, both modelled by the following Moran processes.

Competition. Let an individual A and an individual B compete for reproduction at a rate γ per unit of time. Then, individual A will reproduce and its newborn will replace individual B:

$$A + B \xrightarrow{\gamma\, p_\gamma} 2A, \tag{2.3}$$

with a probability p_γ given by:

$$p_\gamma = \frac{1}{2} + \frac{\omega}{2}\left(f_A - f_B\right), \tag{2.4}$$

where ω is the *selection pressure* parameter. Alternatively, individual B will reproduce and its newborn replace individual A:

$$A + B \xrightarrow{\gamma\, q_\gamma} 2B, \tag{2.5}$$

with probability q_γ:

$$q_\gamma = 1 - p_\gamma = \frac{1}{2} + \frac{\omega}{2}\left(f_B - f_A\right). \tag{2.6}$$

I call these two reactions complementary, because their probability of occurrence always sums up to one (or in other words, their rate of occurrence always sums up to γ). Each probability is composed of a baseline value of $\frac{1}{2}$, and of a fitness-dependent term, proportional on the difference between the fitness value of the two types. By construction, the individual with larger fitness will be more likely to reproduce than to perish. If A is fitter than B (that is $f_A > f_B$), then the first reaction is more likely to occur than the second, and A is more likely to replace B. Contrarily, if A is less fit than B (that is $f_A < f_B$), then the second reaction is more likely to occur, and B is more likely to replace A. The larger the difference between the fitness value of the two individuals, the more skewed the pair of complementary reactions will be towards the more probable. The magnitude of the fitness-dependent contribution with respect to the baseline probability $\frac{1}{2}$ is mediated by the selection pressure parameter ω: the larger (smaller) is ω, the more (less) relevant will be fitness in determining the fate of the individuals. In the case $\omega = 0$, the dependence on fitness disappears and the two reactions occur with same probability: this scenario is known as *neutral dynamics*.

Mutation. Let mutations occur at a constant rate μ per unit of time. An individual

of type A mutates into type B:

$$A \xrightarrow{\mu m_{AB}} B, \tag{2.7}$$

with probability m_{AB}, while and individual of type B mutates into type A:

$$B \xrightarrow{\mu m_{BA}} A, \tag{2.8}$$

with probability m_{BA}.
The above reactions describe the evolutionary dynamics of mutation and selection as microscopic interactions between individuals. A first, simplified approach to describe the system's behaviour can be achieved by invoking the *law of mass action*, that allows to derive the temporal dynamics of the macroscopic quantities N_A and N_B .

2.1.3. The law of mass action

The law of mass action associates a set of differential equations for the concentrations of the types involved, starting from the chemical reactions at play. Introduced by Waage and Guldberg in 1864 in (Waage and Gulberg, 1986), the law can be stated as follows (quoted from Biancalani, 2014):

> Given a chemical equation, the time derivative of a concentration of a certain chemical species, being a reactant or a product, is proportional to the product of the concentrations of the reactants of the reaction. This is multiplied by the reaction constant, which has a plus sign if the species is created or a minus sign if the species is destroyed.

Originally introduced in the context of chemical kinetics, the argument of the law is independent of the phenomenological context, and since then, the law has been employed in a wide variety of applications (Van Kampen, 1992). In the context of

mathematical biology, its most iconic application is provided by the Lotka-Volterra equations, describing the dynamics of prey-predator systems (Murray, 2007). Let $n_A = \frac{N_A}{N}$ and $n_B = \frac{N_B}{N}$ be the concentrations of individuals of the two types, and apply the law of mass action to the above four reactions: the first (second) reaction Eq. (2.3) (Eq. (2.5)) leads to an increment (diminution) term of the number of A type individuals, which is proportional to the competition rate γ, the densities of the two species involved $n_A\, n_B$, and to the probability p_γ (q_γ) of occurrence of the reaction, that is: $+\gamma\, p_\gamma\, n_A\, N_B$ ($-\gamma\, q_\gamma\, n_A\, N_B$). Likewise, the third reaction Eq. (2.7) (fourth reaction Eq. (2.8)) leads to a diminution (increment) term of the number of A (B) type individuals mutating into B (A), which is proportional to the mutation rate μ, to the density of A individuals n_A, and to the probability of occurrence of the mutation m_{AB} (m_{BA}), that is: $-\mu\, m_{AB}\, n_A$ ($+\mu\, m_{BA}\, n_B$).

The differential equation governing the temporal dynamics of the density $n_A(t)$ with initial condition $n_A(t = 0) = n_0$, is then obtained by collecting all contributions. Substituting Eqs. (2.4)-(2.6), recalling that $n_B = 1 - n_A$, and rearranging terms, we obtain:

$$\frac{dn_A(t)}{dt} = 2\gamma\omega\,(f_A - f_B)\,n_A(t)\,(1 - n_A(t)) + \mu\big[m_{BA} - (m_{AB} + m_{BA})\,n_A(t)\big]. \quad (2.9)$$

Eq. (2.9) describes the mutation-selection dynamics for the macroscopic concentration of individuals of A type, derived from invoking the law of mass action on the microscopic interactions of competition and mutation (the corresponding equation for n_B is simply the opposite of Eq. (2.9), since $\frac{dn_A}{dt} = -\frac{dn_B}{dt}$). In the following, I introduce some simplifying assumptions on the parameters of the model.

Let us consider the simple case where mutations occur with the same rate in both directions, and let A denote the fit type and B denote the unfit type, *i.e.*:

$$m_{AB} = m_{BA} = 1, \quad f_A = 1, \quad f_B = 0. \quad (2.10)$$

Inserting Eqs. (2.10) into Eq. (2.9), the dynamics simplifies to:

$$\frac{dn_A(t)}{dt} = 2\gamma\omega n_A(t)\left(1 - n_A(t)\right) + \mu\left(1 - 2n_A(t)\right). \tag{2.11}$$

In Fig. 2.1, I show some temporal trajectories of $n_A(t)$, obtained by means of numerical integration of Eq. (2.11), for two sets of parameters (specified in the figure's caption and legend). For both sets, the system is initialised with two different initial conditions ($n_A(0) = 0.1$ and $n_A(0) = 0.9$). In all cases, the temporal trajectories (smooth solid lines) approach monotonically the asymptotic equilibrium value n_A (indicated with dashed lines), which is obtained by setting Eq. (2.9) to zero:

$$n_A = \frac{1}{2} + \frac{\sqrt{1 + \frac{\delta^2}{4}} - 1}{\delta}, \quad \delta = \frac{2\gamma\omega}{\mu}. \tag{2.12}$$

In absence of competition ($\gamma = 0$), or in absence of selection pressure ($\omega = 0$), the population is equally distributed between the two types, that is $n_A = \frac{1}{2}$. In the presence of competition ($\gamma \geq 0$), selection pressure will bias the equilibrium density towards the fittest type A, as expected. Fig. 2.1 also displays the temporal trajectories of the stochastic dynamics corresponding to Eq. (2.11), which will be introduced and discussed in the following subsection.

2.1.4. The master equation formalism

The microscopic rules of competition and mutations presented in Subsection 2.1.2 have a probabilistic nature, that the law of mass action is unable to capture, due to its deterministic nature: at a certain time t, the population is composed of N_A individuals of type A; reactions have a certain rate of occurrence; upon their occurrence, the number N_A will either increase or decrease by 1. Therefore, the system transits stochastically between different states, characterised by different values of N_A. The master equation describes the temporal dynamics of the probability $P(N_A, t)$ of observing the system

in state N_A at time t. Defining the transition rate per unit of time $T(N_A|N'_A)$ from state N'_A to state N_A, the master equation generally reads:

$$\frac{dP(N_A,t)}{dt} = \sum_{N'_A \neq N_A} T(N_A|N'_A)P(N'_A,t) - \sum_{N'_A \neq N_A} T(N'_A|N_A)P(N_A,t). \tag{2.13}$$

In Eq. (2.13), the first sum represents all the *gain* contributions due to transitions from other states N'_A towards the state N_A; the second sum represents all the *loss* contributions due to transitions from the state N_A towards other states N'_A. In this sense, the master equation can be intended as a balance equation for the probability of each state, specified by the transition rates $T(N_A|N'_A)$.

The chemical reactions Eqs. (2.3), (2.5), (2.7) and (2.8) admit transitions only between states with consecutive numbers, since any event will either increase or decrease N_A by one. Therefore, we have $T(N_A|N'_A) = 0$ if $|N_A - N'_A| > 1$. The only nonzero transition rates are then:

$$T^+(N_A) = T(N_A|N_A - 1) = \gamma\,(1+\omega)\,\frac{N_A}{N}\left(\frac{N-N_A}{N}\right) + \mu\left(\frac{N-N_A}{N}\right) \tag{2.14}$$

$$T^-(N_A) = T(N_A|N_A + 1) = \gamma\,(1-\omega)\,\frac{N_A}{N}\left(\frac{N-N_A}{N}\right) + \mu\frac{N_A}{N}, \tag{2.15}$$

where I have introduced the symbols $T^{\pm}(N_A)$ to lighten the notation. The master equation then simplifies to:

$$\frac{dP(N_A,t)}{dt} = T^+(N_A{-}1)P(N_A{-}1,t){+}T^-(N_A{+}1)P(N_A{+}1,t){-}\left[T^+(N_A) + T^-(N_A)\right]P(N_A,t). \tag{2.16}$$

The Gillespie algorithm provides samples of the probability distribution described by the master equation (Gillespie, 1976, 1977), and corresponding instantiations of the value of the density n_A over time. In Fig. 2.1, I show the example trajectories resulting from Gillespie simulation of the master equation, corresponding to the set of parameters and two initial conditions analysed in the deterministic case. The Gillespie trajectories appear as noisy versions of their deterministic counterparts. Contrary to

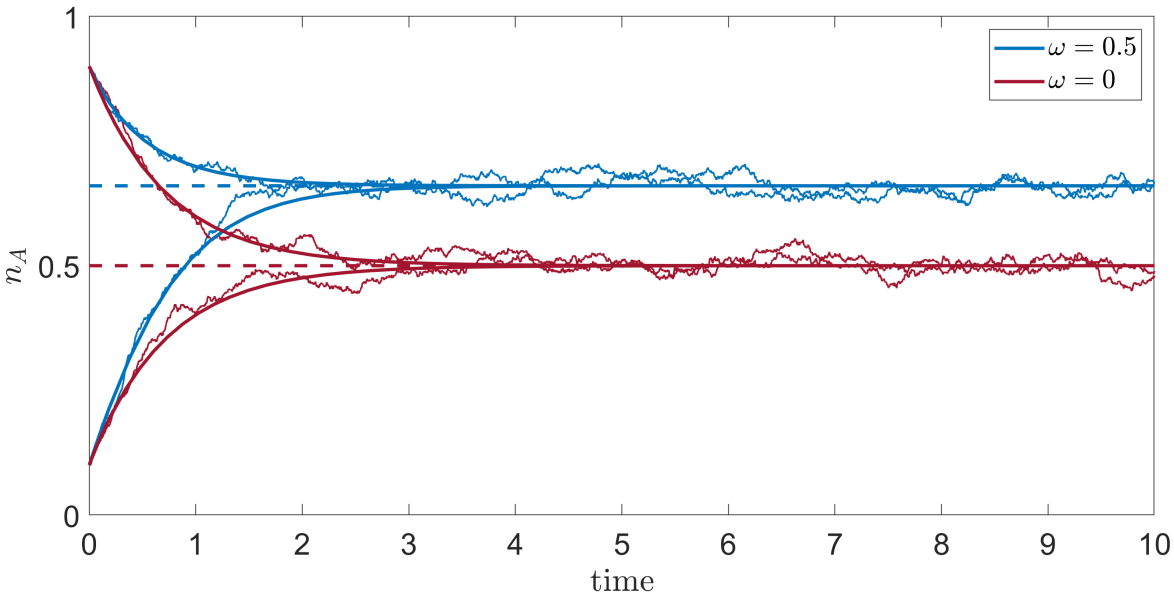

Figure 2.1: **Temporal trajectories of the two-type model.** Temporal trajectories of the two-type mutation-selection dynamics are shown for two values of selection pressure ω. For each ω, two trajectories corresponding to two different initial conditions are shown. Smooth lines correspond to numerical integration of the deterministic Eq. (2.11), while noisy curves correspond to Gillespie simulations of the master Eq. (2.16), with $N = 1000$. Dashed lines correspond to the deterministic equilibrium value of n_A. The mutation rate μ is set to 1.

the deterministic trajectories, after the transient such trajectories fluctuate perpetually around the equilibrium value n_A, due to the stochastic nature of the master equation. Fig. 2.1 seems to suggest that, overall, deterministic and stochastic descriptions deliver the same information on the state and on the dynamics of the evolving system. However, this is not the case, and even for such a simple model, the stochastic dynamics display some behaviours that the deterministic description is not able to capture. In the next subsection, I will present the Fokker-Plank equation, that will serve to illustrate the dual behaviour of the mutation-selection dynamics.

2.1.5. The Fokker-Plank equation

The Fokker-Plank equation is a typical method to obtain approximations of the master equation, and it describes the temporal evolution of the probability density function

$P(n_A)$ to observe the system in the state n_A. By applying the method of the generating function (detailed in the Appendix A.2), one obtains:

$$\frac{\partial P(n_A,\tau)}{\partial \tau} = -\nabla J(n_A,\tau), \tag{2.17}$$

where $\tau = \frac{t}{N}$ is the time rescaled with respect to system size, and $J(n_A,\tau)$ is the probability current:

$$J(n_A,\tau) = a(n_A)P(n_A,\tau) - \frac{1}{2}\frac{\partial}{\partial n_A} b(n_A)P(n_A,\tau), \tag{2.18}$$

with:

$$\begin{cases} a(n_A) = 2\gamma\omega n_A\,(1-n_A) + \mu\,(1-2n_A) \\ b(n_A) = \frac{1}{N}\left[2\gamma n_A\,(1-n_A) + \mu\right]. \end{cases} \tag{2.19}$$

The coefficient $a(n_A)$ is called *drift*, and corresponds to that composing the deterministic Eq. (2.9). The coefficient $b(n_A)$ is called *diffusion*, and describes the purely stochastic contributions to the dynamics: its magnitude is mediated by system size N, in agreement with the fact that stochastic effects tend to disappear for large systems. In the following, I will limit the calculations of the stationary probability distribution to the simple case of neutral dynamics (*i.e.* setting $\omega = 0$), as it is sufficient to show the dual behaviour of the mutation-selection dynamics, and to introduce the difference between monomorphic and polymorphic regimes.

2.1.6. Monomorphic and Polymorphic regimes

In a one-dimensional case such as that I am analysing, the stationary solution of the Fokker-Plank equation is obtained by demanding a vanishing probability current, *i.e.* $J(n_A) = 0 \quad \forall n_A$ (Gardiner et al., 1985). In the case of neutral dynamics ($\omega = 0$), the

probability current reduces to:

$$J_{\text{neutral}}(n_A) = \mu(1-2n_A)P(n_A) - \frac{1}{2N}\frac{\partial}{\partial n_A}\left[2\gamma n_A(1-n_A)+\mu\right]P(n_A) = 0, \quad (2.20)$$

where the time dependence of P has been dropped, because the system is at stationarity. Performing the derivative and rearranging the terms, one obtains:

$$\frac{P'(n_A)}{P(n_A)} = \Gamma(n_A), \quad \Gamma(n_A) = \frac{1-2n_A}{2\gamma n_A(1-n_A)+\mu}(2N\mu - 2\gamma) \quad (2.21)$$

Integrating both sides of Eq.(2.21) between 0 and n_A, one obtains:

$$P(n_A) = \mathcal{Z}e^{\int_0^{n_A}\Gamma(y)dy}, \quad (2.22)$$

with $\mathcal{Z}$ being the normalisation constant. Finally, integrating the function $\Gamma(y)$, I obtain the stationary distribution for the neutral dynamics:

$$P(n_A) = \mathcal{Z}\left[2\gamma n_A(1-n_A)+\mu\right]^{\frac{N\mu}{\gamma}-1}. \quad (2.23)$$

This probability distribution has two distinct behaviours, depending on the value of the compound parameter $\frac{N\mu}{\gamma}$. In the following, I will consider both population size N and competition rate γ fixed, and focus on variations on the order of magnitude of mutation rate μ, because in the biological literature this is considered the parameter discriminating different evolutionary regimes. However, analogous conclusions are obtained if one fixes the latter and varies the order of magnitude of the former.

In Fig. 2.2 I plot some analytical solutions of Eq. (2.23) (red lines), and compare with results from numerical simulations with Gillespie algorithm. The numerical histogram (blue bars) is obtained by running the algorithm 10^5 times, and recording the value of n_A every 10^4 time units. The values of the parameters used in the simulations are specified in the figure's caption. The two distinct behaviours of the stationary probability distribution are separated by a critical mutation rate value $\mu_c = \frac{\gamma}{N}$, for which

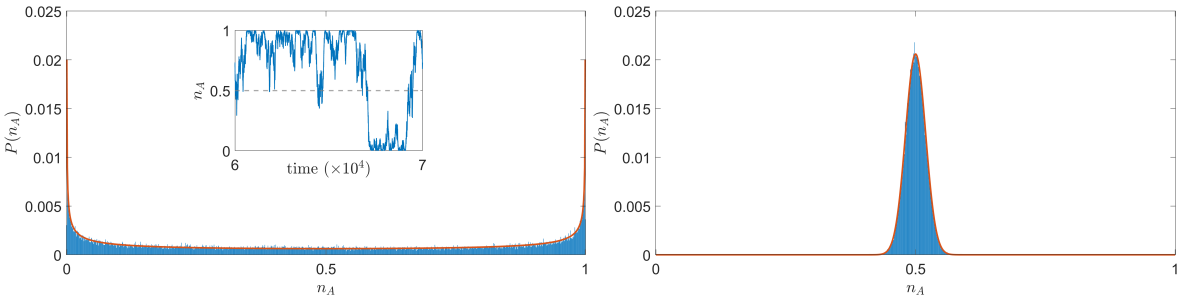

Figure 2.2: **Monomorphic and polymorphic regimes.** Stationary probability distribution of observing n_A individuals. Red lines: analytical solution of the Fokker-Plank equation; blue bars: averages from numerical simulations (number of realisations: 10^5. Time interval between realisations: 10^4 time units). Left panel: the mutation rate is below the threshold value and the population is in the monomorphic regime; inset: temporal trajectory of the simulated master equation. Parameters: $\mu = 0.0005 < \mu_c, \gamma = 1, \omega = 0, N = 1000$. Right panel: the mutation rate is above the threshold value and the population is in the polymorphic regime; parameters: $\mu = 1 > \mu_c, \gamma = 1, \omega = 0, N = 1000$.

$P(n_A)$ becomes uniform.

Monomorphic regime. Below the critical mutation rate (*i.e.* $\mu < \mu_c$), the probability distribution displays two sharp peaks at $x = 0$ and $x = 1$, as illustrated in the left panel. The fraction of individuals of type A is almost always either 0 or 1: therefore, the population is almost always entirely composed of either only type A or only type B individuals, switching from one to another under the effect of demographic noise. In absence of selection pressure ($\omega = 0$), there is no preference between the two types, so that the distribution is not biased towards the fittest one and the two peaks are equivalent. Were selection pressure present ($\omega > 0$), the corresponding probability distribution would preserve the same U shape, but it would be skewed towards $x = 1$, because the dominance of the fitter A type would be favoured by natural selection. This scenario represents an example of *monomorphic* population, because at every time individuals tend to share the same type: at $t = t_0$, all N individuals are of, *e.g.*, A type; at $t = t_1$ a mutation occurs, leading to the emergence of 1 type B individual among $N - 1$ of type A; however, this unique individual will very likely perish during a competition event, before new B types individuals emerge due to mutations; only

occasionally, individuals of type B will be *lucky* enough to *win* all competition events against type A ones, increase in number, and eventually dominate the population, thus reversing the system's composition. If this unlikely event happens, the population will have reached the opposite monomorphic state, and one will have to wait another long time before seeing the re-emergence of A type individuals.

Polymorphic regime. On the other hand (right panel), above the critical mutation rate (*i.e.* $\mu > \mu_c$), the distribution displays a single peak located at $n_A = \frac{1}{2}$, that is the equilibrium point Eq. (2.12), predicted by the deterministic equations: most of the time, the population is equally split between A and B types, because of the absence of selection pressure, but random effects due to demographic noise will make the composition fluctuate around the expected deterministic proportion. Were selection pressure present ($\omega > 0$), the peak of the distribution would be displaced towards $n_A = 1$ (but still coinciding with Eq. (2.12)), because at equilibrium the presence of fitter A type individuals would be favoured by natural selection. This scenario represents an example of *polymorphic* population (note, in this case, bimorphic) because, contrary to the monomorphic case, here mutations are so rapid that individuals of both types are continuously present at every time, and the system is described by specifying how individuals are distributed over the possible types.

This simple example illustrates how the magnitude of mutation rates can discriminate between the two different scenarios, and the transition from one to the other can be appreciated at the variation of μ. However, in more complex situations (*e.g.* involving more than two types and/or more complex microscopic interactions) the calculation of the stationary probability distribution becomes unfeasible, so that being able to describe both regimes and detecting such transition can be difficult. Therefore, a modeller typically has to decide whether to operate below or above the critical mutation rate μ_c. Of course, this choice affects the kind of adaptive phenomena they can describe, and the kind of mathematical tools they will most likely employ. Indeed, the behaviour of a monomorphic population cannot be properly captured by a deterministic approach, as the inset in the left panel of Fig. 2.2 clearly shows: if we track

the state of the system n_A over time during a simulation of the master equation (blue line, inset) we note that very rarely the system is found at the equilibrium state predicted by the deterministic equations (dashed grey line), which has little to do with the bistability typical of a monomorphic population. For this reason, monomorphic populations are generally studied in the context of stochastic processes (Iwasa, 1988; Sella and Hirsh, 2005; Barton and Coe, 2009), where the dynamics is simplified in order to focus on the phenomenon of transition between different monomorphic states over time. In the graphical schematisation of fitness landscapes, the state of a monomorphic population at a certain time can be represented as a point on the fitness landscape, and its evolution as the trajectory performed over time by such point, under the effect of evolutionary processes (see panel **a** of Fig. 2.3).

Instead, the behaviour of a polymorphic population can be studied deterministically, as demonstrated by the agreement between stochastic and deterministic trajectories shown in Fig. 2.1. Models of polymorphic populations usually operate under the assumption of infinite population (Eigen and Schuster, 1977; Eigen et al., 1988), so that stochastic finite size effects can be neglected (although some degree of extension to finite size population is possible Alves and Fontanari, 1998; Saakian and Hu, 2006; Saakian et al., 2009; Park et al., 2010; Saakian et al., 2012.). The state of the system is described by the distribution (be it continuous or discrete) of the various types coexisting in the populations, resulting from the balance between mutation and selection. In the graphical schematisation of fitness landscapes, the state of a polymorphic population at a certain time can be represented as a cloud of points on the fitness landscape, whose distribution varies over time due to evolutionary forces (see panel **b** of Fig. 2.3, adapted from Wilke, 2005). Regardless of the biological details of the system and of the interactions in play, the corresponding deterministic equations have provided insight into universal features of evolutionary dynamics (Page and Nowak, 2002), and are known in the literature as Replicator-Mutator Equations (RME henceforth).

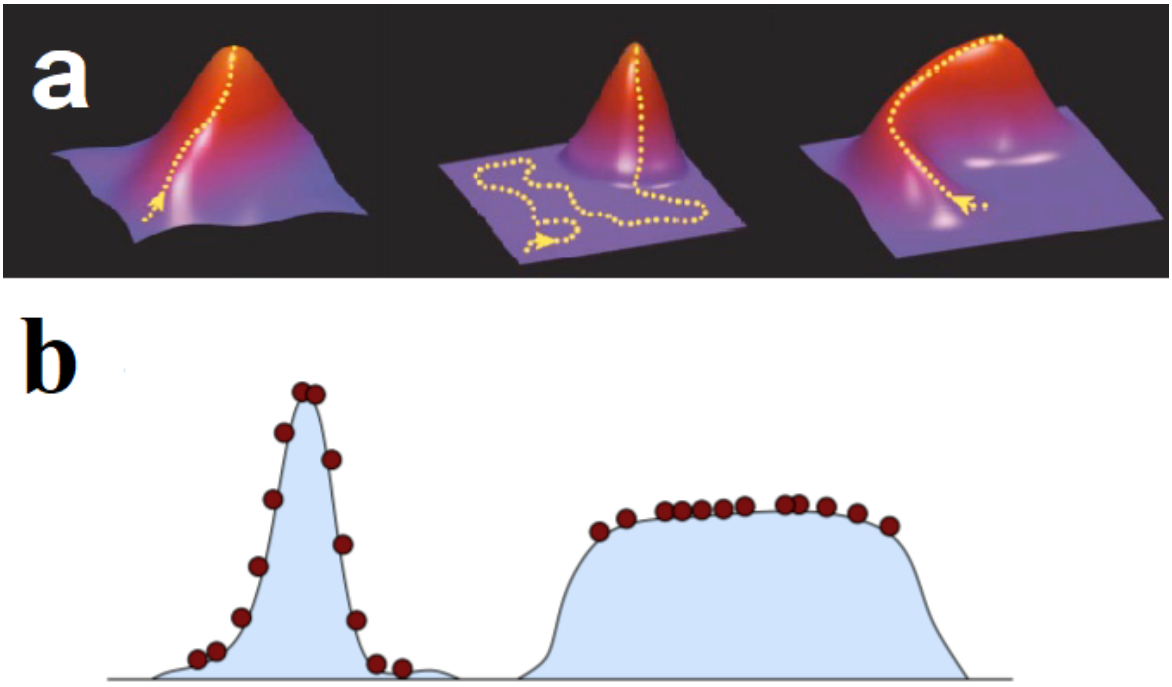

Figure 2.3: **Monomorphic and Polymorphic populations evolving on fitness landscapes.** Panel a: a monomorphic population can be visualised as a single point on the fitness landscape (identifying the dominant phenotype), whose position varies over time, under the effect of evolutionary processes (adapted from Poelwijk et al., 2007). Panel b: a polymorphic population can be visualised as a cloud of points (one for each individual) distributed over the fitness landscape, and evolution as the process shaping such distribution over time (adapted from Wilke, 2005).

2.2. The Replicator-Mutator Equation (RME)

Starting from the simple two-types model analysed in the previous section, I will present a different, more rigorous derivation of the RME, based on mean-field approximation of the stochastic dynamics. Then, I will derive the discrete Replicator-Mutator Equation from the generalisation of the dynamics given by the chemical reactions Eqs. (2.3), (2.5), (2.7) and (2.8), to the case of M finite types. Finally the continuous Replicator-Mutator Equation describing the mutation-selection dynamics of trait-structured populations will be obtained by performing a *continuum approximation* on the discrete version.

2.2.1. The mean field approximation

The master equation also contains the information related to the average behaviour of the stochastic system. Starting from Eq. (2.16), it is possible to derive the equation describing the temporal evolution for the mean number $\langle N_A \rangle$ of individuals of type A, defined as:

$$\langle N_A \rangle = \sum_{N_A} N_A P(N_A, t). \tag{2.24}$$

I multiply Eq. (2.16) by N_A and sum over the possible states $N_A = 0, \ldots, N$. On the left-hand side, we obtain:

$$\sum_{N_A} N_A \frac{dP(N_A,t)}{dt} = \frac{d}{dt} \sum_{N_A} N_A P(N_A,t) = \frac{d}{dt}\langle N_A \rangle = \frac{d}{d\tau}\frac{\langle N_A \rangle}{N}, \tag{2.25}$$

where I have rescaled time $\tau = \frac{t}{N}$, with respect to the system size. On the right-hand side, we obtain:

$$\sum_{N_A} N_A T^+(N_A{-}1)P(N_A{-}1,t){+}N_A T^-(N_A{+}1)P(N_A{+}1,t){-}N_A \left[T^+(N_A)+T^-(N_A)\right] P(N_A,t). \tag{2.26}$$

In the first term of Eq. (2.26), manipulating the sum by rescaling the index $N_A \to N_A + 1$, yields:

$$\sum_{N_A} (N_A + 1)\, T^+(N_A) P(N_A, t). \tag{2.27}$$

Likewise in the second term of Eq. (2.26), manipulating the sum by rescaling the index $N_A \to N_A - 1$, yields:

$$\sum_{N_A} (N_A - 1)\, T^-(N_A) P(N_A, t). \tag{2.28}$$

Substituting Eqs. (2.27) and (2.28) into Eq. (2.26) some terms cancel out, and we are left with:

$$\frac{d}{d\tau}\frac{\langle N_A \rangle}{N} = \sum_{N_A} \left[T^+(N_A) - T^-(N_A)\right] P(N_A) = \langle T^+(N_A) - T^-(N_A) \rangle. \tag{2.29}$$

Substituting the transition rates Eqs. (2.14) into Eq. (2.29), we obtain:

$$\frac{d}{d\tau}\frac{\langle N_A \rangle}{N} = 2\gamma\omega \frac{\langle N_A\,(N - N_A)\rangle}{N^2} + \mu \frac{(N - \langle N_A \rangle)}{N}. \tag{2.30}$$

The deterministic equations are finally obtained by defining the deterministic density n_A of A type individuals as:

$$n_A \coloneqq \lim_{N\to\infty} \frac{\langle N_A \rangle}{N}, \tag{2.31}$$

and by invoking the *mean-field approximation*. The mean-field approximation consists in substituting all many-body with one-body averages, that is:

$$\langle N_A^2 \rangle \approx \langle N_A \rangle^2. \tag{2.32}$$

Substituting Eqs. (2.31) and (2.32) into Eq. (2.29), we obtain:

$$\frac{dn_A(t)}{dt} = 2\gamma\omega n_A(t)\,(1 - n_A(t)) + \mu\,(1 - 2n_A(t))\,, \tag{2.33}$$

in analogy with the derivation based on the law of mass action (Eq. (2.9)). Inspecting the mean-field derivation, one recognises that the mean-field equation can be cast in the following form:

$$\frac{dn_A(t)}{dt} = \langle T^+(n_A) - T^-(n_A) \rangle, \tag{2.34}$$

that is the balance between the average transition rate leading to increase of n_A and that leading to a decrease of n_A. Starting from Eq. (2.34), it is straightforward to generalise the mean-field equation to an arbitrary number of types.

2.2.2. Discrete RME

Let us now generalise the microscopic interactions of mutation and selection introduced in Subsection 2.1.2 to an arbitrary number of types. Let X_i be an individual of type $i = 1, \dots, M$, f_i the fitness value related to type i, and $m_{i,j}$ the probability for an individual of type i to mutate into type j. Then, the chemical reactions describing competition between two individuals of types i and j are:

$$X_i + X_j \xrightarrow{\gamma\left[\frac{1}{2} + \frac{\omega}{2}(f_i - f_j)\right]} 2X_i \tag{2.35.a}$$

$$X_i + X_j \xrightarrow{\gamma\left[\frac{1}{2} + \frac{\omega}{2}(f_j - f_i)\right]} 2X_j, \tag{2.35.b}$$

while the chemical reaction describing an individual of type i mutating into type j is:

$$X_i \xrightarrow{\mu\, m_{i,j}} X_j. \tag{2.36}$$

For a population of size N, the state of the system at a certain time is described by the vector $(N_1, \dots, N_M)$ collecting the number of individuals of each type. The stochastic dynamics undergone by the system is obtained by writing the master equation for each type. Then, defining the deterministic density $n_i := \lim_{N\to\infty} \frac{\langle N_i \rangle}{N}, i = 1, \dots, M$ and performing calculations equivalent to those presented in Subsection 2.2.1, the deterministic equations for the temporal evolution of the densities n_i are given by

(Traulsen et al., 2006):

$$\frac{dn_i(t)}{dt} = \sum_j^M \left(m_{j,i}n_j - m_{i,j}n_i\right) + 2\gamma\omega n_i \sum_j^M n_j \left(f_i - f_j\right). \tag{2.37}$$

The first term in Eq. (2.37) represents the balance between *in* and *out* contributions due to spontaneous mutations. The second term represents the fitness-dependent contribution due to competition, which is positive when the focal type i is competing with a less fit type, and negative otherwise. In the case where $f_i = f_j$, the deterministic contribution to competition is zero, as on average *wins* and *losses* will compensate. Both terms are summed over all types M, in order to account for all possible interactions. Equation (2.37) describes a general mutation-selection dynamics between discrete types, with general mutation scheme (fixed by parameters $m_{i,j}$) and fitness landscape (fixed by f_i); it is sometimes referred as the *parallel* scheme (Baake and Wagner, 2001; Saakian and Hu, 2004), to stress that spontaneous mutations occur as events separated from reproduction due to competition (in opposition to the original model formulated by Eigen, where mutations are *coupled* to competition). Before moving on, I am going to recast Eq. (2.37) in the form in which it usually appears in the literature (Hofbauer et al., 1998). I first define the average fitness $\overline{f}$ as:

$$\overline{f} = \sum_j^M f_j n_j, \tag{2.38}$$

and recall that the following normalisation condition holds:

$$\sum_j^M n_j = 1. \tag{2.39}$$

By using Eqs. (2.38)-(2.39), the equation takes the form:

$$\frac{dn_i(t)}{dt} = \sum_j^M \left(m_{j,i}n_j - m_{i,j}n_i\right) + 2\gamma\omega n_i \left(f_i - \overline{f}\right), \tag{2.40}$$

that is the typical form of the Replicator-Mutator Equation (RME).

2.2.3. From the discrete to the continuous RME

So far, I have employed the generic term *type*, to refer to the different possible biological configurations that individuals may be found in. From a modelling perspective, different types may refer to differences at the genetic or phenotypic level, and are ultimately captured by their different fitness values. The assumption underpinning the RME formalism is that individuals are able to spontaneously mutate from one type to the other, on a timescale that is comparable with the selective timescale. A typical framework where the discrete RME is employed is represented by viral evolution (Domingo et al., 2012): here, types refer to, *e.g.*, particular RNA sequences, each having their own AUGT string of bases; fitness is intended as the rate at which each particular RNA sequence self-replicates; punctual mutations occur at the aminoacids level and change the RNA sequence, hence the type, of the virus.

The continuous formulation aims at describing a different biological context, for which the notion of *type* may be less appropriate. Instead, I will introduce the notion of *trait*: a *trait* is a heritable phenotypic feature of the individual, that is possible to quantify by means of a continuous variable x, and which is exposed to variation due to spontaneous mutations.

Consider two bacterial cells that are identical from the genetic perspective, but their capability to adhere to host cells differs, due to a different level of activity of a certain protein involved in the adhesion process. It would be improper to refer to them as belonging to two different *types* of bacteria; rather, if the level of protein activity is a feature prone to mutations, then it is more appropriate to consider them as two cells of the same *type*, but differing in the magnitude of a common quantitative trait. Such a polymorphic population is also known in literature as *trait-structured* (or *phenotype-structured*), to stress the fact that its composition depends on how the phenotypic trait of interest is structured within the population. In the following, I will present

how to describe the mutation-selection dynamics of trait-structured populations with continuous quantitative traits, by means of a continuous RME.

2.2.4. Continuous RME

The continuous version of the RME was first introduced by Kimura in (Kimura, 1965), based on the assumption that: *i*) mutations can produce an infinite sequence of trait values; every mutation may produce a new trait value different from the pre-existing ones. *ii*) the effect of new trait value on the quantitative character is only slightly different from the parent trait value from which it was derived from a single mutational step. The above assumptions are almost exact quotes of the original sentences written by Kimura in (Kimura, 1965), adapted in order to avoid the introduction of additional biological terms (namely that of *allele*), which do not serve a useful purpose to this thesis. In his original work, the continuous RME is derived starting from *law of mass action*-like arguments. Here, I will derive it by performing a continuum approximation on the discrete Eq. (2.40), although other more general routes are possible (Wakano et al., 2017). The derivation is performed on a simple one-dimensional case, generalisations to multiple dimensions following straightforwardly.

First, I assume that all types are discretised in a one-dimensional lattice space, with lattice spacing Δx. I denote with $i \in [0, \dots, M]$ the lattice site with discrete trait value $x_i = i\Delta x \in [0, 1]$. Therefore, n_i is the density of individuals with trait value x_i. As a result of a single mutation event, an individual of type i moves in the lattice space towards one of the nearest neighbour sites: that is, either $i-1$ or $i+1$, for $i \in (0, M)$. An individual placed at the extreme $i = 0$ ($i = M$) of the lattice space will then move only rightwards (leftwards) towards the site 1 ($M-1$). The set of $M+1$ RME describing the density of individuals at each lattice site is then given by:

$$\frac{dn_0}{dt} = \mu\left(n_1 - n_0\right) + 2\gamma\omega n_0\left(f_0 - \overline{f}\right) \tag{2.41}$$

$$\frac{dn_i}{dt} = \mu\left(n_{i+1} + n_{i-1} - 2n_i\right) + 2\gamma\omega n_i\left(f_i - \overline{f}\right) \tag{2.42}$$

$$\frac{dn_M}{dt} = \mu\left(n_{M-1} - n_M\right) + 2\gamma\omega n_M\left(f_M - \overline{f}\right), \tag{2.43}$$

where f_i is the fitness of type i depending on trait value x_i. Let us now introduce the trait variable $x \in \mathcal{T} = [0,1]$, where $\mathcal{T}$ is the trait space. In the limit of small lattice spacing, I can introduce the following approximations relating the discrete and the continuous descriptions:

$$x_i \approx x, \quad n_i \approx n(x)dx, \quad f_i \coloneqq F(x_i) \approx F(x). \tag{2.44}$$

The first approximation states that x is the continuous counterpart of the discrete trait value x_i; the second approximation states that to each trait value is now associated a density of individuals $n(x)$ per unit of x; the third approximation states that fitness values are now functions of the continuous trait variable x, according to the fitness function F. With the above approximations, the normalisation condition Eq. (2.39) and the average fitness Eq. (2.38) become, respectively:

$$1 = \int_{\mathcal{T}} n(x;t)dx \tag{2.45.a}$$

$$\overline{F}[n(x;t)] = \int_{\mathcal{T}} x\, n(x;t)dx, \tag{2.45.b}$$

where the average fitness $\overline{F}$ is functional of the density $n(x;t)$. In the following, I will refer to the density $n(x;t)$ as the trait distribution of the population at time t. Inserting the above continuum approximations in the discrete RME for the generic i type, I obtain the equation for the temporal evolution of the trait distribution:

$$\frac{dn(x;t)}{dt} = \mu\left(n(x+\Delta x;t) + n(x-\Delta x;t) - 2n(x;t)\right) + 2\gamma\omega n(x;t)\left(F(x) - \overline{F}[n(x;t)]\right). \tag{2.46}$$

Assuming that the trait distribution $n(x;t) \in \mathcal{C}^2$ (that is differentiable functions with continuous first and second derivatives) in both the trait space $\mathcal{T}$ and in the time domain $\mathcal{R}_{\geq 0}$, we can Taylor expand up to second order the terms $n(x+\Delta x;t)$ and

$n(x - \Delta x; t)$ around the point (x, t):

$$n(x \pm \Delta x; t) \approx n(x; t) \pm \Delta x \frac{\partial n(x; t)}{\partial x} + \frac{\Delta x^2}{2} \frac{\partial^2 n(x; t)}{\partial x^2}. \tag{2.47}$$

Inserting the Taylor expansion Eq. (2.47) into Eq. (2.46) and performing basic algebraic calculations, we finally obtain:

$$\frac{dn(x)}{dt} = \mu \frac{\Delta x^2}{2} \nabla^2 n(x; t) + 2\gamma\omega n(x; t) \left(F(x) - \overline{F}[n(x; t)] \right), \tag{2.48}$$

that is the continuous RME of interest (note that the Laplacian notation ∇^2 indicates the partial second derivative with respect to x). The continuous RME (2.48) is a nonlinear integro-differential equation, describing the mutation-selection dynamics of the trait distribution. Changes due to selection preserve the same form of the discrete RME, and I will not discuss it further. Changes due to mutations are modelled by the Laplacian ∇^2, that is the local diffusion operator acting on the trait space $\mathcal{T}$, with corresponding diffusion coefficient given by $\mu \frac{\Delta x^2}{2}$. This term is appropriate when mutations induce small perturbations on the trait, consistently with assumption *ii*) of Kimura's formulation. This modelling choice is also known in the literature as *continuum-of-alleles* formulation (Bu et al., 1988). An antipodal formulation of local mutations is provided by the so-called *house-of-cards* model (Kingman, 1977, 1978), which describes the case when mutations induce major disruptions on the parent trait. Possible interpolating models between *continuum-of-alleles* and *house-of-cards* have also been proposed (Zeng and Cockerham, 1993).

The continuous RME is closed by the no-flux boundary conditions:

$$\frac{\partial n(x; t)}{\partial x} \Big|_{x=0} = \frac{\partial n(x; t)}{\partial x} \Big|_{x=1} = 0 \tag{2.49}$$

describing the behaviour of the system at the boundaries of the trait space: mutations cannot lead outside the trait space, the boundaries $x = 0$ and $x = 1$ act as reflecting barriers. Mutation and selection operate oppositely on the population's

trait composition: the former provides a continuous source of phenotypic variation; the latter instead removes variation by pushing towards fitness increase and deleting less fit traits. At stationarity, these two effects balance, and the system is described by a stationary distribution. The conditions for the existence and uniqueness of the stationary solution have been studied by Bürger in (Bürger, 1986). The proofs are based on methods from the theory of unbounded, self-adjoint operators, an overview of which goes beyond the purpose of this thesis. I just recall that for a continuous, positive and bounded fitness landscape $F(x)$, a positive distribution with initial condition $n(x;t_0) \geq 0$ will always converge to $n(x)$ as $t \to \infty$, where $n(x)$ is solution of the stationary RME (sRME henceforth):

$$\mu \frac{\Delta x^2}{2} \nabla^2 n(x) + 2\gamma\omega n(x) \left(F(x) - \overline{F}[n(x)]\right) = 0. \tag{2.50}$$

All fitness landscapes considered throughout this thesis satisfy the above conditions on F. In Chapter 3, the existence and stability of the solutions employed will not be discussed, as all conditions in (Bürger, 1986) are met. However, such conditions will not be sufficient for the solutions presented in Chapter 4, because the RME will involve a population of non constant size, and agent-based numerical simulations will be used to check the consistency of the analytical results.

The deterministic RME describing the mutation-selection dynamics of a polymorphic population has been derived from mean-field arguments, in the case where phenotypic differences between individuals were captured by a single quantitative trait x. However, the generalisation to multidimensional trait spaces is straightforward.

2.2.5. d-dimensional RME

Let $\underline{\mathbf{x}} \in \mathcal{T}_d$ be a d-dimensional vector belonging to the trait space $\mathcal{T}_d$. Each component x_i of the vector is the quantitative representation of the phenotypic feature i. The collection of the d phenotypic features represents a phenotype. Let $F : \mathcal{T}_d \to [0,1]$ be

the fitness function mapping the phenotype $\underline{\mathbf{x}}$ into its fitness value $F(\underline{\mathbf{x}})$. The evolving system is described by the trait (or phenotype) distribution $n(\underline{\mathbf{x}};t)$. The normalisation condition reads:

$$\int_{\mathcal{T}_d} n(\underline{\mathbf{x}};t)d\underline{\mathbf{x}} = 1, \tag{2.51}$$

and the average fitness is obtained by averaging the fitness function F over all the trait space:

$$\overline{F}[n(\underline{\mathbf{x}};t)] = \int_{\mathcal{T}_d} F(\underline{\mathbf{x}})n(\underline{\mathbf{x}};t)\, d\underline{\mathbf{x}}, \tag{2.52}$$

where $d\underline{\mathbf{x}}$ is the trait space's volume element $d\underline{\mathbf{x}} = dx_1\, dx_2\, \ldots\, dx_d$. Assuming that each trait mutates independently from each other and at the same rate μ (note that the scales of the traits can be defined to make it so, without loss of generality), then mutations over the trait space are modelled by the generalised Laplacian operator ∇_d^2 acting on $\mathcal{T}_d$. The d-dimensional RME is then given by:

$$\frac{dn(\underline{\mathbf{x}};t)}{dt} = \mu\frac{\Delta x^2}{2}\nabla^2 n(\underline{\mathbf{x}};t) + 2\gamma\omega n(\underline{\mathbf{x}};t)\left(F(\underline{\mathbf{x}}) - \overline{F}[n(\underline{\mathbf{x}};t)]\right), \tag{2.53}$$

subject to the boundary conditions:

$$\hat{\mathbf{n}}\cdot\nabla n(\underline{\mathbf{x}};t)\mid_{\underline{\mathbf{x}}\in\partial\mathcal{T}_d} = 0, \tag{2.54}$$

where $\hat{\mathbf{n}}$ is the unit vector normal to the boundary $\partial\mathcal{T}_d$ of the trait space. The condition Eq. (2.54) generalises the one-dimensional no-flux boundary conditions describing the reflecting nature of mutations close to the boundaries of the trait space. Differently from physical systems, where a variety of possible boundary conditions describe different, plausible behaviours, here we are interested only in reflecting boundary conditions: indeed, periodic boundary conditions would connect very phenotypically distant points of the trait space, in contrast with assumption of 'slight mutations'; absorbing boundary conditions would imply that phenotypes at the boundaries of the trait space are lethal, thus behaving as sinks, and in the models that I will study there is no reason to consider lethal phenotypes. Finally, non-zero boundary conditions would imply

the existence of *in* and *out* fluxes of individuals, which are not possible (because the microscopic interactions in play preserve the total number of individuals). Explicit analytical solutions of the sRME are rare because they are hard to obtain (see *e.g.* Alfaro and Carles, 2017; Alfaro and Veruete, 2019; Ruijgrok and Ruijgrok, 2015), and they rely either on further approximations, or on specific choices of the fitness landscape. Instead, I will employ a method allowing to obtain self-consistent solutions, which in principle is applicable to any choice of trait space $\mathcal{T}$ and fitness function F.

2.2.6. Self-consistent solutions of the sRME

At stationarity, the system is described by the time-independent trait distribution $n(x)$. Therefore, the correspondent average fitness $\overline{F}\left[n(x)\right]$ does not change in time any more, and it reaches a constant value $\overline{F}\left[n(\underline{\mathbf{x}})\right] = \phi$. With a fixed average fitness, the sRME loses both the nonlinear and the integro-differential natures, and one can then write the linear sRME:

$$\mu\frac{\Delta x^2}{2}\nabla^2 n_\phi(\underline{\mathbf{x}}) + 2\gamma\omega n_\phi(\underline{\mathbf{x}})\left(F(\underline{\mathbf{x}}) - \phi\right) = 0, \tag{2.55}$$

where $n_\phi(\underline{\mathbf{x}})$ is the solution depending on the unknown average fitness ϕ, subject to the conditions:

$$\begin{cases} \int_{\mathcal{T}} n_\phi(\underline{\mathbf{x}})d\underline{\mathbf{x}} = 1 \\ \hat{\mathbf{n}}\cdot\nabla n_\phi(\underline{\mathbf{x}}) \mid_{x\in\partial\mathcal{T}} = 0. \end{cases} \tag{2.56}$$

Once the linear sRME (2.55) is solved, the right solution $n(\underline{\mathbf{x}})$ is obtained by solving the self-consistent condition on the average fitness:

$$\phi = \int_{\mathcal{T}} F(\underline{\mathbf{x}})n_\phi(\underline{\mathbf{x}})d\underline{\mathbf{x}}. \tag{2.57}$$

Solving the linear sRME (2.55) is, in principle, an easier task than the nonlinear integro-differential version. However, the choice of the method depends on the prop-

erties of both the fitness landscape F and the trait space $\mathcal{T}$. On the other hand, the self-consistent condition will generally have to be solved numerically by means of standard nonlinear system solvers. This semi-analytical procedure represents a parsimonious way to explore the parameter space of the model (which can become large as the complexity of the problem is increased), and it will be applied to solve the RME in all models presented in both Chapter 3 and Chapter 4.

3. Degeneracy-selection trade-off

3.1. Introduction

Most of the mutation-selection models involving trait-structured populations employ one-dimensional trait spaces, where all the biological information of interest is condensed into a single quantitative trait. Therefore the dynamics is typically investigated by means of one-dimensional fitness landscapes. This picture purposely focuses the attention on the traits providing selective advantage to the evolving individual, thus neglecting contributions provided by neutral traits. Despite not providing selective advantage to the carrier, neutral traits (that will be properly defined in the following) contribute to shape the fitness landscape upon which the population evolves, and become particularly relevant when they are related to selective traits through a trade-off. Understanding the interplay between neutrality and selection is considered one of the major challenges in the contemporary theory of biological evolution (Wagner, 1999; Ciliberti et al., 2007a; Wagner, 2008; Barghi et al., 2020; Manrubia et al., 2020), aiming to bridge the gap between two historically antipodal theories (Nei, 2013): selectionism and neutralism. Such interplay has been well documented in the case of monomorphic populations, leading to a complete formal theory known as free-fitness. In the complementary, polymorphic case (to which trait-structured populations belong), theoretical investigations have been limited to special cases, or to effective formulations inspired by free-fitness. In this Chapter, I shall explore the interplay between neutrality and selection in trait-structured populations, by means of degenerate fitness landscapes

featuring both neutral and selective traits, related by a minimal but universal trade-off. I will calculate the trait distributions on symmetric and asymmetric degenerate landscapes, and compare their behaviour with non degenerate cases. Then, I will calculate the marginal fitness distributions and show the emergence of a dual behaviour, due to the presence of a trade-off between neutral and selective traits. I will show that asymmetries of the fitness landscape lead to a characterisation of neutral contributions that drastically differ from the free-fitness approach.

3.1.1. Neutralism

The concept of neutrality was introduced by the population genetist Mooto Kimura to explain the patterns of aminoacid substitution, experimentally observed in animal haemoglobin molecules (Kimura et al., 1968). Since then, neutralism developed as an approach complementary to selectionism, in the study of biological evolution. The neutralist viewpoint reverses the role played by mutations during evolution (Nei, 2013): in the selectionist viewpoint, mutations provide the source of variation, while fitness differences drive competition by natural selection; in the neutralist viewpoint, fitness differences between possible configurations are neglectable, when compared to the rate at which such configurations mutate: despite two aminoacid sequences presenting different rate of replications, which in principle would eventually lead to the domination of the faster replicating, in practice they will be disrupted by mutation before this occurs.

In his first works, Kimura acknowledged that *degeneracy* in the genetic code (Kimura, 1968) is manifested mainly in two ways: first, several aminoacid sequences code for the same protein; second, many (if not most) of the possible mutations in a polypeptide chain have little effect on the biological activity of the protein. These two considerations highlight the two possible sources of neutrality in a living organism: on the one side, there exist way more possible genotypes (e.g. aminoacid sequences) than observed phenotypes (*e.g.* the coded proteins), hence the mapping between the two

levels of description is inevitably degenerate. On the other side, not all phenotypic changes are relevant. The extent to which these two phenomena distinguish or overlap depends on the modelling context and on the system under consideration. In the following, I will first briefly discuss the first of such sources of neutrality, in the context of genotype-phenotype (GP) maps. Then I will focus on the second source, and on its applications to trait-structured populations.

3.1.2. Degeneracy of GP maps

In molecular evolution, the concept of degeneracy is well described by the general notion of *genotype network*, introduced by Maynard Smith in (Smith, 1970): genotypes are defined as the nodes of a network, representing the entire genotype space; two genotypes are then linked by an edge if they are separated by a single mutational step. A mutation connecting genotypes with identical phenotype is then called neutral. The degeneracy of GP mappings stems from the basic fact that the number of possible genotypes is much larger than that of phenotypes, so that such maps must be degenerate (Wagner, 2011; Greenbury et al., 2016; Ahnert, 2017). This schematic representation is widely used in molecular evolution to model gene regulation, metabolism and protein folding, and is at the foundation of the concept of mutational robustness (Wagner, 2011): under the effect of mutations and random sampling, the evolving system is perpetually exploring the genotype space, with the potential of discovering novel, innovative, phenotypes (Wagner, 2005). However, besides providing fitness advantage, the successful phenotype must also display some degree of robustness with respect to mutations, which continuously attempt to disrupt its corresponding genotype. In this framework, mutational robustness emerges as a macroscopic property depending on the topology of the underlying genotype network (Van Nimwegen et al., 1999; Fontana, 2006; Ciliberti et al., 2007b; Aguirre et al., 2009).

3.1.3. Degeneracy of phenotypic traits

Molecular evolution has provided an exceptional field to investigate the role of degeneracy in GP maps and test theoretical results, thanks to the increasing empirical evidence unveiled by technological advance (Manrubia et al., 2021). However, such a domain is less suitable to investigate the role played by the relevance of phenotypic changes, that is the second source of neutrality formalised by Kimura. While it is (in principle) fairly simple to connect a mutation on a RNA sequence to the increase (or decrease) of its self-replication rate (thus to its fitness), connecting a mutation leading to the increase in a pathogen's level of activity of a protein related to drug transporter production, with a potential selective advantage for the pathogen, may be less straightforward. Indeed, such mutation may be beneficial, if the pathogen is exposed to a pesticide whose chemicals are more easily cleared by such drug transporters; on the other hand, in absence of a pesticide the mutation may be detrimental, if it just represents additional metabolic cost with respect to pathogens not carrying this mutation; alternatively, the mutation may also be neutral, if it simply does not provide any relevant phenotypic change. This example demonstrates how the potential neutral nature of a phenotypic trait is strictly related to the environmental conditions and to the interactions between environment and individuals, thus to the fitness landscape on which the population is evolving. If ones identifies a phenotype as the collection of distinct traits endowing the individual with some phenotypic features, then it is natural to expect that some of such traits will provide selective advantage and some of them will not; that is, such collection is expected to include both selective and neutral traits.

The aim of this Chapter is to investigate mutation-selection dynamics of individuals whose phenotypes feature both selective and neutral traits. As explained in Chapter 2, the rate at which mutations occur delineates a major distinction between monomorphic and polymorphic regimes. In the monomorphic regime, a complete theory accounting also for neutral effects due to degeneracy has been developed in

(Khatri and Goldstein, 2015). Providing an exhaustive overview of this topic goes beyond the scope of this Section. Rather, the aim of the following Subsection is to provide an insight into some well established concepts regarding degeneracy in the monomorphic regime, with respect to which the results regarding polymorphic, trait-structured populations will be compared and discussed.

3.1.4. Monomorphic regime: the free-fitness approach

The role of neutrality in fitness landscapes has been extensively studied in the monomorphic regime, where the evolutionary dynamics is described by a stochastic process determining the probability to jump from a resident phenotype to a mutant one, which may take over the resident and become dominant (as explained in Subsection 2.1.6). For this event to occur, the mutant phenotype has to: *i*) be mutationally adjacent to the resident one; *ii*) fixate in the population. Point *i*) will depend on the topology of the mutations, as well as on the degeneracy of the mutant phenotype: the larger it is, the more likely such mutation will naturally occur. Point *ii*) will depend on the fitness difference between resident and mutant: the larger is the mutant fitness with respect to the resident one, the more likely it will invade and eventually fixate in the population. Consider a population of size N, which can express any phenotype ξ of a phenotype space Ξ. Each phenotype is characterised by a fitness $F(\xi)$ and a degeneracy $S(\xi)$. The equilibrium probability $P(\xi)$ that the population is found with phenotype ξ is given by:

$$p(\xi) \propto e^{N\,\Phi(\xi)}, \tag{3.1}$$

where:

$$\Phi(\xi) = F(\xi) + \frac{S(\xi)}{N} \tag{3.2}$$

is the free fitness of phenotype ξ (Khatri and Goldstein, 2015). Drawing a connection with equilibrium statistical mechanics, $\Phi(\xi)$ is interpreted as the potential that is

maximised at equilibrium by the evolving system, akin to the free energy of a thermal system. Hence, rather than just fitness, phenotypes shall maximise a combination of fitness and degeneracy. The degeneracy term $S(\xi)$ is also called *sequence entropy*, to stress the analogy with thermal systems: under the same selective conditions (same fitness), the population will drift into states that can be realised through a larger portion of the phenotype space; that is, phenotypes with larger degeneracy (*i.e.* larger sequence entropy) have larger probability to be explored by the system. The magnitude of this *entropic* contribution is mediated by population size N (which acts as an inverse temperature), so that its effect will be larger in smaller populations. The phenotypic free-fitness extends a concept introduced by Iwasa in (Iwasa, 1988), and subsequently rediscovered in (Sella and Hirsh, 2005). This expression highlights a crucial property of degenerate mappings: indeed, for Eq. (3.2) to be a relevant tool, fitness F and sequence entropy S must behave oppositely with respect to phenotypes: that is, phenotypes with large fitness must have small degeneracy, and vice-versa. In other words, a trade-off between degeneracy and fitness is expected to hold.

3.1.5. The degeneracy-selection trade-off

In presence of a trade-off, fitness and degeneracy act as opposing tendencies which are eventually balanced at equilibrium. Conversely, if a phenotype were able to maximise both fitness and degeneracy, then it would trivially dominate the evolutionary trajectory. It has been argued that this trade-off should be regarded as a universal feature of any kind of fitness landscapes (Khatri and Goldstein, 2019): ultimately, highly fit individuals are so because they have a phenotype better suited than others to their environment, but such higher functionality will stem from a *specific* feature that most of the other phenotypes do not provide; however, the specificity of such highly functional configuration is paid in terms of degeneracy. Hence, the concept of neutrality of genotypes with respect to phenotypes can be extended to phenotypes with respect to fitness, and the same kind of degeneracy is expected to hold, so that

very fit phenotypes would typically not be also highly degenerate.

In models of molecular evolution, degeneracy is generally assigned *ad hoc* to each phenotype, thus treated as set of parameters of the model. Instead, here I will consider it as a structured feature of fitness landscapes, which was explicitly encapsulated since the very first attempts to visualise them. Indeed, in their iconic two-dimensional representation introduced by Wright (Wright, 1932), fitness landscapes exhibit a hill-shaped topography: every phenotype is assigned a height proportional to its fitness, hence the optimum is represented by the top of the hill (see panel **a** of Fig. 2.3, adapted from Poelwijk et al., 2007). Neutrally related phenotypes, *i.e.* those sharing the same fitness value, are located at the same height, so that a height contour represents a neutral subset. Since the length of a contour (*i.e.* the size of the neutral subset) grows with distance from the summit, very fit phenotypes are rare, whereas less fit ones tend to be more abundant. Hence a degeneracy-fitness trade-off occurs, akin to that of genotype-phenotype maps. Simple two-dimensional fitness landscapes therefore represent a minimal tool for the modelling of polymorphic population featuring both selective and neutral degrees of freedoms. Unsurprisingly, characterising the role of neutral contributions in the case of polymorphic populations is far more difficult than in the monomorphic regime, as I will discuss in the next Subsection.

3.1.6. Polymorphic regime

In the polymorphic regime, the modeller would ideally be able to derive a coarse-grained description accounting for both selective and neutral degrees of freedom, such as free-fitness. However, despite some attempts to bridge the gap with the monomorphic regime (Khatri, 2018b), in the polymorphic regime it is not possible to rely on such a complete formalism. Indeed, when the population is polymorphic, the possibility to derive an exact coarse-grained dynamics passing from phenotypes to fitness demands special assumptions on the topology of mutations (Sato and Kaneko, 2007),

that is that their rates have to depend only on the resulting (mutant) fitness value, regardless of the starting (parent) phenotype. Although this demanding condition holds for many models of molecular phenotypes (Tsimring et al., 1996; Gerland and Hwa, 2002; Marchi et al., 2021), the implications of its violation are much less clear (Khatri, 2018a). Alternatively, one needs to rely on a phenomenological description of phenotypic robustness. For instance, in (Draghi et al., 2010) the authors consider a simplified version of GP networks, which drastically (and purposely) bypasses their complexity: phenotype neighborhoods are composed of both neutral and fitter configurations, and reshuffle randomly over time. The aim is to investigate the relationship between times of adaptation and the phenomenological parameters describing phenotypic robustness (namely the probability for a mutation to be neutral and the size of the neighborhood). In (Rigato and Fusco, 2020), the authors consider a discrete RME-like equation such as Eq. (2.40), where mutation rates $m_{i,j}$ are multiplied by a probability ρ (that they define as *phenotypic robustness*) that the mutation preserves fitness (that is neutral).

In this work, I shall preserve the form of the RME dynamics, without the addition of phenomenological terms capturing phenotypic robustness. Rather, I will consider explicit degenerate fitness landscapes. When a trait-structured population evolves on degenerate fitness landscapes, if the phenotype and fitness levels of descriptions cannot be disentangled, then they are likely to convey different information about the evolutionary state of the system.

3.2. Methods

In this Section, I present the minimal degenerate fitness landscapes employed to investigate the interplay between neutrality and selection, as well as the analytical and numerical methods used to calculate the trait distributions of the evolving system.

3.2.1. Degenerate fitness landscapes

I consider phenotypes to be composed of both selective traits (on which fitness depends) and neutral traits (on which it does not), so that the dynamics will be captured by simple fitness landscapes featuring degeneracy. Degeneracy will be minimally modelled by considering two-dimensional landscapes, where a selective and a neutral trait interact by virtue of a universal degeneracy-selection trade-off. Let $\mathcal{T}_2$ be the trait space, and its elements $\underline{\mathbf{x}} = (x, y) \in \mathcal{T}_2$ be the possible phenotypes; the components x, y represent respectively the value of the two quantitative traits defining the phenotype. Each phenotype $\underline{\mathbf{x}}$ maps into its corresponding fitness value $f = F(\underline{\mathbf{x}})$ according to the smooth fitness function $F(\underline{\mathbf{x}})$; the particular choice of $F(\underline{\mathbf{x}})$ determines the fitness landscape of the system. Two phenotypes $\underline{\mathbf{x}}_A$ and $\underline{\mathbf{x}}_B$ are defined to be *neutrally* related if they share the same fitness, that is if $F(\underline{\mathbf{x}}_A) = F(\underline{\mathbf{x}}_B)$. Then, a *neutral subset* with fitness value f is the collection of all neutrally related phenotypes $\underline{\mathbf{x}}_A$ with fitness $F(\underline{\mathbf{x}}_A) = f_A$. For the sake of simplicity we will consider only single-peak landscapes, which have been employed in a variety of biological contexts (Gil et al., 2019), the study of more complex topographies going beyond the scope of this work.

Degeneracy of the landscape is ultimately due to the degeneracy of the fitness function F. Here, I shall compare two possible versions of such degeneracy, symmetric (panel **a** Fig. 3.1) and asymmetric (panel **b** Fig. 3.1). In panel **a** of Fig. 3.1, phenotypes are identified by the trait coordinates $\underline{\mathbf{x}} = (x, y)$. However, their fitness $F(\underline{\mathbf{x}})$ depends only on the distance $r(x, y)$ from the centre. Phenotypes lying on the circle of radius r will share the same fitness value regardless of their angular position θ, thus forming neutral subsets. Hence, from the pair of trait variables x and y, we can construct a pair of (respectively) selective and neutral variables (r, θ), with which both the phenotype and the fitness dynamics can be described. The phenotype distribution of a population evolving on the symmetric landscape is described by the function $n(x, y)$ in the original traits coordinates, or equivalently by $n(r, \theta)$ in the corresponding polar coordinates. Given the circular symmetry, the marginal fitness distribution $\mathcal{N}^s(r)$ is

obtained by integrating the phenotype distribution over the angular coordinate θ:

$$\mathcal{N}^s(r) = \int_0^{2\pi} n(r,\theta)\, r\, d\theta, \tag{3.3}$$

that is the radial distribution. I remark that the landscape exhibits the aforementioned degeneracy-fitness trade-off, as the size of neutral subsets varies (linearly in this minimal model) in opposition to fitness. In the asymmetric case, I assume that the traits x and y directly express, respectively, selective and neutral effects. So the x axis will represent the selective direction, and the y axis the neutral direction (panel **b** of Fig. 3.1), with the fitness function F depending on x only. The trait space is then closed by the boundary curve $\mathcal{B}(x)$. Neutral subsets are given by vertical lines, that are the collections of points with equal value of the selective trait x. From the phenotype distribution $n(x,y)$ in the original trait coordinates, the marginal fitness distribution $\mathcal{N}^a(x)$ in the asymmetric landscape is given by integration over the neutral variable y:

$$\mathcal{N}^a(x) = \int_0^{\mathcal{B}(x)} n(x,y)\, dy. \tag{3.4}$$

The size of neutral subsets depends on the choice of $\mathcal{B}(x)$: taking a monotonically decreasing function of x leads to the desired degeneracy-fitness trade-off, equivalent to the symmetric landscape. Symmetric and asymmetric degenerate fitness landscapes display the same degeneracy-selection trade-off of interest. Nonetheless, the nature of such trade-offs is mechanistically different: in the symmetric case, neutrality stems from the property that fitness is given by a combination of the traits composing the phenotype, such combination being degenerate; instead, in the asymmetric case neutrality stems from explicitly considering a completely neutral trait concomitantly with a completely selective trait. Then, degeneracy is due to the inherent geometry of the resulting phenotype space, rather than to the degeneracy of the fitness function. For these reasons, I consider the two cases to be suited to qualitatively distinct biological

contexts: for instance, the symmetric landscape dates back to the Fisher Geometric Model and has been widely employed in the field of molecular evolution, where the existence of a target optimal configuration of traits is assumed, and any mutation away from it is deleterious (Tsimring et al., 1996; Orr, 2006; Gerland and Hwa, 2002).

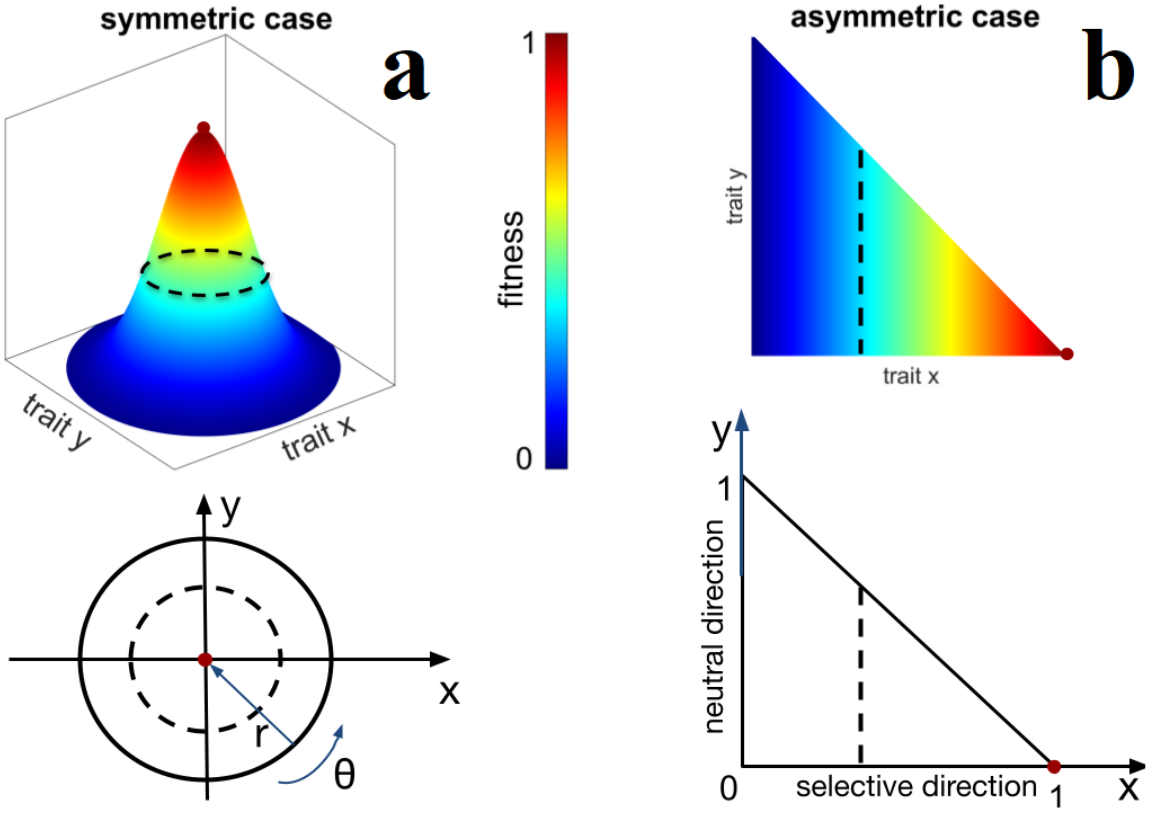

Figure 3.1: **Minimal degenerate fitness landscapes.** Panels **a** - **b**: respectively, symmetric and asymmetric degenerate fitness landscapes, and projections of the correspondent phenotype spaces, in the trait coordinates (x, y). For the symmetric case, fitness depends on the radial distance r from the optimum, regardless of the angular position θ. For the asymmetric case, fitness is proportional to the trait x determining the direction, while the trait y is neutral. Dashed black lines represents examples of neutral subsets. Red dots identify the optimum of the respective landscapes. In both cases, the size of the neutral subsets decreases in the selective direction, by virtue of the degeneracy-fitness trade-off.

3.2.2. Analytical solutions of the sRME

The deterministic mutation-selection dynamics of the trait distribution distribution $n(\underline{\mathbf{x}};t)$, evolving on a fitness landscape $F(\underline{\mathbf{x}})$, is given by the RME (2.53). In this work, I shall focus on the stationary trait distribution, which is the solution of the following sRME:

$$\nabla^2 n(\underline{\mathbf{x}}) + \delta\, n(\underline{\mathbf{x}})\,(F(\underline{\mathbf{x}}) - \phi) = 0, \tag{3.5}$$

where ϕ is the population average trait, and $\delta = \frac{4\gamma\omega}{\mu\Delta x^2}$ is the relevant compound parameter determining the relative importance of selection and mutation at stationarity. In the following, I shall present the analytical solutions to the sRME in the case of non-degenerate one-dimensional fitness landscape, and of degenerate two-dimensional ones, introduced in Subsection 3.2.1. In both cases, I shall employ the self-consistent resolution method presented in Subsection 2.2.6.

3.2.2.1 Non-degenerate landscape

I will consider a very simple instance of non-degenerate fitness landscape, and use it to provide baseline results for comparison with degenerate landscapes, in order to elucidate the effects of the degeneracy-selection trade-off. Let the one-dimensional variable $x \in \mathcal{T}_1 = [0,1]$ be the mathematical description of the single quantitative trait of interest. Let $F(x)$ be a non-degenerate monotonically increasing function, such that $x = 1$ ($x = 0$) is the fittest (least fit) trait value. For the sake of simplicity, I shall consider the linear fitness function $F(x) = x$, for which analytical stationary solutions can be found. However, any monotonic fitness function will produce qualitatively equivalent distributions. Clearly, since $F(x)$ is not degenerate, the corresponding fitness landscape is not degenerate; each phenotype is composed of a single trait,

whose value uniquely determines the corresponding phenotype's fitness. Therefore, x simultaneously determines the trait, the phenotype and the fitness of the individual. The RME is given by Eq.(2.48), subject to boundary conditions Eq. (2.49). Performing the transformation of variable $z = \sqrt[3]{\delta}\,(\phi - x)$, the equation for the stationary solution $n(x)$ becomes:

$$\frac{\partial^2 n(z)}{\partial z^2} - z\, n(z) = 0, \tag{3.6}$$

that is the well known Airy differential equation (Abramowitz and Stegun, 1964). The solution is a linear combination of the Airy functions of first and second kind which, back in the original variable, reads:

$$n(x) = \mathcal{Z}\Big\{ \mathrm{Ai}\left[\sqrt[3]{\delta}\,(\phi - x)\right] + \mathcal{C}\,\mathrm{Bi}\left[\sqrt[3]{\delta}\,(\phi - x)\right] \Big\}, \tag{3.7}$$

with $\mathcal{Z}$ and $\mathcal{C}$ constants of integration given by (prime notation indicates the x derivative):

$$\begin{cases} \mathcal{C} = -\dfrac{\mathrm{Ai}'\left(\sqrt[3]{\delta}\phi\right)}{\mathrm{Bi}'\left(\sqrt[3]{\delta}\phi\right)} \\ \mathcal{Z}^{-1} = \int_0^1 \mathrm{Ai}\left[\sqrt[3]{\delta}\,(\phi - x)\right] + \mathcal{C}\,\mathrm{Bi}\left[\sqrt[3]{\delta}\,(\phi - x)\right] dx. \end{cases} \tag{3.8}$$

Equation (3.8) represents the self-consistent trait distribution of the one-dimensional sRME. In order to plot the closed form the solution, the proper average fitness value ϕ is computed numerically by using the definition of the average fitness ϕ Eq. (2.57). In order to perform this last numerical step, I have used a simple MATLAB code employing the *fsolve*() function. The function *fsolve*(fun,x_0) is a standard routine to solve the nonlinear equation $\mathrm{fun}(x) = 0$, starting from the point x_0. Similarly to other of such functions, it is sensitive to the choice of the initial guess x_0. However, I have found that the starting point $x_0 = 1$ always provides the correct result, for any value of the parameters explored.

3.2.2.2 Asymmetric degenerate landscape

In this case, the dynamics takes place in the trait space $\mathcal{T}_2^{\mathrm{a}} = \{0 \leq x \leq 1, 0 \leq y \leq \mathcal{B}(x)\}$, with fitness function $F(x,y) = F(x) = x$. A phenotype is specified by the values of the two quantitative traits x and y. The x axis represents the selective direction, because it determines the phenotype's fitness value. The y axis represents the neutral direction, because the fitness function is degenerate with respect to y. The degeneracy-selection trade-off is encapsulated in the boundary profile $\mathcal{B}(x)$, which I choose linear for sake of simplicity, that is:

$$\mathcal{B}(x) = 1 - x. \tag{3.9}$$

The resulting trait space is then a right triangle, where the optimal phenotype is unique (hence not degenerate) and it occupies the right edge of coordinates $(1, 0)$. The two-dimensional stationary trait distribution $n(x,y)$ is the solution of the following sRME:

$$\nabla^2 n(x,y) + \delta\, n(x,y)\Big(F(x) - \phi\Big) = 0, \tag{3.10}$$

with average fitness given by:

$$\phi = \int_0^1 \int_0^{1-x} F(x)\, n(x,y)\, dxdy, \tag{3.11}$$

and boundary conditions given by:

$$\begin{cases} \int_0^1 \int_0^{1-x} n(x,y)\, dxdy = 1 & \text{population conservation} \\ \frac{\partial n(x,y)}{\partial x}\,|_{x=0} = \frac{\partial n(x,y)}{\partial y}\,|_{y=0} = \frac{\partial n(x,y)}{\partial x} + \frac{\partial n(x,y)}{\partial y}\,|_{y=1-x} = 0 & \text{no-flux} \end{cases} \tag{3.12}$$

Despite the apparent simple form of Eq. (3.10), the separation of variables method fails due to the non trivial no-flux condition at the boundary $y = \mathcal{B}(x)$. Thus, I have employed a spectral method to solve the equation (detailed in the Appendix A.3). The

spectral solution takes the form of a linear combination of the eigenfunctions $e_{i,j}$ of the Laplacian on the trait space $\mathcal{T}_2^{\mathrm{a}}$:

$$n(x,y) = \sum_{i,j} a_{i,j} e_{i,j}(x,y), \tag{3.13}$$

where $a_{i,j}$ are the corresponding coefficients of the expansion. Writing the solution in this form allows to convert the problem of solving the partial differential equation into the problem of solving a linear system of equations, giving the coefficients of the expansion. This system being in principle infinite, in practice one needs to truncate the solution to a finite number M of eigenfunctions. Throughout this work, I have found that using the first $M = 8$ eigenfunctions leads to solutions in good agreement with numerical simulations. Therefore, all results related to this Subsection will refer to the choice $M = 8$.

3.2.2.3 Symmetric degenerate landscape

In the symmetric case, the dynamics takes place in the trait space $\mathcal{T}_2^{\mathrm{s}} = \{x, y \mid x^2 + y^2 \leq 1\}$. The optimal phenotype occupies the centre $(0,0)$, has maximum fitness value $f = 1$, and again is not degenerate. Fitness decreases proportionally to the distance from the optimum. Hence, it is useful to describe the dynamics in the polar coordinates (r, θ), obtained from the trait variables via the usual coordinates transformation:

$$\begin{cases} x = r\ \cos\theta \\ y = r\ \sin\theta, \end{cases} \tag{3.14}$$

with which fitness becomes function of the sole radial variable r, that is $F = F(r)$. Describing the problem in polar coordinates (r, θ), we recognise r as the selective variable, and θ as the neutral one: phenotypes lying on the same circle (*i.e.* with same r) will share the same fitness value, regardless of their value of θ, as shown in Fig. 3.1, panel **a**. It is then useful to write the two-dimensional sRME for the trait distribution

$n(r,\theta)$ in polar coordinates. Transforming the Replicator term of the sRME from cartesian (x,y) to polar (r,θ) is straightforward due to the symmetry of the fitness function:

$$n(x,y)\left(F(x,y)-\phi\right) \Longrightarrow n(r,\theta)\left(F(r)-\phi\right). \tag{3.15}$$

The Mutator term of the sRME is transformed by replacing the Laplacian in cartesian coordinates with its corresponding in polar coordinates:

$$\left(\frac{\partial^2}{\partial x^2}+\frac{\partial^2}{\partial y^2}\right) n(x,y) \Longrightarrow \left(\frac{1}{r^2}\frac{\partial^2}{\partial r^2}+\frac{1}{r}\frac{\partial}{\partial r}+\frac{\partial^2}{\partial \theta^2}\right) n(r,\theta). \tag{3.16}$$

Finally, the sRME in polar coordinates describing the dynamics in the symmetric degenerate landscape reads:

$$\left\{\frac{\partial^2}{\partial r^2}+\frac{1}{r}\frac{\partial}{\partial r}\ +\frac{1}{r^2}\frac{\partial^2}{\partial \theta^2}\right\} n(r,\theta)\ +\ +\delta\left(F(r)-\phi\right) n\left(r,\theta\right)=0, \tag{3.17}$$

with average fitness:

$$\phi=\int_0^1\int_0^{2\pi} F(r)\, n(r,\theta)\, r\, dr d\theta, \tag{3.18}$$

and boundary conditions:

$$\begin{cases} \int_0^1\int_0^{2\pi}\ n(r,\theta)\, r\, dr d\theta = 1 & \text{population normalisation} \\ \frac{\partial\, n(r,\theta)}{\partial\, r}\ |_{r=1}= 0 & \text{no-flux} \end{cases} \tag{3.19}$$

Differently from the asymmetric case, separation of variables can be applied since the *no-flux* boundary condition only depends on the selective variable r. Hence, the solution can be found in the form $n(r,\theta)=R(r)Y(\theta)$, where radial $R(r)$ and angular $Y(\theta)$ contribution are factorised and describe, respectively, selective and neutral contributions to the trait distribution. The angular contribution can be eliminated by integrating Eq. (3.17) over the angular variable θ:

$$\int_0^{2\pi}\left\{\frac{\partial^2}{\partial r^2}+\frac{1}{r}\frac{\partial}{\partial r}\ +\frac{1}{r^2}\frac{\partial^2}{\partial \theta^2}\right\} n(r,\theta)\, d\theta\ +\ +\delta\int_0^{2\pi}\ \left(F(r)-\phi\right) n\left(r,\theta\right)\ d\theta =$$

$$\frac{\partial^2}{\partial r^2}R(r)\int_0^{2\pi}Y(\theta)d\theta+\frac{1}{r}\frac{\partial}{\partial r}R(r)\int_0^{2\pi}Y(\theta)d\theta+$$

$$+\frac{1}{r^2}R(r)\int_0^{2\pi}\frac{\partial^2}{\partial\theta^2}Y(\theta)d\theta+\delta\left(F(r)-\phi\right)R(r)\int_0^{2\pi}Y(\theta)d\theta=$$

$$\frac{\partial^2}{\partial r^2}R(r)\mathcal{Y}+\frac{1}{r}\frac{\partial}{\partial r}R(r)\mathcal{Y}+\frac{1}{r^2}R(r)[\frac{\partial}{\partial\theta}Y(\theta)]_0^{2\pi}+\delta\left(F(r)-\phi\right)R(r)\mathcal{Y}=0, \tag{3.20}$$

with $\mathcal{Y}=\int_0^{2\pi}Y(\theta)d\theta$ being the normalisation constant of the angular contribution. The third term appearing in Eq. (3.20) is zero because $\frac{\partial Y(2\pi)}{\partial\theta}=\frac{\partial Y(0)}{\partial\theta}$, by symmetry. Finally, the constant $\mathcal{Y}$ can be eliminated from the equation, and I am left with:

$$\frac{\partial^2R(r)}{\partial r^2}+\frac{1}{r}\frac{\partial R(r)}{\partial r}+\delta\,R(r)\left(F(r)-\phi\right)=0, \tag{3.21}$$

that is the radial equation for the selective variable, with average fitness:

$$\phi=\int_0^1F(r)R(r)rdr, \tag{3.22}$$

and simplified boundary conditions:

$$\begin{cases}\int_0^1 R(r)\,r\,dr=1\\ \frac{\partial R(r)}{\partial r}\mid_{r=1}=0.\end{cases} \tag{3.23}$$

Unsurprisingly, the trait distribution will be constant along the neutral variable θ, due to the circular symmetry of the landscape, and it will vary along the selective variable r, according to the radial equation (3.21). Similarly to the asymmetric case, I solve the radial equation by means of spectral method (detailed in the Appendix A.3).

3.2.3. Agent-based numerical simulations

In this Section, I present the algorithm employed to simulate the agent-based dynamics on both degenerate and non degenerate landscapes. The algorithm used to simulate the microscopic mutation-selection interactions is based on a rejection-free Gillespie algorithm, adjusted to account for continuity of the trait variables. It can be applied to simulate any mutation-selection dynamics with continuous variables, regardless of the choice of the fitness function, of the dimension and shape of the adaptive space.

3.2.3.1 The algorithm

Let $\mathcal{T}_d$ be the d-dimensional trait space. The population is composed of N individuals. This size is preserved over timesteps, because the simulation employs only Birth-Death processes. The system is represented by an array of dimension N. Each element i of the array represents an individual, and contains the array of trait values $\underline{\mathbf{x}}_i \in \mathcal{T}_d$, identifying the individual's phenotype. Each trait has value $x_i^j \in [0,1]$, where the subscript $i = 1, \ldots, N$ identifies the individual, and the superscript $j = 1, \ldots, d$ the trait. The system is initialised assigning to each trait value a random number sampled from a uniform distribution $\in [0,1]$, although any other kind of initialisation can be employed (as long as the inputs are positive). This will only affect the transient dynamics, but not the asymptotic behaviour which in all cases studied coincides with the deterministic predictions. The agent-based dynamics is composed of *Mutation events*, occurring at rate μ per individual, and *Competition events*, occurring at rate γ per pair of individuals. The total reaction rate r_{tot} is given by $r_{tot} = \mu + \gamma$ (demonstration in the Appendix A.4). All rates are constant over time because the population size is fixed. A single timestep is composed of N iteration steps. During an iteration step, two pseudorandom numbers $r_{1,2} \in [0,1]$ are sampled: r_1 is used to determine the time

to the next reaction τ, given by:

$$\tau = \frac{1}{r_{tot}} \log\left(\frac{1}{r_1}\right), \tag{3.24}$$

and update the time of the next reaction to $t+\tau$ (rescaled with respect to system size). The second pseudorandom number r_2 is used to determine which of the two events occur. If $r_2 \leq \frac{\mu}{r_{tot}}$, a Mutation event occurs, otherwise a Competition event occurs.

Mutation event. I define $\underline{\zeta} \in \mathcal{R}^d$ a vector of random variables. The components ζ_j, with $j = 1, \ldots, d$, are independently extracted from the same probability distribution $\mathcal{U}$, and represent the potential random modification to trait j, due to mutation. Upon occurrence of a mutation event, an integer pseudorandom number $i \in [1, N]$ is sampled to determine which individual undergoes mutation. Then, its phenotype $\underline{\mathbf{x}}$ is modified according to the following reaction:

$$\underline{\mathbf{x}}_i \xrightarrow{\mu} \underline{\mathbf{x}}_i + \underline{\zeta}, \tag{3.25}$$

If the new mutant phenotype would cross the border of the adaptive space, the mutation is rejected and the individual retains its original phenotype, that is reflecting boundary conditions are considered. For the analysis provided in this thesis I have employed a uniform probability distribution $\mathcal{U}(\zeta)$, defined as follows:

$$\mathcal{U}(\zeta) = \begin{cases} \frac{1}{2\epsilon} & \text{if } -\epsilon \leq \zeta \leq +\epsilon \\ 0 & \text{otherwise.} \end{cases} \tag{3.26}$$

The moments of the probability distribution read:

$$\begin{cases} \text{mean} & E[\xi] = 0 \\ \text{variance} & \sigma^2 = E[(\xi - E[\xi])^2] = \frac{\epsilon^2}{3}, \end{cases} \tag{3.27}$$

and they determine important properties of the process. The *zero* mean implies that mutations are unbiased, that is the trait space is explored with same probability in any direction (with the exception of the reflecting behaviour close to the boundaries), and no distinction between deleterious, beneficial or neutral mutations is made. The variance σ^2 corresponds to the small increment Δx^2 appearing in the RME (Kimura, 1965).

Competition event. Upon occurrence of a competition event, two integer pseudorandom numbers $i, j \in [1, N]$ are sampled to determine the couple of competing individuals. In the (unlikely) case that $i = j$, another index is sampled again. Competition is modelled by a fitness-dependent Birth-Death process, where one individual perishes and the other reproduces. The two possible outcomes are schematised by the chemical reactions Eqs. (2.35).

The codes produce the numerical results appearing in this Chapter have all population size 10^5. The algorithm is run for 12000 timesteps, and the scatter profiles of the trait distributions are obtained by averaging over the last 10000 timesteps (the first 2000 are discarded due to transient dynamics). The Processing code employed for the agent-based dynamics of the asymmetric degenerate fitness landscape is reported in the Appendix A.1.1.

3.3. Behaviour of the trait distributions

In this Section, I present the analytical trait distributions obtained by solving the sRME with the methods presented in Subsection 3.2.2, for both non-degenerate and degenerate fitness landscapes. The non-degenerate case will provide the baseline results for comparison with results on degenerate landscapes, to elucidate the effects of the degeneracy-fitness trade-off.

3.3.1. Equilibrium trait distribution on non-degenerate landscape

In Fig. 3.2, I plot the analytical trait distribution $n(x)$ solution of the sRME (3.7) for different values of δ (solid lines), and compare it with results from numerical simulations of the agent-based dynamics (circles and squares). For $\delta = 0$, that is in the *purely neutral* scenario, the distribution is trivially uniform (dashed line): since every phenotype is equally likely to survive competition regardless of their fitness value, no particular trait value will be preferred by natural selection. For $\delta > 0$, the distribution is monotonically increasing, always showing an absolute maximum at $x = 1$ (the optimal phenotype), as well as an absolute minimum at $x = 0$ (the least fit one). These profiles represent qualitatively the prediction of the standard *survival-of-the-fittest* paradigm: the distribution is biased towards the phenotype endowed with the fittest trait ($x = 1$); most of the population lies on top of the fitness landscape, and progressively fewer individuals are found as one moves away from the peak. The least successful individuals are those carrying the least fit trait ($x = 0$). On increasing δ (that is, increasing selection strength or decreasing mutation diffusion coefficient), the distribution gets narrower around the maximum.

3.3.2. Equilibrium trait distribution on degenerate landscapes

In Fig. 3.3, I show the analytical two-dimensional trait distributions $n(x, y)$ in the case of degenerate landscapes, for different values of δ. The asymmetric case is shown in panels **a** and **c**, where I plot the iso-density contour lines on the trait plane (x, y); the symmetric case is shown in panels **b** and **d**, where I plot the color-map projection on the trait plane (x, y). The color code quantifies the magnitude of the density of $n(x, y)$, according to the respective color-bars. With the exception of the purely neutral scenario $\delta = 0$, for which the distribution would be trivially uniform (not shown), in all

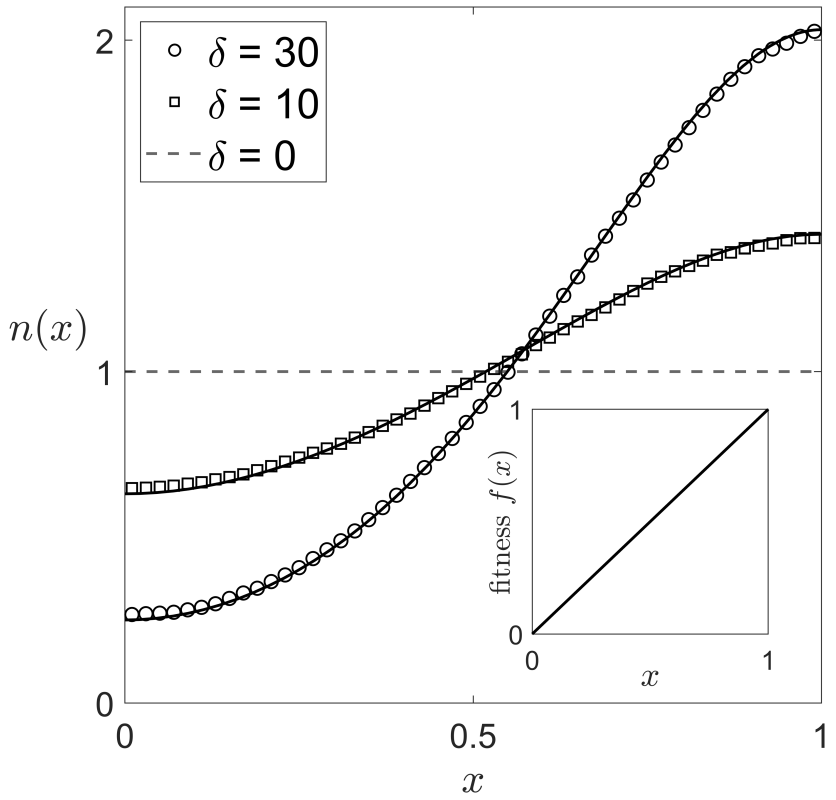

Figure 3.2: **Trait distribution on non-degenerate landscape.** Solid lines: analytical solution; circles and squares: agent-based numerical simulations with $N = 10^5$ individuals. With the exception of the neutral case $\delta = 0$ (dashed line), the distribution is always monotonically increasing towards the optimal trait $x = 1$, indicating the standard survival-of-the-fittest scenario. Inset: linear fitness landscape $F(x) = x$.

other cases the trait distributions increase monotonically along the selective direction: that is, along the x axis for the asymmetric case; along the radial axis for the symmetric one. In both cases, and for all values of $\delta > 0$, the distributions display an absolute maximum located at the optimal trait combination (the right edge of the triangle for the asymmetric, and the center of the circle for the symmetric case). Similarly to the non-degenerate case, these results again indicate a *survival-of-the-fittest* paradigm, where fitter individuals are more abundant in the population, and the other types are distributed around the optimal with density that decreases as the distance from the optimum increases. The difference in the geometry of the two landscapes affects the behaviour of the trait distributions on the neutral subsets: on the one hand, $n(x, y)$ is

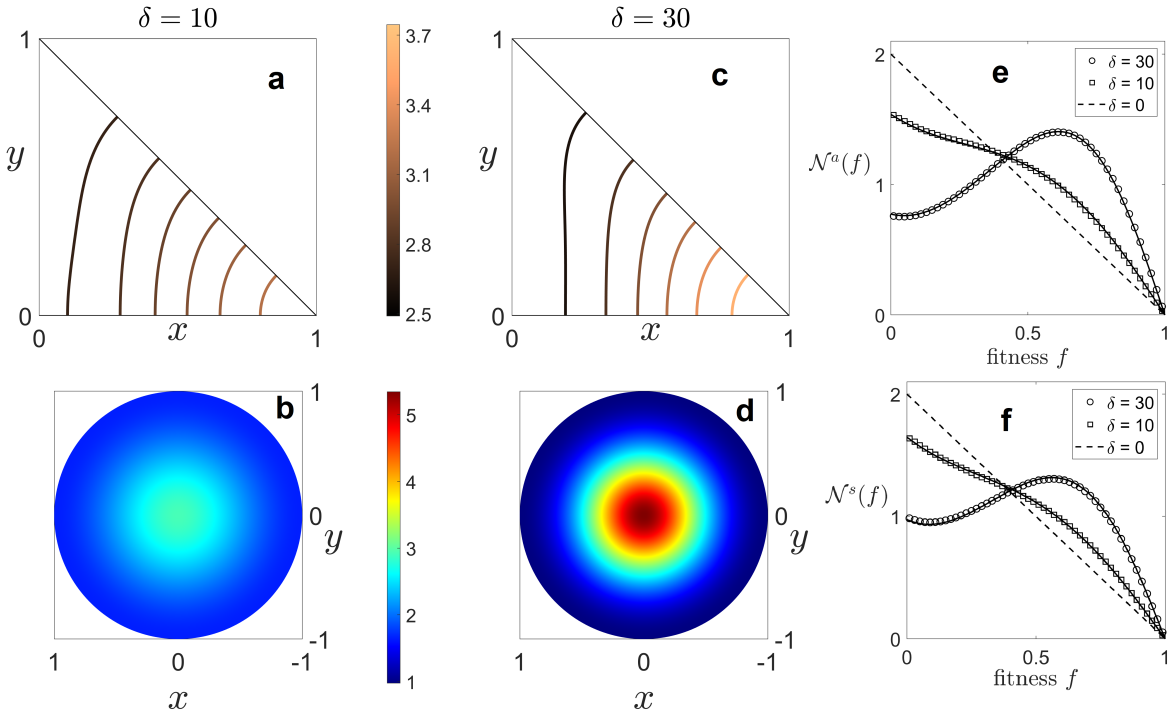

Figure 3.3: **Stationary phenotype distributions and marginal fitness distributions for degenerate landscapes.** Phenotype distributions: contour lines of iso-density are shown for the asymmetric case (**a** and **c**), while colormaps are shown for the symmetric case (**b** and **d**). In both cases and for every value of $\delta > 0$, the distribution has maximum density in correspondence of the optimal trait (that with max fitness), exhibiting a survival-of-the-fittest behaviour. However, the corresponding marginal fitness distributions (**e-f**) display rather different behaviours depending on the value of δ. Particularly, we distinguish the degeneracy-dominated profile (squares $\delta = 10$), where the most degenerate fitness values are favoured; and the sub-optimal profile (circles $\delta = 30$), where the fitness distributions exhibit maximum at a value, smaller than the optimal one. Solid lines refer to analytical solutions of the RME, while scatter plots to agent-based simulations with $N = 10^5$ individuals.

constant along each of the neutral subsets of the symmetric landscape (circles of radius $0 \leq r \leq 1$); on the other hand, $n(x, y)$ is not constant along the neutral subsets of the asymmetric case (vertical lines of fixed x): rather, I remark a non-trivial variation along the $y-$axis, which results from the asymmetric behaviour of mutations close to the boundaries of the trait space.

The distributions displayed in Fig 3.3 provide full information on all traits composing the phenotypes. However, if one is solely interested in selective traits, then they have

to focus on the marginal fitness distribution, which is obtained upon integration of the full distribution over the neutral subsets of the fitness landscapes. In the next Section, I will show the marginal fitness distributions and compare their behaviour with that of the full trait distributions.

3.4. Behaviour of the marginal fitness distributions

In this Section, I focus on the behaviour of the marginal fitness distributions, describing how selective traits are distributed in the population. First, I will show that the presence of a degeneracy-fitness trade-off leads to non-monotonic fitness distributions, drastically different from the non-degenerate case. Second, I will derive the exact equations governing the temporal dynamics of the marginal fitness distribution, and show that effects of asymmetries in degenerate landscapes.

3.4.1. Equilibrium marginal fitness distributions

I now consider the behaviour of the marginal fitness distribution $\mathcal{N}^s(f)$ and $\mathcal{N}^a(f)$ for, respectively, symmetric and asymmetric landscapes, defined in Eq. (3.3) and Eq. (3.4). In panels **e-f** of Fig. 3.3, I compare analytical (solid lines) and numerical (circles and squares) profiles, corresponding to the trait distributions presented in panels **a-d**.
For $\delta = 0$, the purely neutral scenario, the solution is straightforward: I recall that in this case, the full trait distribution is uniform over the trait space, *i.e.* $n(x, y) = C$. In the asymmetric landscape, the marginal fitness distribution is then given by:

$$\mathcal{N}^a(f) = \int_0^{1-f} C\, dy = C\,(1-f)\,. \tag{3.28}$$

The constant C is fixed by imposing normalisation:

$$1 = \int_0^1 \mathcal{N}^a(f) = \int_0^1 C\,(1-f)\, df = C\frac{f\,(1-f)}{2} = \frac{C}{2} \Longrightarrow C = 2. \tag{3.29}$$

Hence, $\mathcal{N}^a(f) = 2\,(1-f)$, and likewise for the symmetric landscape. Therefore the marginal fitness distribution is a monotonically decreasing function of fitness, the linear dependence reflecting the linearity of the degeneracy-fitness trade-off. For values of $\delta > 0$, the marginal fitness distributions are obtained by firstly calculating the full trait distribution, and then by performing the integration over the corresponding neutral subsets (Eqs. (3.3)-(3.4)). For small values of δ, the profiles are still monotonically decreasing yet considerably different from the purely neutral case, displaying an increase in the density for intermediate fitness values (see $\delta = 10$ case). For larger values of δ, the fitness profiles become non-monotonic: a new pair of local minimum and maximum emerge, at intermediate fitness values (see $\delta = 30$ case).

In Fig. 3.4, the positions of the extrema of the fitness profile are shown for a wide

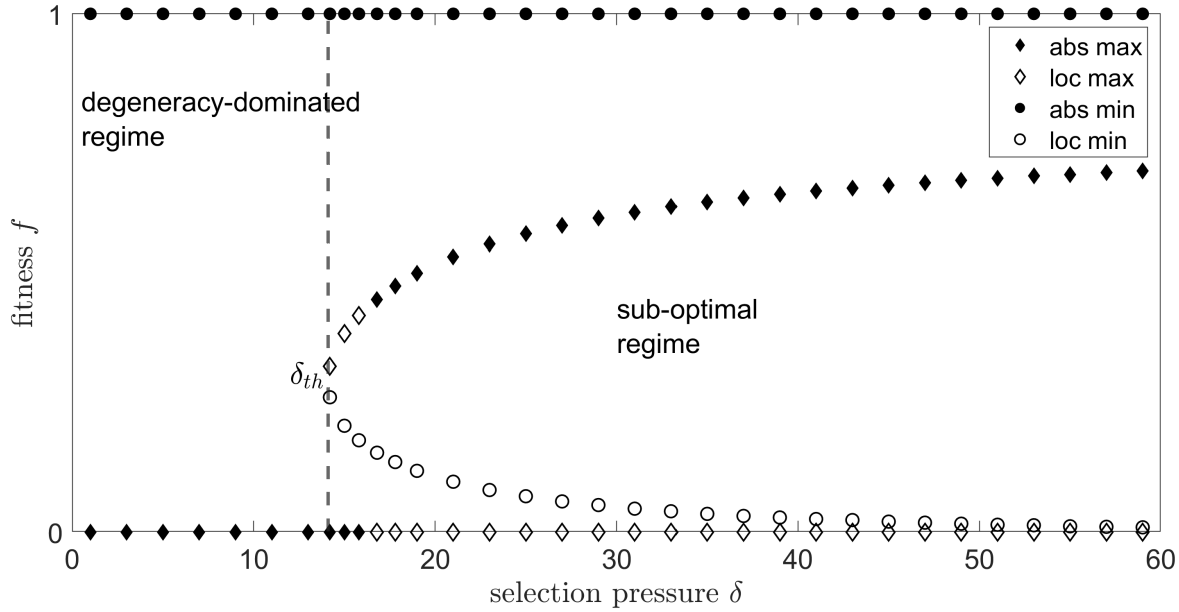

Figure 3.4: **Marginal fitness behaviour.** The different regimes of the marginal fitness distribution $\mathcal{N}^a(f)$ are identified by tracking the extrema of its spectral solution at the variation of selective pressure δ. Diamonds (circles) refer to maxima (minima). Filled (empty) symbols refer to absolute (local) extrema. A threshold value $\delta_{\rm th} \simeq 14$, estimated with the perturbative solution, separates the two qualitative behaviours. Below $\delta_{\rm th}$, the fitness distribution is dominated by the most degenerate fitness value (degeneracy-dominated regime). Above $\delta_{\rm th}$, the distributions exhibit sub-optimality, as they are dominated by intermediate fitness values. Then, the survival-of-the-fittest scenario is recovered in the limit of very large selection ($\delta \to \infty$).

range of effective selection pressure values, for asymmetric landscape (the symmetric case is not shown, as it provides the same qualitative result). For $\delta \lesssim 14$, the profiles are all monotonically decreasing and have an absolute maximum at $f = 0$; I call this phase *degeneracy-dominated*, because the most degenerate fitness value is the most abundant in the population. When δ crosses a threshold value δ_{th}, monotonicity is broken, with the emergence of a new peak in the fitness profile. Initially, the new maximum is local (the absolute one still being located at $f = 0$), and it eventually becomes absolute as δ is increased; I call this the *sub-optimal* phase, since the new maximum is located at an intermediate fitness value, which does not correspond to the optimal one ($f = 1$). Increasing selection pressure, the maximum shifts progressively towards the value $f = 1$.

For small values of δ (known as the weak selection limit), in the asymmetric case with linear fitness and triangular shape, a closed analytical approximation of the marginal fitness distribution $\mathcal{N}^a(f)$ can be obtained. In the Appendix A.5, I show that performing a linear perturbation expansion on δ, one gets:

$$\mathcal{N}^a(f) = 2(1-f) + \delta\,\mathcal{N}^a_{\text{I}}(f) + O\left(\delta^2\right), \tag{3.30}$$

with

$$\mathcal{N}^a_{\text{I}}(f) = \frac{4}{3}(1-f)B_4\left(\frac{f}{2}\right) - \frac{8}{15}B_5\left(\frac{f}{2}\right) + \frac{4}{15}B_5\left(f\right), \tag{3.31}$$

where $B_k(z)$ is the k^{th} Bernoulli polynomial of the variable z. This approximation then predicts that the average fitness of the population ϕ at stationarity increases linearly with selection pressure, according to:

$$\phi = \frac{1}{3} + \frac{1}{189}\,\delta + O\left(\delta^2\right). \tag{3.32}$$

This approximation also predicts the emergence of intermediate local maxima and minima in the marginal fitness distribution for $\delta_{\text{th}} \simeq 14$ (see Fig. A.1 in the Appendix),

which is consistent with the results obtained with the spectral solution.

The two phases displayed in Fig. 3.4 highlight a behaviour that cannot be captured by observing the full trait composition: in the presence (or absence) of low selection pressure, the absolute maximum of the marginal distribution is found at $f = 0$, which is the most degenerate fitness value. Thus, fitness values belonging to the largest neutral subset outperform the others, even if they posses less fitness. This scenario is consistent with the so-called *survival-of-the-flattest* effect (Wilke, 2005; Codoner et al., 2006; Beardmore et al., 2011), a term coined in iconic antithesis to the survival-of-the-fittest paradigm: flatter (that is less fit) regions of the fitness landscape are favoured, because the advantage provided by degeneracy overcomes the disadvantage provided by being far from the landscape's peak. In my setting, such advantage is inherent in the degeneracy-selection trade-off, rather than in a phenomenological representation of phenotypic robustness. For this reason, the *degeneracy-dominated* behaviour emerges only at the marginal level. Upon increasing selection pressure, the trade-off leads to the emergence of a *sub-optimal* phase, where the most successful fitness value possesses both non-zero degeneracy and some degree of selective advantage. Eventually, for very large values of effective selection pressure ($\delta \to \infty$), the distribution's sub-optimum reaches the optimal fitness value $f = 1$, and the survival-of-the-fittest scenario is recovered. The location of the new maximum is non trivial, and in general will depend both on the geometry of the trait space $\mathcal{T}$ and on the fitness function F.

Contrary to their non degenerate counterpart (always displaying fittest-like patterns, Fig. 3.2), I have shown that degenerate landscapes display a dual behaviour, depending on the dynamics' level of description: full phenotype distributions exhibit fittest-like patterns (Fig. 3.3, panels **a-d**), where most of the population lies in proximity of the landscape peak; on the other hand, their correspondent marginal fitness distributions may exhibit *sub-optimal* patterns (Fig. 3.3, panels **e-f**), where most of the population displays less fit but more degenerate traits (Fig. 3.4). A proper characterisation of neutral contributions is crucial to understand the dual behaviour between full and marginal trait distributions. One may be tempted to interpret the different phases

of the marginal fitness distribution as the result of a balance between fitness and degeneracy, akin to the free-fitness potential presented in Subsection 3.1.4, allowing to predict when one or the other contributions are favoured. For this purpose, in the next Section, I will derive the exact equations governing the dynamics of the marginal dynamics in both symmetric and asymmetric landscapes.

3.5. Deriving the marginal dynamics

We have seen that neutral information featuring degenerate landscapes is often modelled by introducing effective contributions mimicking phenotypic robustness (see Subsection 3.1.6), *e.g.* by biasing mutations (Beardmore et al., 2011; Draghi et al., 2010; De Martino et al., 2016, 2019; Rigato and Fusco, 2020). In these effective formulations, the marginal fitness distribution $\mathcal{N}(f)$ would be governed by some effective RME dynamics depending only on the selective variable f, such as:

$$\frac{d\mathcal{N}(f;t)}{dt} = \widehat{M}_{\text{eff}}\left[\mathcal{N}(f;t)\right]\mathcal{N}(f;t) + \mathcal{N}(f;t)\,\left(F_{\text{eff}}(f) - \overline{F}_{\text{eff}}[\mathcal{N}(f;t)]\right) \tag{3.33}$$

where the interplay between neutrality and selection would be described by either/both a modified 'mutational operator' $\widehat{M}_{\text{eff}}\left[\mathcal{N}(f;t)\right]$, and/or a modified 'effective fitness' function F_{eff}(f) (similarly to the case of monomorphic populations). However, I shall show that the above effective formulation is not general, and is not appropriate unless the landscape is symmetric. Note that in the following, I operate a slight change of notation in order to lighten the equations, and the symbol μ will directly represent the full mutation coefficient related to mutational diffusion.

3.5.1. Marginal dynamics on symmetric landscape

In the symmetric landscape, the marginal fitness distribution is straightforwardly found from the radial contribution $R(r;t)$, as integrating over the neutral variable

θ one obtains:

$$\mathcal{N}^s(r;t) = \int_0^{2\pi} n(r,\theta)\, r\, d\theta = \int_0^{2\pi} R(r;t) Y(\theta;t)\, r\, d\theta = r\, R(r;t). \tag{3.34}$$

Taking the first and second derivatives with respect to r of Eq. (3.34), I obtain the following relationships:

$$\begin{cases} \frac{\partial \mathcal{N}^s(r;t)}{\partial r} = R(r;t) + r\frac{\partial R(r;t)}{\partial r} \\ \frac{\partial^2 \mathcal{N}^s(r;t)}{\partial r^2} = 2\frac{\partial R(r;t)}{\partial r} + r\frac{\partial^2 R(r;t)}{\partial r^2}. \end{cases} \tag{3.35}$$

Multiplying by r the temporal equation for the radial contribution I get:

$$r\frac{d\, R(r;t)}{dt} = \mu \left\{ r\frac{\partial^2 R(r;t)}{\partial r^2} + \frac{\partial R(r;t)}{\partial r} \right\} + \gamma r R(r;t) \left[F(r) - \overline{F} \right] \tag{3.36}$$

Replacing the expressions Eqs. (3.34)-(3.35) into the above equation, I obtain:

$$\frac{d\mathcal{N}^s(r;t)}{dt} = \mu \left\{ \frac{\partial^2 \mathcal{N}^s(r;t)}{\partial r^2} - \frac{1}{r}\frac{\partial \mathcal{N}^s(r;t)}{\partial r} + \frac{\mathcal{N}^s(r;t)}{r^2} \right\} + \gamma \mathcal{N}^s(r;t) \left[F(r) - \overline{F} \right], \tag{3.37}$$

which can be rewritten in the following more compact form:

$$\frac{d\mathcal{N}^s(r;t)}{dt} = \mu \left\{ \frac{\partial^2 \mathcal{N}^s(r;t)}{\partial r^2} + \frac{\partial}{\partial r}\left[v(r) \mathcal{N}^s(r;t) \right] \right\} + \gamma\, \mathcal{N}^s(r;t)\, (F(r) - \overline{F}), \quad \text{with} \quad v(r) = -\frac{1}{r}. \tag{3.38}$$

Finally, recalling that for the symmetric landscape the fitness variable is $f = 1 - r$, the temporal equation governing the dynamics of the marginal fitness distribution reads:

$$\frac{d\mathcal{N}^s(f;t)}{dt} = \mu \left\{ \frac{\partial^2 \mathcal{N}^s(f;t)}{\partial f^2} + \frac{\partial}{\partial f}\left[v(f) \mathcal{N}^s(f;t) \right] \right\} + \gamma\, \mathcal{N}^s(f;t)\, (F(f) - \overline{F}[\mathcal{N}^s(f;t)]) = 0, \tag{3.39}$$

with

$$v(f) = \frac{1}{1-f}. \tag{3.40}$$

In the symmetric landscape, marginalisation leads to a new drift term $\frac{\partial}{\partial f}\, v(f)$, where $v(f)$ plays the role of a velocity field whose magnitude increases with fitness, thus pushing individuals away from the optimum $f = 1$. The marginal dynamics Eq. (3.39) is consistent with the effective RME formulation Eq. (3.33), with:

$$\widehat{M}_{\text{eff}}\left[\mathcal{N}(f;t)\right] = \mu \left\{ \frac{\partial^2}{\partial f^2} + \frac{\partial}{\partial f} v(f) \right\} \tag{3.41}$$

being the new effective mutational operator biasing mutations in favour of smaller fitness values, due to their higher degeneracy. This mutational operator is referred as 'mutational entropy' in (Tsimring et al., 1996; Gerland and Hwa, 2002), in analogy with the free fitness fitness potential presented in Subsection 3.1.4. However, contrary to the free-fitness potential, this entropic contribution relies on the symmetry of the landscape and is far from being general, as the following calculations on asymmetric landscapes will show.

3.5.2. Marginal dynamics on asymmetric landscape

For an asymmetric landscape of general boundary $\mathcal{B}(x)$, I obtain the marginal fitness distribution $\mathcal{N}^a(f;t)$ by integrating the RME (2.53) over the neutral variable y:

$$\begin{aligned} \frac{d\,\mathcal{N}^a(x;t)}{dt} &= \int_0^{\mathcal{B}(x)} \frac{d\,n(x,y;t)}{dt}\, dy = \mu \int_0^{\mathcal{B}(x)} \frac{\partial^2\, n(x,y;t)}{\partial\, x^2}\, dy \\ &+ \mu \int_0^{\mathcal{B}(x)} \frac{\partial^2\, n(x,y;t)}{\partial\, y^2}\, dy + \gamma \mathcal{N}^a(x;t) \Big(F(x) - \overline{F}[\mathcal{N}^a(x;t)] \Big). \end{aligned} \tag{3.42}$$

The second integral term on the right hand side of Eq. (3.42) is straightforward to handle. Applying the Fundamental Theorem of Integral Calculus to the second integral term, I obtain:

$$\int_0^{\mathcal{B}(x)} \frac{\partial^2\, n(x,y;t)}{\partial\, y^2}\, dy = \frac{\partial\, n(x,y;t)}{\partial\, y} \Big|_{y=0}^{y=\mathcal{B}(x)} = \frac{\partial\, n(x,y;t)}{\partial\, y} \Big|_{y=\mathcal{B}(x)}, \tag{3.43}$$

where I have used the no-flux boundary condition Eq. (3.12) in the last passage. Performing a similar calculation on the first integral term of the right hand side of Eq. (3.42) and using the no-flux boundary condition Eq. (3.12), I obtain the following equality:

$$\int_0^{\mathcal{B}(x)} \frac{\partial^2 n(x,y;t)}{\partial y^2}\, dx = \tag{3.44}$$

$$\frac{d^2\mathcal{N}^a(x;t)}{dx^2} - 2\mathcal{B}'(x)\frac{\partial n(x,y;t)}{\partial x}|_{y=\mathcal{B}(x)} + \mathcal{B}'^2(x)\frac{\partial n(x,y;t)}{\partial y}|_{y=\mathcal{B}(x)} - \mathcal{B}''(x)n(x,y;t)_{y=\mathcal{B}(x)}$$

Finally, substituting Eqs. (3.43)-(3.44) into Eq. (3.42), and recalling that the fitness value is $f = x$, I obtain:

$$\frac{d\mathcal{N}^a(f;t)}{dt} = \mu\left\{\frac{d^2\mathcal{N}^a(f;t)}{df^2} + \mathcal{F}_1(f;t) + \mathcal{F}_2(f;t)\right\} + \gamma\mathcal{N}^a(f;t)\left(F(f) - \overline{F}[\mathcal{N}^a(f;t)]\right) = 0, \tag{3.45}$$

with:

$$\mathcal{F}_1(f;t) = \left[\mathcal{B}'^2(f) - 1 - 2\mathcal{B}'(f)\right]\frac{\partial n(f,y;t)}{\partial f}|_{y=\mathcal{B}(f)} \tag{3.46.a}$$

$$\mathcal{F}_2(f;t) = -\mathcal{B}''(f)\, n(f,y;t)|_{y=\mathcal{B}(f)}, \tag{3.46.b}$$

where the prime notation indicates the derivative with respect to the selective variable f. In the asymmetric landscape, marginalisation generates contributions of crucially different nature with respect to the symmetric landscape. In Eq. (3.45), mutations and competition are still captured by, respectively, a local diffusion term and a replicator term, acting on the marginal distribution $\mathcal{N}^a(f)$. However, marginalisation also generates the new contributions $\mathcal{F}_1(f;t)$ and $\mathcal{F}_2(f;t)$, which depends on the landscape's geometry, that is, respectively, on the slope $\mathcal{B}'(f)$ and on the curvature $\mathcal{B}''(f)$ of the boundary profile. Moreover, from Eq. (3.46) we observe that these contributions depend on the full two-dimensional trait distribution $n(f,y;t)$, thus making the marginal

dynamics Eq. (3.45) an inhomogeneous differential equation. Therefore, neutral contributions deriving from asymmetric landscapes do not lead to an equation in $\mathcal{N}(f)$ alone, with effective operators acting on the fitness level of description. This imposes severe limitations on the exactness of effective formulations, for trait-structured populations. Indeed, my calculations have shown that solving the high-level fitness dynamics still requires the knowledge of the underlying low-level trait details, and that this issue will occur whenever asymmetries in the trait-space are present.

The new terms due to asymmetry, $\mathcal{F}_1(x;t)$ and $\mathcal{F}_2(x;t)$, have the appearance of effective source contributions to the dynamics, analogous to a spontaneous generation of individuals, if interpreted in the context of a lower-dimensional (non-degenerate) fitness landscape. Note that the marginal one-dimensional profiles, shown in Fig. 3.3 panels **e**-**f**, display a non-zero gradient at the boundaries of the fitness domain, which would require a flux to be present in a truly one-dimensional system. This feature cannot be present in profiles generated by one-dimensional RME models, due to the physical constraints (as, we recall, the total population size is conserved and the system has no flux boundary conditions), unless they are introduced *ad hoc*. I call these emerging sources *effective* because they are generated by the asymmetry in the neutral degrees of freedom, that are unobserved at the marginalised fitness level. These sources are also doubly local: indeed, they depend locally on the full trait distribution $n(f, y; t)$, and locally on the landscape's geometry of the boundary $\mathcal{B}(x)$, through its slope and curvature.

Describing the marginal dynamics of multidimensional trait-structured populations hence requires perfect knowledge of the landscape and of the full trait distribution. The ability to capture neutral contributions by means of effective entropic terms is coincidental and demands special symmetries to hold. In all other cases, the introduction of effective operators should be made carefully, and fundamentally it should be motivated by stronger arguments than a simple (and comfortable) analogy with the monomorphic case. When studying trait-structured populations involving multiple quantitative traits, there is no reason to expect perfect symmetry along all neutral

variables. Rather, asymmetric landscapes are expected to be encountered in a variety of biological applications, as I will discuss in the next Subsection.

3.5.3. Biological pertinence of asymmetric landscapes

While the neutral or selective neutral of traits will depend on the environment and on the interactions at play (see Subsection 3.1.3), in general, asymmetric landscapes are expected to be found whenever a trade-off of some nature holds between the various traits composing the phenotype. For instance, the MacArthur's consumer-resource model (MacArthur, 1970), is employed to investigate the coexistence of communities competing for a common pool of resources (Pacciani-Mori et al., 2020; Gupta et al., 2021). When multiple resource types are present, the different rates of consumption can be modelled as mutating quantitative traits. If an energetic constraint limits cells' ability of consumption due to metabolic trade-offs, then the population will evolve on an asymmetric trait space (Amicone and Gordo, 2020).

Similar mechanisms are expected to lead to asymmetric landscapes, in presence of life-history trade-offs. An ideal pathogen would be characterised by high infection transmission, and low induced mortality. In practice, such *super-pathogens* are rarely observed, whereas milder strains are more frequent. This observation is generally explained by acknowledging the existence of a life-history trade-off between transmission and virulence (Bull, 1994; Alizon et al., 2009), that, in fitness terms, might relate to trade-offs akin to degeneracy-selection, leading to asymmetric shapes. Asymmetric landscapes also emerge whenever the trait space effectively available is bounded by Pareto-like fronts, outside of which lie all those phenotypic configurations that long-term evolution has excluded, due to their systematic inefficiency (Shoval et al., 2012; Xue et al., 2019). Such trait spaces have been proposed to explain observed patterns in gene regulation (Weiße et al., 2015), and bacterial growth (Klumpp and Hwa, 2014). Triangular-shaped landscapes, that herein have been used to facilitate calculations, have actually been observed in animal morphology

(McGhee, 2006; Wilson, 1980; Norberg and Rayner, 1987). In game theory, triangular geometries also characterise three-strategies games (Boccabella et al., 2011), and have been recently observed to emerge in a numerical study of a rapidly mutant version of the Ultimatum Game (Evans, 2018).

3.6. Conclusions

To conclude, I consider the results herein presented to be general and to be relevant whenever trait-structured populations evolve on asymmetric degenerate fitness landscape. They do not depend on the specifics of the model (which here have been chosen in order to facilitate the mathematical analysis). My results convey an important message: in general, neutral effects will not be properly captured by effective formulations of phenotypic robustness; rather, they will generate effective sources at the marginalised fitness-level description. In general, these new contributions will depend on the geometry of the landscape, and on the trait composition of the population, so that all the microscopic trait information (even for the neutral traits) must be retained in order to properly derive the observable fitness dynamics.

The mathematical procedure herein employed allows the explicit calculation of equilibrium trait distributions and could be employed to straightforwardly implemented in previous one-dimensional models, so as to include neutral effects in the mutation-selection dynamics. Ultimately, my study suggests that the experimental quantification of the landscape's asymmetries in the neutral directions is as important as that of selective traits. To interpret experimental patterns in the trait distributions and characterise them theoretically, it will be important to consider the relationship between the relevant selective components of traits, as well as their the degree of degeneracy in all of the other, neutral, components.

4. Control strategies for heterogeneous plant pathogens

4.1. Introduction

The study of mutation-selection models of pathogen populations is at the foundation of the domain of evolutionary epidemiology. Models of evolutionary epidemiology are composed of the epidemiological interactions occurring between pathogens and hosts, and of the evolutionary processes affecting (either or both) the two populations. In general, the epidemiological dynamics of a disease may influence the way natural selection manifests, by shaping the rules according to which competition occurs; concomitantly, changes in the evolutionary composition of the evolving population will affect the epidemiological interactions at play. Therefore, complex feedbacks are expected to occur between the two dynamical levels, and understanding the outcome of such complex interactions is the main purpose of evolutionary epidemiology. Analogously to the problem analysed in Chapter 2, the rate at which pathogens mutate determines the mathematical tool employed in the analysis. In the case of monomorphic populations, the aim is to determine which mutant of the pathogen will be able to invade and replace the resident one (Dieckmann et al., 2005; Day, 2005). In the case of polymorphic populations, multiple pathogen strains coexist in the population, and compose a trait-structured population (Day and Proulx, 2004). In this Chapter, I will again focus on the polymorphic case. Particularly, I will study the problem in the

context of agricultural pest management, with the aim of understanding how to optimise the production of healthy yield, when the crop is infected by a rapidly mutating, heterogeneous population.

4.1.1. The use of pesticides

'*Crop pathogens and pests are responsible for reduction in the yield and quality of agricultural production. They cause important economic losses and reduce food security at household, national and global level (Savary et al., 2019). Nowadays, although alternative practices to protect crops are gaining scientific support (Lechenet et al., 2017; Begg et al., 2017), the use of chemical pesticides is still the primary means of pest control and faces an increasing food demand worldwide (Lamichhane et al., 2016). Although the use of pesticides, among other practices, has led to a greater than twofold increase in food production during the last century (Pretty et al., 2018), worldwide surveys have documented the contamination and impact of pesticide residues in soils, terrestrial and aquatic ecosystems, and their toxic effects on humans and nonhuman biota (Pretty et al., 2018; Carvalho, 2017), as well as on biodiversity of crop fields(Dudley and Alexander, 2017). A reduction in the use of pesticide is sought worldwide and demanded by the EU pesticide Regulation N 1107/2009. A report on pesticide residues in food is due every year by the European Food Security Agency (Medina-Pastor and Triacchini, 2020)*'(quoted from Miele et al., 2021b). Recent works suggest that pesticide use could be reduced, without impacting crop productivity and profitability, through the adoption of new production strategies and optimisation; this is particularly true in those cases with high pesticide use (Lechenet et al., 2017; Pretty et al., 2018). Mathematical modelling provides an excellent tool to explore different control strategies and assess their efficacy, whilst avoiding the inevitable expenses of field experiments (Gilligan and van den Bosch, 2008; Gilligan, 2008; Ristaino et al., 2021).

4.1.2. Mathematical modelling of pest management

The success of modelling depends upon the availability of biologically plausible models together with adequate consideration of social and economical constraints. Only recently have epidemiological models started to incorporate economic aspects of control strategies (Forster and Gilligan, 2007a; Laxminarayan, 2010; Mbah et al., 2010). Crop models have provided insights into optimal control under constraints imposed by environmental regulation, *e.g.* imposing a maximum level of chemical treatments (Jørgensen et al., 2017). Significant attention has been devoted to design and explore different strategies to overcome the problem of pesticide resistance (Russell, 2005). In this case, models are often framed in terms of sensitive *versus* resistant pathogen strains (van den Bosch and Gilligan, 2008; Elderfield et al., 2018; Hall et al., 2007), and aim at understanding optimal spatial (Parnell et al., 2006; Débarre et al., 2009), and temporal (Van den Berg et al., 2016; Shi et al., 2009) patterns of pesticide release. However, such two-strains models fail at describing the effects of a broader kind of heterogeneity affecting pathogen's traits involved in their life cycle.

4.1.3. The problem of heterogeneous pathogens

Foreseeing the consequences of a prolonged use of pesticide is particularly tricky when the pathogen displays a more general heterogeneity, *i.e.* when the composition of the pathogen population is more complex than simply resistant versus sensitive. In these populations, individuals characterised by genetically related variants, may differ from each other by phenotype traits possibly involved in the pathogen's virulence, transmission, viability etc. This phenomenon is ubiquitous in plant pathogens, including viruses (González et al., 2019), bacteria (Perrier et al., 2019; Schröter and Dersch, 2019) and fungi (Dutta et al., 2020; Jain and Fries, 2009; Hewitt et al., 2016). Such heterogeneity is often maintained through time (rather than being a transient property eventually cleared by stabilising selection), suggesting the existence of a mechanism continuously

fuelling it. In this case, the pathogen can be described as a trait-structured population. In such populations, the overall effect of a control strategy will depend on the trait distribution of the heterogeneous pathogen, which in turn will be affected by the control's selective pressure (Galvani, 2003; Day and Gandon, 2006). Ultimately, the performance of any management scenario will result from the complex interplay between the epidemiological plant-pathogen interactions, and the pathogen's evolutionary dynamics. However, despite few exceptions (*e.g.* see Shaw, 2000), in the context of pest management, heterogeneous pathogen populations are modelled only rarely.

Heterogeneity in plant pathogens is always perceived as a threat for the control strategy, limiting its efficacy. In this Chapter, I shall move away from the sensitive/resistant duality, to investigate the role of continuous heterogeneity in pest control, and show that the implementation of trait-dependent control can harness heterogeneity in pathogen populations to our advantage. In the framework of a classical epidemiological model, I will consider a trait-structured pathogen population, and investigate the evolutionary dynamics of its trait distribution (Day and Proulx, 2004). The trait variable will determine the pathogen levels of virulence, transmission and the pesticide sensitivity. This framework will account for the transmission-virulence trade-off, as well as to possible heterogeneous pesticide effects.

4.1.4. Trait-dependent trade-offs

The transmission-virulence trade-off hypothesis, introduced to explain the evolution of intermediate levels of virulence (Bull, 1994; Lipsitch et al., 1995), assumes a positive correlation between the two traits, so that an increase in the former comes at the expenses of an increase in the latter. In fact, pathogen spread is generally favoured by high levels of transmission and low levels of virulence (Bull, 1994). Despite its validity still being the subject of lively debate (Alizon et al., 2009), this hypothesis has found popularity in epidemiological models, and some evidence has been collec-

ted in the context of plant pathology (Froissart et al., 2010; Laine and Barrès, 2013). Whenever such a trade-off holds, then control strategies (*e.g.* vaccination Gandon et al., 2001 or antibiotic treatment Porco et al., 2005) may lead to possible different outcomes, with consequent selection for high or low virulent strains. Such models however, typically investigate the long-term evolution of virulence, within the context of adaptive dynamics (Dieckmann et al., 2005). In the termilogy of this thesis, these works would then provide the analysis of the evolution of a monomorphic population (see Subsection 2.1.6). Here, I shall extend the study of control strategies to the case of polymorphic, trait-structured populations.

On the other hand, the introduction of a trait-dependent sensitivity of the pesticide is, to the best of my knowledge, a novelty in agricultural disease management literature. The rationale is that, if a pesticide differentially affects pathogens with heterogeneous traits (*e.g.* virulence or transmission), complex population effects resulting from the balance of control and selection are expected (Patyka et al., 2016). Modelling pesticide treatment, a distinction is typically made between protectant and eradicant (or curative) effects (Castle and Gilligan, 2012). The former is described by reducing the infection's transmission, while the latter by increasing hosts' recovery. Here, I shall focus solely on the eradicant effect, and discuss future extensions accounting for protection as well, at the end of the Chapter. Particularly, I will allow pesticide-induced eradication to depend on the pathogen trait. That is, I will model a spectrum of possible pesticide types with different degrees of specialisation – *e.g.* more effective on highly virulent (or transmitting) pathogens, or more effective on less virulent (or transmitting) ones, or generically effective – and investigate the performance, in terms of both economic and environmental objectives, of different control strategies characterised by the type (*i.e.* specialist or generalist) and the quantity (*i.e.* rate of application) of the pesticide used.

The minimal model here developed allows for mathematical tractability, analytical investigation of the pathogen's trait distribution and of the endemic crop yield at equilibrium, and is potentially extendable to different management, ecological and

epidemiological scenarios. Particularly, it allows to disentangle the role of the different ecological interactions in shaping the optimal pesticide, and can therefore provide qualitatively guidelines for pesticide choice, starting from basic ecological information on the system.

4.2. Methods

In this Section, I will first present the classical formulation of the epidemiological model employed. Then, I will present the equivalent heterogeneous formulation, describing infections of trait-structured pathogens, and I will show how to relate the problem with the RME. I will introduce minimal recipes to describe the trait-dependent trade-offs of interest, and the modelling of control strategies. I will also present the agent-based numerical simulations employed to check the validity of my analytical results.

4.2.1. Classical SIS epidemiological formulation

The starting epidemiological model is an SIS model (Kermack and McKendrick, 1927), adapted to account for characteristics typical of plant-pathogen systems (Hethcote, 2000). The host population is divided into (S)usceptible and (I)nfected individuals. The pathogen's dynamics is implicit in the description of infected hosts, and it is not explicitly accounted for, as it is commonly done when dealing with microparasites (Anderson and May, 1981). The dynamics is summarised as follows: (*i*) susceptible hosts are replanted at a constant rate, and (*ii*) they become infected at a rate proportional to the amount of infected hosts; transmission events are modelled with a density-dependent term, since we assume the area of the crop to remain constant (Begon et al., 2002); (*iii*) hosts share an equal harvesting rate that removes them from the system, regardless of their epidemiological class; (*iv*) infected hosts experience additional mortality due to the virulent charge of the pathogen; (*v*) the host recovers

from the infection proportionally to the rate of pesticide application, with the effect of reallocating the host in the susceptible class (Forster and Gilligan, 2007b).
The deterministic equations governing the dynamics of S and I hosts is typically obtained by applying the law of mass action (see Subsection 2.1.3), to points (i)-(v). The following system of ordinary differential equations is so obtained:

$$\frac{dS}{dt} = \theta - \delta S - \beta SI + c\phi I \tag{4.1.a}$$

$$\frac{dI}{dt} = \beta SI - [\delta + \nu + c\phi]\, I, \tag{4.1.b}$$

where θ is the replanting rate; δ is the harvesting rate; β and ν are, respectively, the pathogen's rate of infection transmission and virulence. The term $c\phi$ is the rate of eradication, where parameter c is the application rate of the pesticide, and ϕ pesticide sensitivity to the pathogen. Theoretical and experimental pesticide literature typically employ saturating, non-linear functions relating pesticide effects with its dose, known as dose-response curves (Elderfield et al., 2018). My choice implies a linear dose-response curve, so as to maintain the model as simple as possible, and to emphasise the role of pathogen heterogeneity in the dynamics.

4.2.1.1 Equilibrium points

The equilibrium points of the system Eq. (4.1) are obtained by setting the temporal derivatives to zero. There is a trivial equilibrium point $(\widehat{S}_0; \widehat{I}_0)$ of coordinates:

$$\left(\widehat{S}_0 = \frac{\theta}{\delta};\ \widehat{I}_0 = 0\right), \tag{4.2}$$

corresponding to the extinction of the infection, where consequently the host population is entirely susceptible. I will refer to this equilibrium point as the disease-free

equilibrium. In addition, there is a non trivial equilibrium point $(\widehat{S};\widehat{I})$ of coordinates:

$$\left(\widehat{S}=\frac{\delta+\nu+c\phi}{\beta}\,;\,\widehat{I}=\frac{\beta\theta-\delta\left(\delta+\nu+c\phi\right)}{\beta\left(\delta+\nu\right)}\right), \tag{4.3}$$

corresponding to the co-existence of susceptible and infected hosts. I will refer to this equilibrium point as the endemic equilibrium. The existence and stability of the two equilibria are determined by value of the basic reproduction number R_0, defined as:

$$R_0=\frac{\theta}{\delta}\frac{\delta+\nu+c\phi}{\beta}. \tag{4.4}$$

The disease-free equilibrium is always biologically feasible, and is asymptotically stable when $R_0<1$. On the other hand, the endemic equilibrium has biological meaning only when $R_0>1$; in this case, it is also asymptotically stable (Korobeinikov and Wake, 2002). Therefore, the system is always characterised by a sole asymptotic stable equilibrium point, depending on the value of R_0. In Fig. 4.1, I show the temporal trajectories of the number of S and I hosts, obtained by means of numerical integration of Eq. (4.1), for two sets of parameters corresponding to $R_0\gtrless 1$ (specified in the figure's caption). In both cases, after a transient depending on the initial conditions, the temporal trajectories (solid lines) approach their corresponding equilibrium points (dashed lines), that is the endemic equilibrium $\left(\widehat{S};\widehat{I}\right)$ in the left panel (where $R_0>1$), and the disease-free equilibrium $\left(\widehat{S}_0;\widehat{I}_0\right)$ in the right panel (where $R_0<1$). Starting from the classical one-strain formulation of the dynamics, I shall now derive the equivalent heterogeneous formulation.

4.2.2. Heterogeneous SISx formulation

4.2.2.1 From SIS to SISx formulation

Following (Day and Proulx, 2004; Gudelj et al., 2006; Bolzoni and De Leo, 2013; Korobeinikov, 2018; Day et al., 2020) I elaborate the formulation equivalent to the

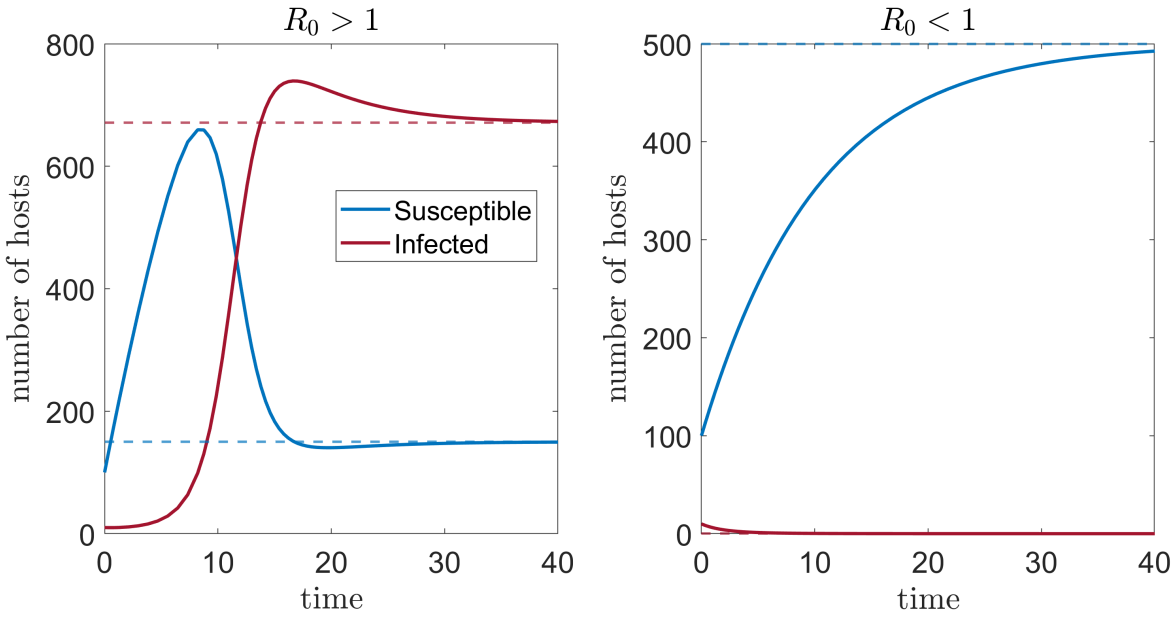

Figure 4.1: **Temporal trajectories classical SIS model.** Left panel: the temporal trajectories for the number of S and I hosts (solid lines) approach the endemic equilibrium (dashed lines), since $R_0 > 1$; parameters: $\theta = 100, \delta = 0.04, \beta = 0.001, \nu = 0.1, c = 0.01, \phi = 1$. Right panel: the temporal trajectories for the number of S and I hosts (solid lines) approach the disease-free equilibrium (dashed lines), since $R_0 < 1$; parameters: $\theta = 50, \delta = 0.1, \beta = 0.001, \nu = 0.5, c = 0.01, \phi = 1$.

Table 4.1: **List of the variables and parameters used in the model.**

Name	Description
S	Number Susceptible hosts
I	Number Infected hosts
x	Trait variable
$i(x)$	Trait distribution
$\overline{x}$	average trait value
μ	Mutations diffusion coefficient
θ	Replanting rate of S hosts
δ	Harvesting rate
c	Pesticide application rate
$\nu(x)$	Trait-dependent virulence (additional mortality)
ν_0	Baseline virulence rate
ν_1	Trait-dependent virulence coefficient
$\beta(x)$	Trait-dependent transmission
β_0	Baseline transmission rate
β_1	Trait-dependent transmission coefficient
$\phi(x)$	Pesticide sensitivity to trait
ϕ_1	Type of pesticide

one-strain model Eq. (4.1), in the case of a trait-structured pathogen. The parameters of the model and their description are summarised in Table 4.1. The following assumptions are introduced: (*i*) The pathogen has a *continuum-of-strains*, mathematically described by a continuous trait variable $x \in \mathcal{T} = [x_{\min}, x_{\max}]$, where $\mathcal{T}$ is the trait space. I denote with $I(x)$ the number of hosts infected by a pathogen with trait value x. Heterogeneity is described by the trait distribution $i(x)$, that is the density of hosts infected with trait x. (*ii*) The trait determines the pathogen's levels of virulence, transmission, and pesticide sensitivity, which are now represented by the functions $\nu(x), \beta(x), \phi(x)$. (*iii*) Pathogens undergo rapid within-host mutations which induce small changes in their traits, and maintain heterogeneity among the infected population; mutation rates are unbiased and no preferential direction is assumed; mutations are modelled by allowing the trait distribution to diffuse over the trait space, with mutational diffusion coefficient μ (in analogy with Kimura's model, see Subsection 2.2.4).

The dynamics of the heterogeneous system is given by the following equations:

$$\frac{d\,S}{dt} = \theta - \delta S - S\int_{\mathcal{T}} \beta(x)I(x)dx + c\int_{\mathcal{T}} \phi(x)I(x)dx \tag{4.5.a}$$

$$\frac{d\,I(x)}{dt} = \mu\nabla^2 I(x) + \beta(x)I(x)S - \left[\delta + \nu(x) + c\phi(x)\right] I(x), \tag{4.5.b}$$

where in Eq. (4.5.a), the transmission and eradication terms are integrated over the trait space in order to account for contribution from all strains. In contrast to the one-strain model, this heterogeneous system is composed of an ordinary differential equation and of a partial differential equation. The Eq. (4.5.b) is subject to *no-flux* boundary conditions:

$$\frac{\partial I(x)}{\partial x}\,|_{x=x_{\min}} = \frac{\partial I(x)}{\partial x}\,|_{x=x_{\max}} = 0, \tag{4.6}$$

corresponding to the reflecting nature of mutations at the boundaries of the trait space (likewise the model presented in Chapter 3). In the following, I will recast the dynamics in a form that will highlight the ecological and evolutionary levels of description of the dynamics, and that will allow me to solve the problem within the context of the RME formalism.

4.2.2.2 The RME

First, I define the total number of infected hosts I as:

$$I := \int_{\mathcal{T}} I(x)dx, \tag{4.7}$$

that is obtained integrating $I(x)$ over the trait space. Then, I define the trait distribution $i(x)$ as:

$$i(x) := \frac{I(x)}{I}. \tag{4.8}$$

The trait distribution is the density of individuals infected by trait x, and is a dynamical quantity varying over time. As such it is normalised to one upon integration over the trait space:

$$\int_{\mathcal{T}} i(x)\,dx = \int_{\mathcal{T}} \frac{I(x)}{I}\,dx = \frac{I}{I} = 1. \tag{4.9}$$

The trait distribution allows me to define average quantities over the infected population. Given a function $f(x)$ of the trait variable, I will refer to its average with the bar notation, that is:

$$\overline{f}\,[i(x);t] := \int_{\mathcal{T}} f(x)i(x)dx. \tag{4.10}$$

In general, such average quantities will be function of the trait distribution, and of time, since both total number of I hosts and trait composition vary during the dynamics. In the following however, I will drop the functional dependence of the average quantities of $i(x)$, and retain just the temporal one, so as to lighten the notation. The temporal dynamics for I is obtained by integrating Eq. (4.5.b) over the trait space:

$$\begin{aligned}\frac{dI}{dt} &= \int_{\mathcal{T}} \beta(x)SI(x)dx - \int_{\mathcal{T}} \delta I(x)dx - \int_{\mathcal{T}} \nu(x)I(x) - \int_{\mathcal{T}} c\phi(x)I(x) \\ &= \overline{\beta(t)}IS - \left[\delta + \overline{\nu(t)} + c\overline{\phi(t)}\right] I,\end{aligned} \tag{4.11}$$

where in the second line I have used the definition Eq. (4.10) for transmission, virulence and pesticide sensitivity. According to the above equation, the total number of infected hosts variate proportionally to the average quantities of the trait-dependent epidemiological functions. Note that, upon integration, the Laplacian term disappears due to the boundary conditions Eq. (4.6), since mutations do not increase nor decrease the total number of infections. In order to highlight the evolutionary nature of the dynamics, I shall derive the equation for the temporal evolution of the trait distribution $i(x)$. By taking the temporal derivative of its definition Eq. (4.8), and applying

the chain rule I obtain:

$$\frac{d\,i(x)}{dt} = \frac{d}{dt}\frac{I(x)}{I} = \frac{1}{I}\frac{dI(x)}{dt} - \frac{I(x)}{I^2}\frac{dI}{dt} = \tag{4.12}$$

$$\mu\nabla^2\frac{I(x)}{I} + \beta(x)S\frac{I(x)}{I} - [\delta + \nu(x) + c\phi(x)]\frac{I(x)}{I} - \frac{I(x)}{I}\left(\overline{\beta(t)}S - \left[\delta + \overline{\nu(t)} + c\overline{\phi(t)}\right]\right),$$

where in the second line I have replaced Eq. (4.5.b) and Eq. (4.11). Finally, recalling the definition Eq. (4.8), I obtain:

$$\frac{d\,i(x)}{dt} = \mu\nabla^2 i(x) + i(x)\left[\beta(x)S - \nu(x) - c\phi(x) - \left(\overline{\beta(t)}S - \overline{\nu(t)} - c\overline{\phi(t)}\right)\right], \tag{4.13}$$

subject to the boundary conditions Eq. (4.6) (upon replacing $I(x)$ with $i(x)$) and to normalisation Eq. (4.9). The heterogeneous dynamics is fully described by the equations for the total number of S and I hosts, as well as by that for the trait distribution $i(x)$, which I recollect in the following system of equations:

$$\frac{d\,S}{dt} = \theta - \delta S - \overline{\beta(t)}SI + c\overline{\phi(t)}I \tag{4.14.a}$$

$$\frac{d\,I}{dt} = \overline{\beta(t)}SI - \left[\delta + \overline{\nu(t)} + c\overline{\phi(t)}\right]I \tag{4.14.b}$$

$$\frac{d\,i(x)}{dt} = \mu\nabla^2 i(x) + i(x)\left[\beta(x)S - \nu(x) - c\phi(x) - \left(\overline{\beta(t)}S - \overline{\nu(t)} - c\overline{\phi(t)}\right)\right]. \tag{4.14.c}$$

In the above system, Eqs. (4.14.a)-(4.14.b) describe the epidemiological SIS dynamics at the demographic level, and are determined by the ecological interactions between plant and pathogen. They are equivalent to the classical formulation Eqs. (4.1), upon replacing the single-strain parameters ν, β, ϕ with their population average counterparts $\overline{\nu(t)}, \overline{\beta(t)}, \overline{\phi(t)}$.

The last Eq. (4.14.c) describes the mutation-selection dynamics of the trait distribu-

tion, and takes the form of a RME. Phenotypic mutations are captured by diffusion over the trait space, with corresponding coefficient diffusion μ; concomitantly, pathogens compete between each other for the infection of a limited number of hosts, according to the trait-dependent function $F(x) = \beta(x)S - \nu(x) - c\phi(x)$. The overall success of pathogens with trait x depends on the difference between their value of $F(x)$ and the population average, as in a replicator dynamics (see Subsection 2.2.4). Contrary to the problem studied in Chapter 3, the function $F(x)$ driving such competition is not assumed, rather it behaves as a fitness landscape emerging from the ecological interactions (Doebeli et al., 2017; Day et al., 2020): the transmission term $\beta(x)S$ contributes to the increase of trait x density, whereas virulence $\nu(x)$ and sensitivity $\phi(x)$ contribute to its decrease. This equation is evolutionary, as it governs the changes in the pathogen composition *within* the infected population, due to mutations and competition for infection.

The system Eqs. (4.14) shows neatly the intertwining of ecological and evolutionary levels of descriptions: on the one hand, the demography of the population (given by S and I) depends on the trait composition $i(x)$ via the average quantities $\overline{\nu(t)}, \overline{\beta(t)}, \overline{\phi(t)}$; on the other hand, the trait composition depends on the population state via the ecological interactions (as transmission depends on S). The solution (and the methods needed to obtain it) of the heterogeneous problem depends on the choices of the trait-dependent epidemiological rates, which are detailed in the following subsection.

4.2.3. Modelling the trait dependence of epidemiological rates

In my model, the pathogen's virulence, transmission and sensitivity to pesticide are considered functions of the trait value x. The mathematical choices presented in the following aim at capturing the basic biological features regarding the trade-offs of interest, whilst preserving mathematical tractability.

Virulence. I assume that the pathogen virulence ν may vary linearly with the trait

x:

$$\nu(x) = \nu_0 + \nu_1 x, \tag{4.15}$$

with the parameters ν_0 being the baseline virulence, and ν_1 the trait-dependent contribution (Day and Proulx, 2004; Bolzoni and De Leo, 2013; Porco et al., 2005). For sake of simplicity, I shall also consider the unit segment $\mathcal{T} = [0, 1]$ as trait space. The generalisation to any positive interval $[x_{\min}, x_{\max}]$ is straightforward, and can be mapped to the unit interval upon rescaling of the parameters.

Transmission. Similarly, I assume that transmission rate β may be linearly affected by the trait variable x, that is:

$$\beta(x) = \beta_0 + \beta_1 x, \tag{4.16}$$

where β_0 is the baseline transmission rate, and β_1 the trait-dependent contribution. For values of both ν_1 and $\beta_1 > 0$, pathogens with higher transmission will also have higher virulence, consistent with the Transmission-Virulence trade-off hypothesis. Although nonlinear, concave-down functions are typically considered (Galvani, 2003; Bolzoni and De Leo, 2013; Porco et al., 2005; Pugliese, 2002), a simpler linear choice has the following advantages: first, it is sufficient to capture the essential biological features we are interested in, that is the cost paid in virulence terms for the pathogen to increase transmission; second, it allows to fully exploit mathematical analysis; finally, it provides the baseline results against which one can in future compare nonlinear functions, so as to disentangle the role of nonlinearities from the role of the trade-off alone. Possible extensions to other functions will be discussed at the end of the chapter.

Pesticide sensitivity. Finally, the pesticide sensitivity $\phi(x)$ is considered to depend on the heterogeneous trait, and is maximal of the extreme values of the trait space $(0, 1)$. Consistently with (Porco et al., 2005), I choose a linear dependence:

$$\phi(x) = C_{\phi_1} + \phi_1 x, \tag{4.17}$$

where the parameter ϕ_1 represents the pesticide's degree of correlation with the trait, and C_{ϕ_1} is a normalisation factor. A graphical summary of the pesticides spectrum is shown in Fig. 4.2 panel B (note that the bound $|\phi_1| < 2$ ensures a positive $\phi(x)$).
Equations (4.15)-(4.17) allow to account for all the possible trade-offs occurring between the considered epidemiological traits: if $\beta_1 = 0$, sensitivity of the eradication correlates only with virulence, and transmission is trait independent: this is the Virulence-Eradication (VE) case. If $\nu_1 = 0$, sensitivity correlates only with transmission, and virulence is trait independent: this is the Transmission-Eradication (TE) case. Finally, the case $\beta_1, \nu_1 \neq 0$ corresponds to the scenario with full complexity; I call this the Transmission-Virulence-Eradication (TVE) case. Note that $\phi_1 = 0$ describes the case when sensitivity of eradication is trait independent, *i.e.* the pesticide has a purely generalist effect over the trait space, and can be considered as a sub-case of TVE.

4.2.4. Modelling control strategies

I assume that the environmental and economic cost of pesticide use is inherent and proportional to its application rate c, regardless of the type. The degree of correlation ϕ_1 with the heterogeneous trait determines the type of pesticide: a positive ϕ_1 models a pesticide with maximal eradicant effect on pathogens that may also be the most virulent (and/or most transmitting), and minimal effect on the least virulent (and/or least transmitting) one; instead, a negative ϕ_1 models the opposite scenario.
The normalisation factor $C_{\phi_1} = 1 - \phi_1/2$ ensures that $\int_{\mathcal{T}} \phi(x)\mathrm{d}x$ is always normalised to 1, for any type ϕ_1. Besides removing one arbitrary degree of freedom, this condition also imposes a plausible constraint on the pesticide design, and allows the comparison between different choices. In fact, while the ideal pesticide has maximum effect on all pathogens, in practice a *specialist-generalist* trade-off is expected to hold. By virtue of this trade-off, a high maximal eradication effect on a particular trait value should

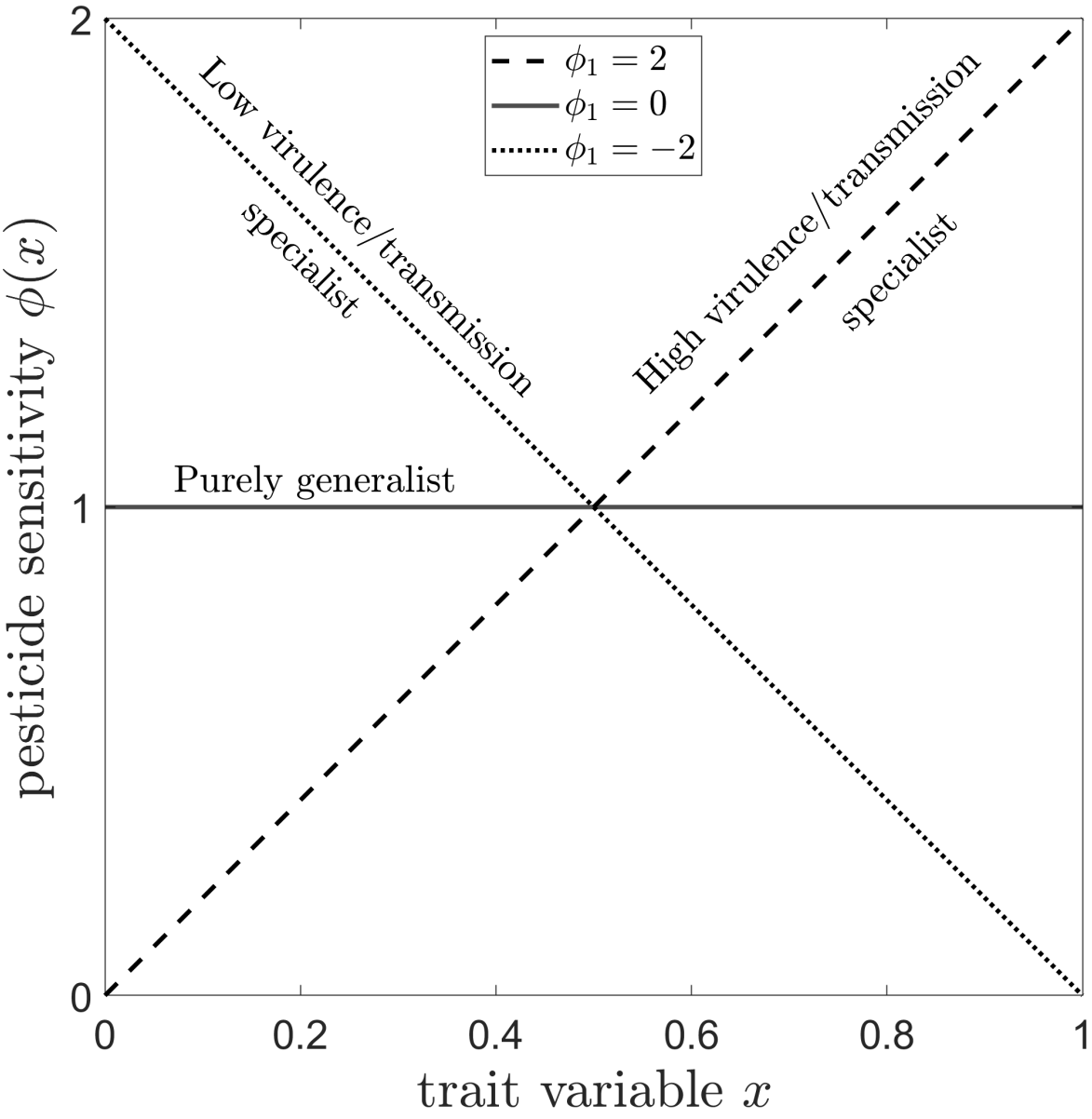

Figure 4.2: **Spectrum of pesticides with trait-dependent sensitivities.** The type of pesticide is determined by the sign and the magnitude of the parameter $\phi_1 \in [0, 2]$: positive ϕ_1 models types with maximal effect on pathogens with higher virulence and/or transmission ($x = 1$); negative ϕ_1 models types with maximal effect on pathogens with lower virulence and/or transmission ($x = 0$). Large $|\phi_1|$ are specialised in targeting extreme values of the trait; small $|\phi_1|$ are generalist types with more uniform action.

come at the expenses of a general reduction of the effect on the others; concomitantly, generalist pesticides will affect more uniformly over the trait space, with a reduction of the maximal eradicant effect. The parameter ϕ_1 is then a control parameter modelling the pesticide choice, out of a spectrum of possible degrees of correlation with the heterogeneous trait.

Henceforth, with the term 'specialist' will refer to pesticides with large degree of correlation (large $|\phi_1|$), and the term 'generalist' will refer to pesticides with small degree of correlation (small $|\phi_1|$). Particularly, the choices $\phi_1 = \pm 2$ represent the most specialised types; the choice $\phi_1 = 0$ represents the most generalist type, with a homogeneous effect over the trait space. A control strategy is specified by choosing both application rate c and pesticide type ϕ_1. For my purposes, the aim of the pest management is then to assess which type of pesticide maximises the amount healthy yield at equilibrium.

4.2.5. Numerical simulations

The agent-based dynamics is based on a Montecarlo algorithm simulating the ecological interactions between susceptible and infected hosts, each occurring at a rate consistent with the deterministic Eqs. (4.14). The purpose is to provide a numerical validation of the existence and stability of the endemic equilibrium solution predicted by the theory.

At each timestep, the system is composed of a certain number of susceptible and infected hosts. The former is represented by the scalar number S of total susceptible hosts in the population. The latter is represented by an array of dimension I, where I is the total number of infected hosts. Each element i of the array represents an infected host, and contains the strain value x_i determining its trait-dependent functions. The system is initialised assigning a starting total number of S and I, as well as the value of each element $I[i]$. In my code, the elements $I[i]$ are initialised using a uniform distribution $\in [0, 1]$. Any other distribution can be used to initialise the

infected population. Alternatively, they can also be all initialised with the same value. This will only affect the transient dynamics, but not the asymptotic behaviour.

The agent-based dynamics is composed of the following events: *Mutation*, *Infection*, *Harvesting*, *Disease induced death*, *Eradication*, *Replanting*. Each event is represented by a stochastic process e occurring at a rate r_e. During a time-step, each event is simulated once. For each event, a uniformly distributed random number r_1 is sampled and compared to $r_i\Delta\tau$, where $\Delta\tau$ is the time-step of the numerical simulation. If $r_1 < r_e\Delta\tau$, then the event i occurs, and the state of the population is updated. Provided a small enough $\Delta\tau$ (I choose $\Delta\tau = 10^{-4}$), the discrete-time dynamics is expected to converge to the deterministic continuous-time one. In the following, the rates of all the events are presented.

Mutation. All infected hosts have the same probability to mutate. A mutation occurs if $r_1 < \mu_0\, I\, \Delta\tau$, where μ_0 is the per capita rate of mutation per unit of time. Upon occurrence, an infected host is randomly extracted, and its trait value is updated analogously to the procedure employed in Subsection 3.2.3

Infection. Each infected host i has a probability of infection that depends on their own trait value x_i. In order to simulate this event, I first sample at random an infected host. Then, the infection occurs if $r_1 < \beta(x_i)\, I\, S\Delta\tau$, where the trait-dependent transmission rate $\beta(x_i)$ is computed according to Eq. (4.16). Upon occurrence of the event, a susceptible host becomes infected. Hence, the total number S is decreased by one, and a new element is appended to the array I, with trait value equal to x_i.

Harvesting. All hosts have the same harvesting rate δ. Hence, if $r_1 < \delta\, I\, \Delta\tau$, a random element of the array I is deleted. If $r_1 < \delta\, S\, \Delta\tau$, the total number S is decreased by one.

Disease induced death. Similarly to infection, each infected host has its own probability to die due to the disease, that depends on its own trait value. This process is simulated likewise for infection events. First, an infected host i is chosen at random from the array I. Then, the element $I[i]$ is deleted if $r_1 < \nu(x_i)\, I\, \Delta\tau$, where the level of virulence $\nu(x_i)$ is computed according to Eq. (4.15).

Eradication. This event is analogous to the previous event, upon replacing $\nu(x_i)$ with $c\,\phi(x_i)$, where c is the pesticide application rate, and $\phi(x_i)$ is the pesticide sensitivity to trait x_i, computed according to Eq. (4.17).

Replanting. Susceptible hosts are replanted at constant rate. Hence, if $r_1 < \theta\Delta\tau$, then the total number S is increased by one.

The Python code employed to simulate the above process is reported in the Appendix A.1.2. An example of the simulated temporal trajectories (and their agreement with the deterministic theory) is shown in Fig. 4.5.

4.3. Results

4.3.1. Ecological equilibrium

The equilibrium solution of the heterogeneous system is obtained by setting to zero the temporal derivatives of Eqs. (4.14). The ecological states at equilibrium are found by solving the algebraic conditions for S and I. In the following, I will refer to S as the *yield*: assuming that the infected quantity goes wasted, S is the amount of harvest with economic value, therefore the quantity that the producer would want to maximise at equilibrium. Since the functional form of the equations is analogous to the classical formulation Eqs. (4.1), the form of the equilibrium points is analogous as well. The system has a trivial equilibrium point trivial equilibrium point $(\widehat{S}_0; \widehat{I}_0)$ of coordinates:

$$\left(\widehat{S}_0 = \frac{\theta}{\delta};\, \widehat{I}_0 = 0\right), \tag{4.18}$$

corresponding to the disease-free equilibrium. Moreover, the system has a non trivial equilibrium point $(\widehat{S}; \widehat{I})$ of coordinates:

$$\left(\widehat{S} = \frac{\delta + \nu + c\overline{\phi}}{\overline{\beta}};\, \widehat{I} = \frac{\overline{\beta}\theta - \delta\left(\delta + \overline{\nu} + c\overline{\phi}\right)}{\overline{\beta}\left(\delta + \overline{\nu}\right)}\right), \tag{4.19}$$

corresponding to the endemic equilibrium. Analogally to the classical formulation, the endemic equilibrium is biologically meaningful when:

$$R_0 = \frac{\theta}{\delta}\frac{\delta + \overline{\nu} + c\overline{\phi}}{\overline{\beta}}, \tag{4.20}$$

that is the trait-structured version of the basic reproduction number. Contrary to the classical formulation, however, such equilibrium depends on the average quantities $\overline{\nu}, \overline{\beta}, \overline{\phi}$ which are not known *a priori*. Rather, they depend on the equilibrium trait distribution $\widehat{i(x)}$, which is the solution of the sRME:

$$\mu\nabla^2\widehat{i(x)} + \widehat{i(x)}\left[\beta(x)\widehat{S} - \nu(x) - c\phi(x) - \left(\overline{\beta}\widehat{S} - \overline{\nu} - c\overline{\phi}\right)\right] = 0. \tag{4.21}$$

Note that in Eq. (4.20) and Eq. (4.21), the temporal dependence of the average quantities has been dropped, because at equilibrium they have reached a constant value. Again, the sRME has a trivial solution $\widehat{i_0(x)}$, which obviously corresponds to the disease-free equilibrium. Moreover, there is a non-trivial solution $\widehat{i(x)}$, determining the trait composition of the endemic equilibrium. Like the classical formulation, the basic reproduction number R_0 determines the existence and stability of the two equilibria. If $R_0 \leq 1$, then the system evolves towards disease extinction; otherwise for $R_0 > 1$, the system evolves towards the endemic equilibrium. Contrary to the classical formulation though, the above condition cannot be directly computed in terms of the epidemiological *SIS* model alone. Hence, a way to determine the fate of the system given a set of parameters, is to solve the trait distribution $\widehat{i(x)}$, compute the corresponding equilibrium average quantities $\overline{\nu}, \overline{\beta}, \overline{\phi}$, and finally check whether $R_0 \lessgtr 1$. As pointed out in papers employing RME-like equations (Beardmore et al., 2011; Lorenzi et al., 2020), when the total population size is not fixed (which is instead the case in the models studied in Chapter 3), a rigorous proof of the stability of the endemic equilibrium is not known (for the moment). Therefore (and likewise those papers), existence and stability are checked by means of numerical simulations of the agent-based dy-

namics. For all set of parameters explored, I find that the system approaches towards either the disease-free or the endemic equilibrium, according to condition Eq. (4.20) on R_0. In the following, I will focus on the characterisation of the endemic equilibrium of both the ecological and evolutionary levels.

4.3.2. Trait distribution equilibrium

Assuming that the system has reached endemic equilibrium, then I can replace the endemic value $\widehat{S}$ Eq. (4.19) into the sRME (4.21) for $\widehat{i(x)}$:

$$\mu\nabla^2\widehat{i(x)} + \frac{\widehat{i(x)}}{\overline{\beta}}\left[\beta(x)\Big(\delta+\overline{\nu}+c\overline{\phi}\Big) - \overline{\beta}\Big(\delta+\nu(x)+c\phi(x)\Big)\right] = 0. \tag{4.22}$$

Inserting the trait-dependent functions Eqs. (4.15)-(4.17), the above equation becomes:

$$\mu\nabla^2\,\widehat{i(x)} + \frac{\Omega}{\beta_0+\beta_1\overline{x}}\,\widehat{i(x)}\,[x-\overline{x}] = 0, \tag{4.23}$$

with

$$\Omega = \beta_1\,(\delta+\nu_0) - \beta_0\nu_1 + c\,[\beta_1 - \beta_1\phi_1/2 - \beta_0\phi_1]\,. \tag{4.24}$$

where $\overline{x}$ is the average trait value. The above equation can be recast in the form of an Airy differential equation, likewise the one analysed in Subsection 3.2.2. The procedure to solve it follows the same line of the non-degenerate model, therefore I will omit to report all calculations here, and refer to the Appendix A.6 for details.
The behaviour of the solution is entirely determined by the compound parameter Ω. In Fig. 4.3, I plot some examples of the endemic trait distribution for three different values of Ω, obtained by varying ν_1 and fixing the other parameters (specified in the figure's caption). Particularly, if $\Omega < 0$, the solution is monotonically decreasing and the trait distribution is mostly distributed close to the trait $x = 0$, that is the trait value providing lowest virulence and/or lowest transmission. I refer to this kind of distribution as belonging to the *low-virulence* and/or *low-transmission* state,

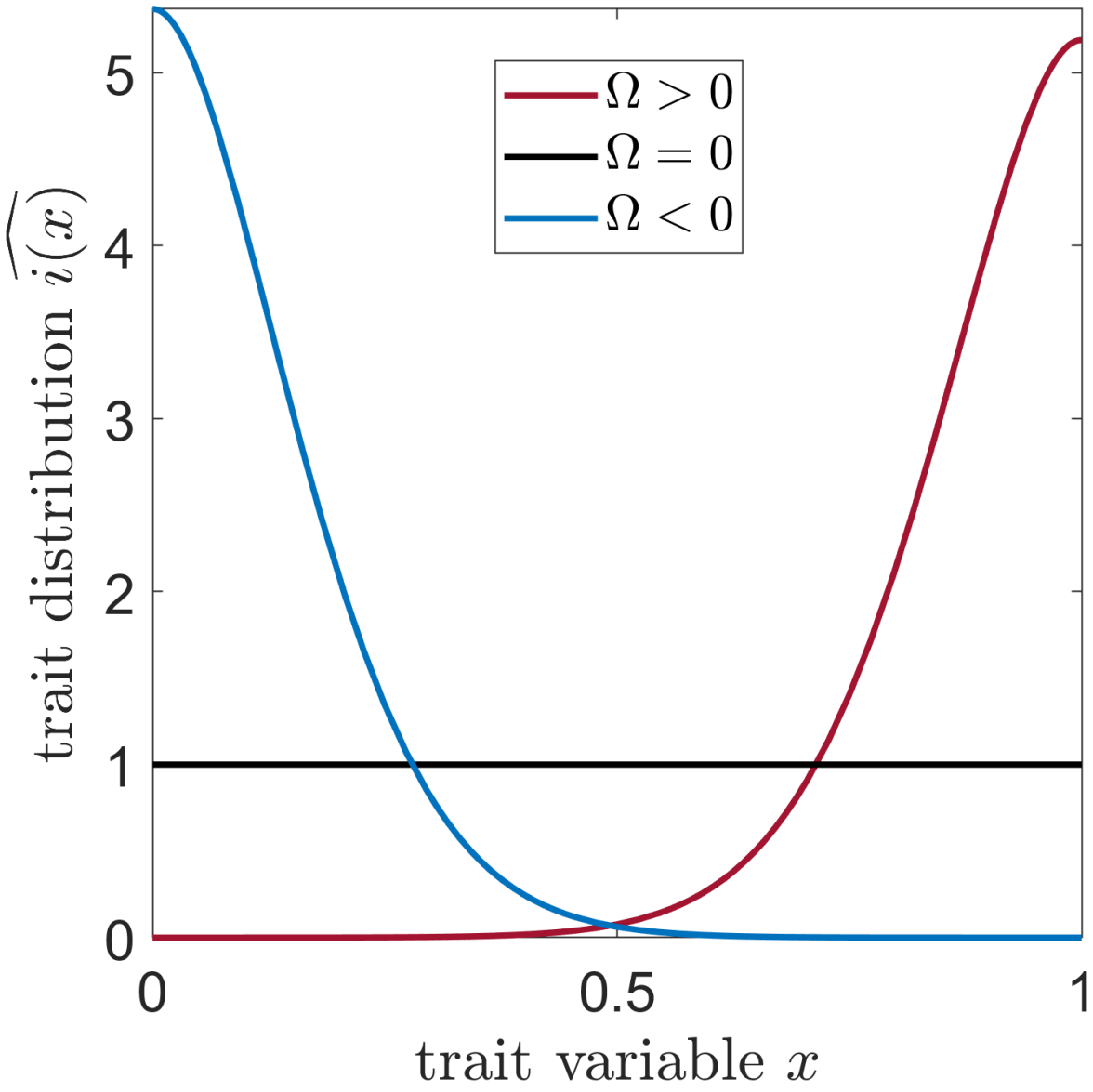

Figure 4.3: **Possible behaviours of the trait distributions.** The value of Ω determines the behaviour of the trait distribution. Here, I plot three solutions for the set of parameters $(\beta_0 = \beta_1 = 0.0001, \mu = 0.00007, \delta = 0.06, \nu_0 = 0.1, c = 0)$, and different values of ν_1. For $\nu_1 = 0.1$, Ω is positive and the profile is monotonically increasing, that is a *high* state. For $\nu_1 = 0.16$, Ω is zero and the profile is degenerately uniform. For $\nu_1 = 0.2$, Ω is negative and the profile is monotonically decreasing, that is a *low* state.

because it represents an endemic equilibrium where most of the population is infected by pathogens with low values of virulence and/or transmission. On the other hand, if $\Omega > 0$, the solution is monotonically increasing and the trait distribution is mostly distributed close to the trait $x = 1$, that is the trait value providing highest virulence and/or highest transmission. I refer to this kind of distribution as belonging to the *high-virulence* and/or *high-transmission* state, because it represents an endemic equilibrium where most of the population is infected by pathogens with high values of virulence and/or transmission. These two antipodal behaviours are separated by a degenerate case, corresponding to $\Omega = 0$, for which the trait-dependent replicator term of the sRME (4.23) disappears, and the trait distribution becomes uniform. In the following, I characterise the phase diagrams of all the possible trade-offs that the model can account for, both in the presence and absence of pesticide treatment.

Virulence-Eradication VE case. In this case, the pesticide sensitivity $\phi(x)$ and virulence $\nu(x)$ both depend on the trait x. The transmission of infection is then homogeneous, that is $\beta_1 = 0$. The relevant compound parameter of Eq. (4.24) reduces to $\Omega_{\mathrm{VE}} = -\beta_0 (\nu_1 + c\phi_1)$. In absence of pesticide (*i.e.* $c = 0$, corresponding to the x-axis in panel A of Fig. 4.4), Ω_{VE} is always negative, meaning that the distribution is in the low-virulence state for any combination of the parameters. When pesticide is employed, if its application rate c exceeds the threshold $c_{\mathrm{th}} = -\frac{\nu_1}{\phi_1}$, the sign of Ω_{VE} reverses, and a distribution in the high-virulence state is obtained. For this to occur, one needs to employ a pesticide type with negative ϕ_1, since for positive ϕ_1 the change would occur for negative c. The larger the degree of correlation $|\phi_1|$, the lower the threshold c_{th} will be (panel B of Fig. 4.4, parameters).

The adaptation towards the two possible states is shown in Fig. 4.5, where I plot the trajectories of the simulated agent-based dynamics (solid lines), differing for the pesticide type employed. The other parameters (specified in the figure's caption) and initial conditions are identical. For $\phi_1 = 1$, the system adapts towards the low virulence state, and towards the high virulence state for $\phi_1 = -1$. Consequently, the quantity of yield reached at equilibrium differs in the two cases (the relationship between yield and

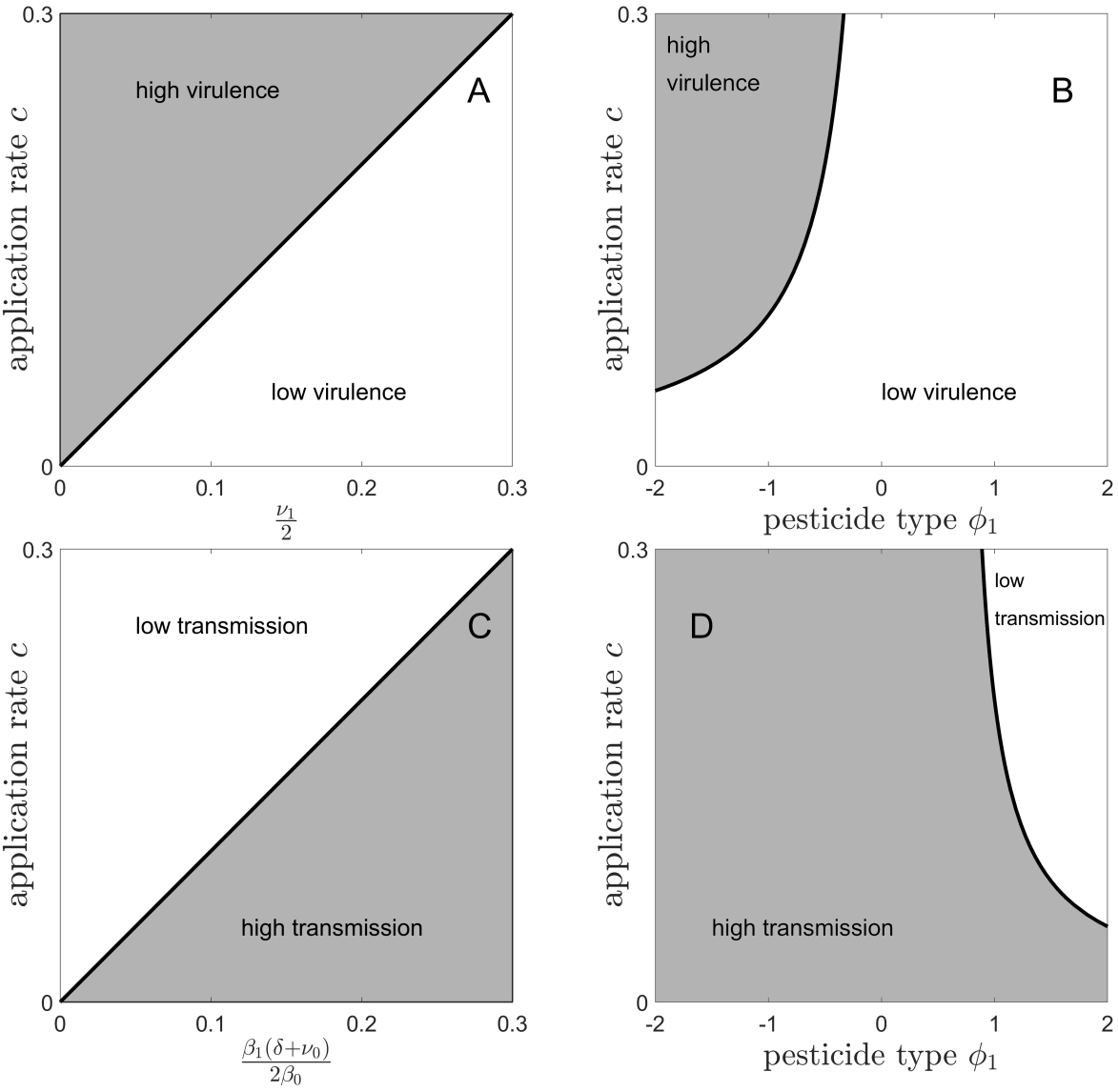

Figure 4.4: **Trait distribution states - VE & TE cases.** Color code: white (grey) region refers to *low* (*high*) states. Panel A: VE case for a fixed pesticide (*i.e.* $\phi_1 = -2$). In absence of pesticide ($c = 0$), the infected population is always in the *low* state, regardless of the trait-dependent virulence contribution ν_1. In the presence of pesticide ($c > 0$), the system can adapt towards the *high* state, for sufficiently high c. Panel B: state diagram for control strategy parameters c and ϕ_1 (with fixed $\nu_1 = 0.1$). Panel C: TE case for a fixed pesticide (*i.e.* $\phi_1 = 2$). In absence of pesticide ($c = 0$), the infected population is always in the *high* state. In the presence of pesticide ($c > 0$), the system can adapt towards the *low* state, for sufficiently high c. Panel D: state diagram for control strategy parameters (with fixed $\beta_0 = \beta_1 = 0.0001, \delta + \nu_0 = 0.1$).

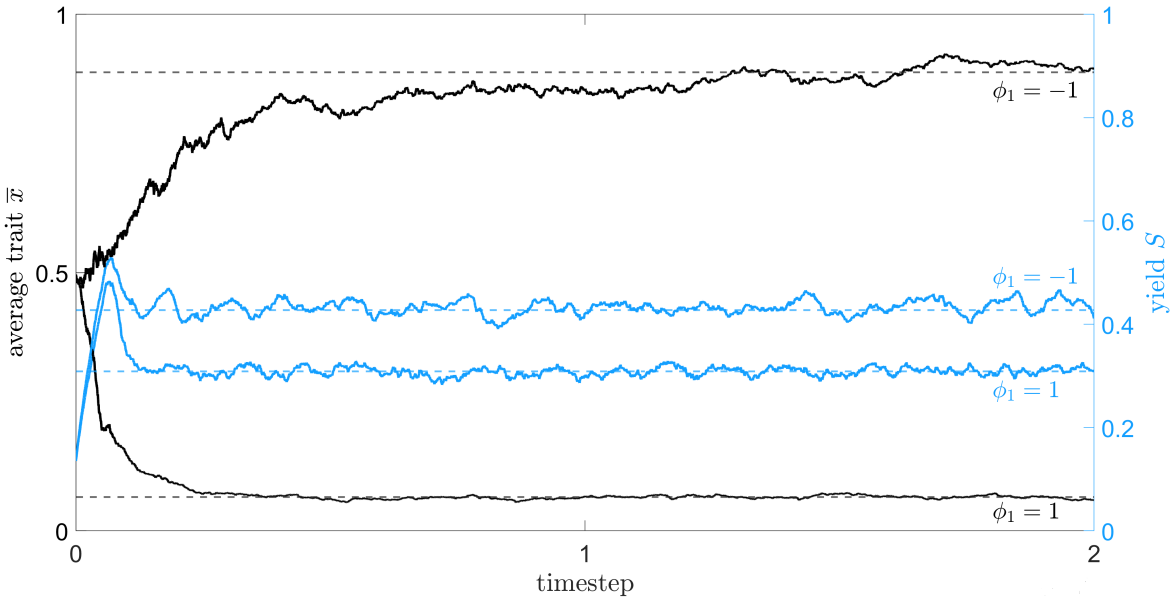

Figure 4.5: **Simulated temporal trajectories.** Solid lines: Temporal trajectories of the yield ($\widehat{S}$, rescaled with respect to $\widehat{S}_0$) and of the average trait ($\overline{x}$), obtained from agent-based numerical simulations of the dynamics. Dashed lines: analytical equilibrium values. The system is initialised with identical initial conditions and same application rate ($c = 0.15$), but different pesticide type. For $\phi_1 = -1$ ($\phi_1 = 1$), the system adapts towards the high (low) state. Other parameters: $\theta = 300, d = 0.04, \beta_0 = 0.0001, \beta_1 = 0, \nu_1 = 0.1, \nu_1 = 0.1, \mu = 0.00007$.

pesticide type will be analysed extensively later). The figure also shows the agreement between the analytical predictions for the equilibrium values, and the agent-based SISx dynamics, which holds for all sets of parameters considered in the study.

Transmission-Eradication TE case. In this case, pesticide sensitivity $\phi(x)$ and transmission $\beta(x)$ both depend on the trait x. Virulence is then homogeneous, that is $\nu_1 = 0$. The relevant compound parameter of Eq. (4.24) reduces to $\Omega_{\mathrm{TE}} = \beta_1 (\delta + \nu_0) + c[\beta_1 (1 - \phi_1/2) - \beta_0 \phi_1]$. In absence of pesticide (*i.e.* $c = 0$, corresponding to the x-axis in panel C of Fig. 4.4), Ω_{TE} is always positive, meaning that the distribution is in the high-transmission state for any combination of the parameters. Upon employment of a pesticide positively correlated with the trait ($\phi_1 > 0$, thus focusing the effect on the most transmitting pathogens), the system may adapt towards the low-transmission state: panel C of Fig. 4.4 shows that for this to occur, the ap-

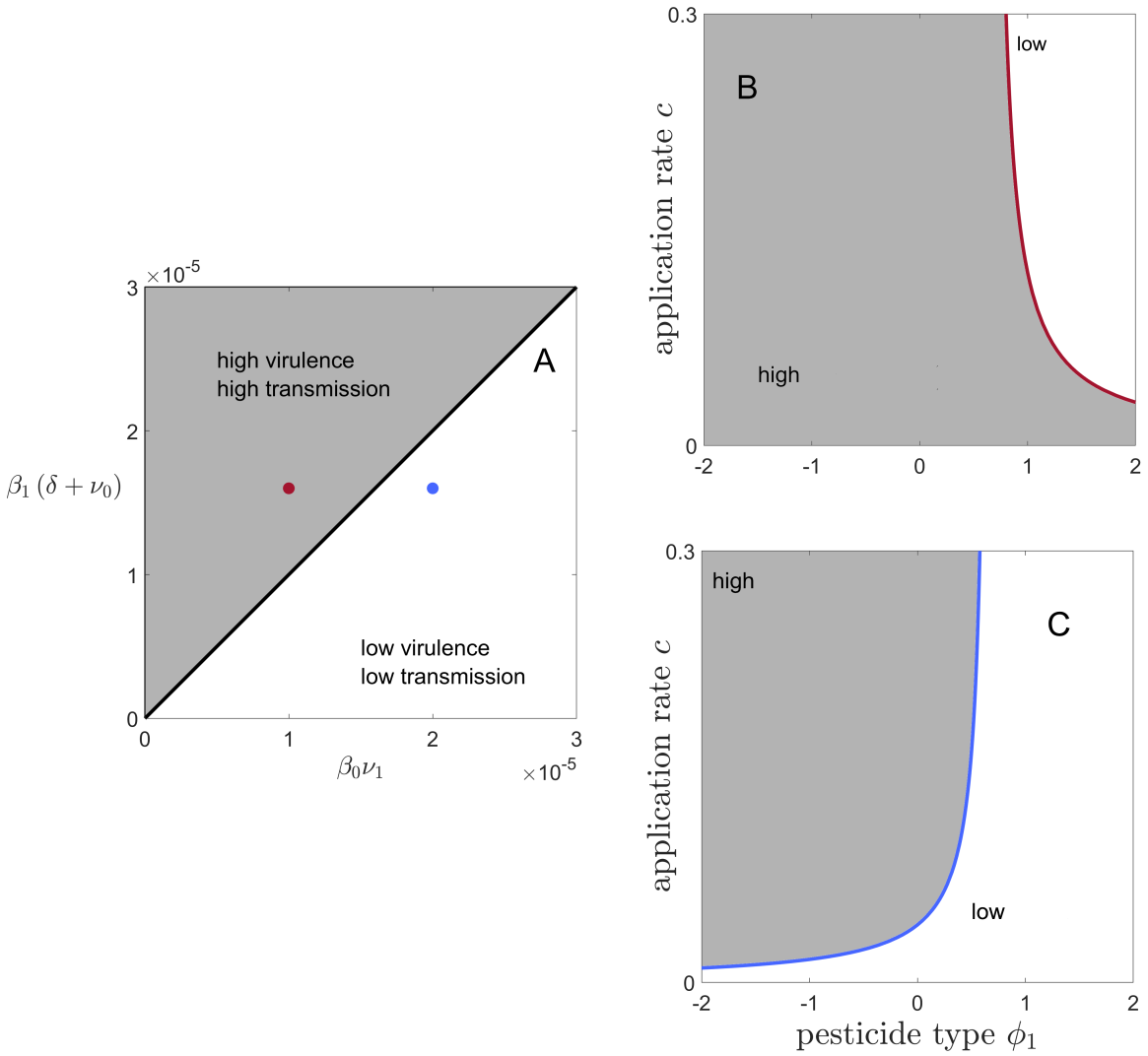

Figure 4.6: **Trait distribution states - TVE case.** Panel A: state diagram of the trait distribution in absence of pesticide. The infected population can adapt towards either the high-virulence and high-transmission state, or the low-virulence and low-transmission state. Large β_1, harvesting rate δ and baseline virulence ν_0 push the system towards the *high* state; instead, large baseline transmission β_0 and trait-dependent virulence contribution ν_1 push it towards the *low* state. Panel B: a system initially in the *high* state (red point panel A) can switch towards the *low* state under a range of control strategies. The red curve separates the two regions of the control parameters. Panel C: likewise, a system initially in the *low* state (blue point panel A) can switch towards the *high* state under a range of control strategies. The blue curve separates the two regions of the control parameters. Parameters: $\delta = 0.06, \nu_0 = 0.1, \beta_0 = \beta_1 = 0.0001$.

plication rate c must exceed a threshold value that increases with the trait-dependent transmission β_1, and with $\delta + \nu_0$, (here we have fixed the pesticide type $\phi_1 = 2$), while it decreases with baseline transmission β_0. In general, for fixed values of β_1, ν_0, δ, such threshold value decreases as correlation ϕ_1 increases (panel D of Fig. 4.4).

Transmission-Virulence-Eradication TVE case. In the TVE case, the heterogeneous trait simultaneously determines all three epidemiological interactions. The relevant compound parameter is then given by the Ω of Eq. (4.24). Contrary to the cases previously shown, in absence of pesticide (*i.e.* $c = 0$), the pathogen population can already be found in both *high* or *low* states. With reference to panel A of Fig. 4.6, *low* states will be favoured for large baseline transmission β_0 and trait-dependent virulence contribution ν_1; instead, high transmission-high virulence states will be favoured for large trait-dependent transmission β_1, harvesting rate δ and baseline virulence ν_0. The presence of pesticide may lead to a change of state, depending on both the rate of application c and the degree of correlation ϕ_1 with the heterogeneous trait. In panel B of Fig. 4.6, I show how a system initially in the *high* state adapts after pesticide application, as a function of the management control parameters c and ϕ_1. For low use of pesticide (*i.e.* low c), the infected population remains in the *high* state, regardless of the type of pesticide employed. However, increasing pesticide application will eventually bring the system into the *low* state, if positive ϕ_1 or generalist types are employed. If the system is initially in the *low* state in absence of pesticide (panel C of Fig. 4.6, same parameters as panel A but ν_1 doubled), the complementary behaviour is observed.

Besides affecting the evolutionary state (that is the average trait value $\overline{x}$) of the system at the endemic equilibrium, numerical simulations of the dynamics have shown that the type of pesticide employed also affects the quantity of healthy yield produced. The aim of the next Section is to characterise mathematically the relationship between control strategy and yield production, with the aim of understanding the optimal control strategy.

4.3.3. Optimising pesticide use

At endemic equilibrium, the average virulence, transmission and pesticide sensitivity, respectively, are:

$$\begin{cases} \overline{\nu} = \nu_0 + \nu_1 \overline{x} \\ \overline{\beta} = \beta_0 + \beta_1 \overline{x} \\ \overline{\phi} = \phi_1 \overline{x} + 1 - \phi_1/2. \end{cases} \tag{4.25}$$

Inserting the above equations into the endemic equilibrium yield $\widehat{S}$ Eq. (4.19), I get:

$$\widehat{S} = \frac{\delta + \nu_0 + \nu_1 \overline{x} + c\phi_1 \overline{x} + c\,(1 - \phi_1/2)}{\beta_0 + \beta_1 \overline{x}}. \tag{4.26}$$

Note that the equilibrium average trait $\overline{x}$ is function of the control strategy (ϕ_1, c), as the equilibrium trait distribution $\widehat{i(x)}$ depends on such parameters. Therefore, Eq. (4.26) provides all information about the complex relationship between yield production and pest management, and it allows systematic exploration of the whole parameter space. In the following, I will focus on a particular set of parameters exemplar of the possible non trivial behaviours of the system. In Fig. 4.7, I plot the equilibrium yield $\widehat{S}$ (rescaled with respect to the disease-free yield $\widehat{S}_0$), as a function of application rate c, and compare the effect of five different types of pesticides: $\phi_1 = -2, -1, 0, 1$ and 2. The set of parameters correspond to the TVE case, with the system in the *low* state in absence of pesticide (white region in panel A of Fig. 4.6, other parameters specified in the figure's caption); the complementary case starting in the *high* state is not shown, but it preserves the same qualitative behaviour.

Employing a pesticide type inconsistent with the state of the trait distribution in absence of control (*e.g.* $\phi_1 = 2$ in this example), leads to a small increase of yield as the dose is increased (green curve). Instead, employing a pesticide extremely specialised on *low* trait values ($\phi_1 = -2$), initially leads to a more significant increase in yield, for

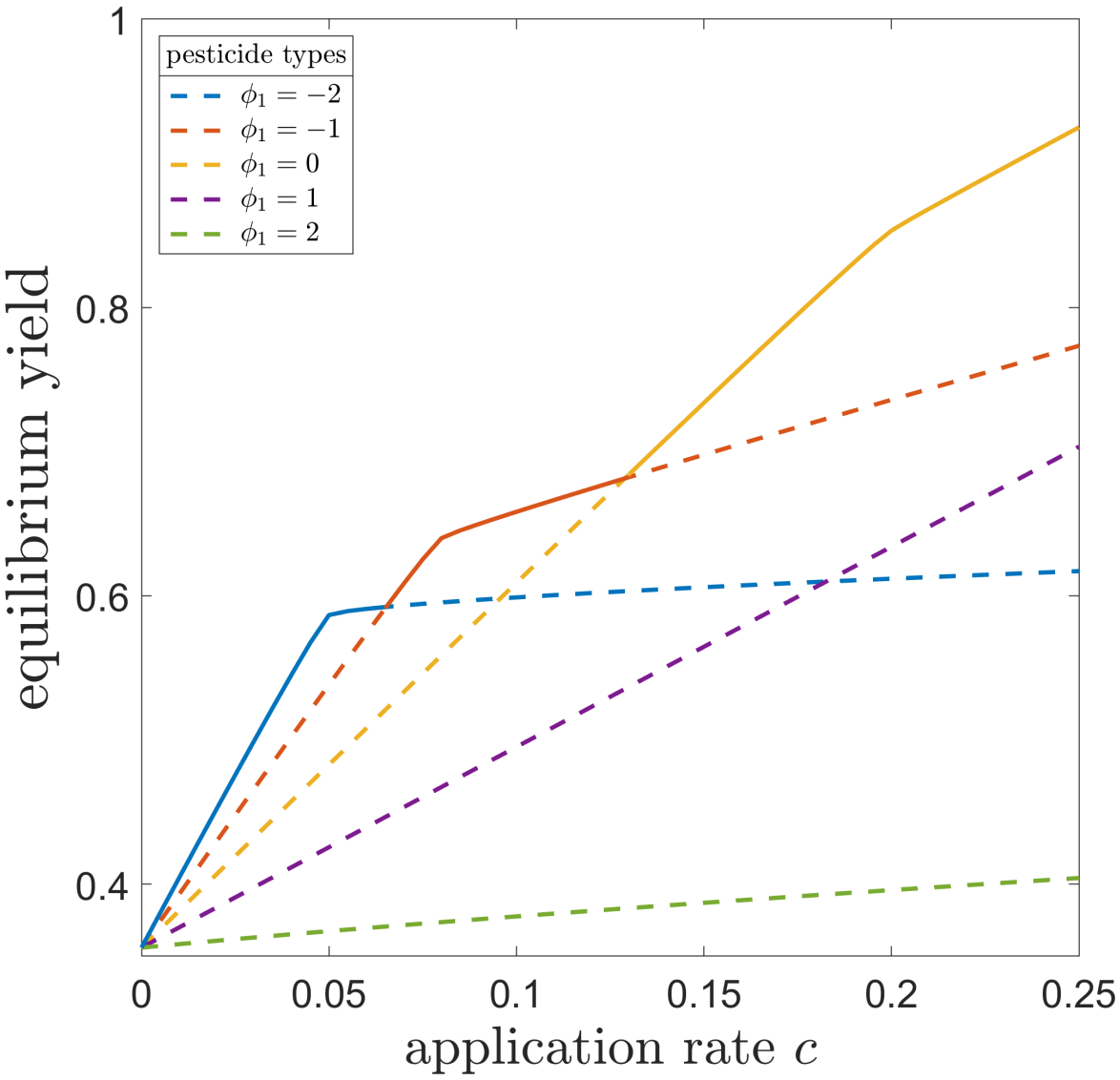

Figure 4.7: **Equilibrium yield as function of pesticide application rate - TVE case.** The yield at equilibrium $\widehat{S}$ obtained using five different pesticide types, as function of application rate c (the y-axis is normalised with respect to the disease free yield $\widehat{S}_0$). In absence of pesticide, the system is in the low-virulence state. Very specialised pesticides (*e.*g. $\phi_1 = -2$) are optimal for low c, but their correspondent gain in yield quickly saturates as application rate is increased. For higher values of c, switching to more generalist types grants a higher return. The Pareto-efficient solutions of the control strategy as function of application rate are highlighted with solid curves. Parameters: $\mu = 0.00007, \theta = 150, \delta = 0.04, \beta_0 = \beta_1 = 1e-4, \nu_0 = 0.08, \nu_1 = 4\nu_1$.

low application rates (blue curve). However, as increasing application rate leads the system towards the opposite *high* state, this extremely specialist pesticide becomes less effective, and the gain in yield eventually saturates. At this point, switching to a more moderate ($\phi_1 = -1$) or to a generalist ($\phi_1 = 0$) type provides more gain in yield, rather than increasing further the rate of application c (red and yellow curves). Depending on the value of the replanting rate θ, the system may eventually reach the disease-free equilibrium (where $\widehat{S} \equiv \widehat{S}_0$), as the dose is further increased. Overall, I remark that, regardless of the choice, increasing c always corresponds to an increase of the yield. Hence, it is evident that maximising yield and minimising pesticide application are contrasting objectives. Nonetheless, this picture shows that, for a given application rate c, it is possible to optimise its use by choosing the right type ϕ_1. In the next subsection, I will exploit the linear form of the trait-dependent functions, so as to obtain analytical formula for the optimal pesticide type.

4.3.3.1 Optimal pesticide choice

I have shown that in general, for a given value of pesticide application rate c, there will exist an optimal pesticide type ϕ_1^{opt} maximising the yield $\widehat{S}$ at the endemic equilibrium. Under the linear assumptions Eqs. (4.15)-(4.17), the optimal pesticide can be computed analytically. For a given set of the parameters $\theta, \delta, \nu_0, \beta_0, \beta_1$ and c, the pesticide type ϕ_1 that maximises the equilibrium yield satisfies:

$$\frac{\partial \widehat{S}}{\partial \phi_1} = 0 \quad , \quad \frac{\partial^2 \widehat{S}}{\partial \phi_1^2} < 0. \tag{4.27}$$

Performing the first derivative with respect to ϕ_1 of $\widehat{S}$ (Eq. (4.26)), I get:

$$\frac{\partial \widehat{S}}{\partial \phi_1} = \frac{\left[\nu_1 \overline{x}_{\phi_1} + c\overline{x} + c\phi_1 \overline{x}_{\phi_1} - c/2\right]\left[\beta_0 + \beta_1 \overline{x}\right] - \left[\delta + \nu_0 + \nu_1 \overline{x} + c\phi_1 \overline{x} + c - c\phi_1/2\right]\beta_1 \overline{x}_{\phi_1}}{\left(\beta_0 + \beta_1 \overline{x}\right)^2}, \tag{4.28}$$

where the subscript notation indicates the derivative with respect to ϕ_1. Arranging terms (and neglecting the denominator which is always positive), I get:

$$\frac{\partial \widehat{S}}{\partial \phi_1} = 0 \Longleftrightarrow [\overline{x} - 1/2]\,[c + \beta_1\, c\, \overline{x}] - \Omega\, \overline{x}_{\phi_1} = 0. \tag{4.29}$$

The above condition is readily solved by observing that $\Omega = 0$ for $\overline{x} = 1/2$. Hence, the candidate for the optimal type is:

$$\phi_1^{\text{opt}} \quad \text{such that} \quad \overline{x} = \frac{1}{2}. \tag{4.30}$$

The second derivative with respect to ϕ_1 of $\widehat{S}$ gives:

$$\frac{\partial^2 \widehat{S}}{\partial \phi_1^2} = \frac{(\beta_0 + \beta_1 \overline{x})^2 \left[\overline{x}_{\phi_1} (c\beta_0 + c\beta_1 \overline{x}) \left(\overline{x} - \frac{1}{2}\right) c\beta_1 \overline{x}_{\phi_1} - \Omega_{\phi_1} \overline{x}_{\phi_1} - \Omega \overline{x}_{\phi_1 \phi_1}\right] - 2\beta_1 \overline{x}_{\phi_1} \left(\overline{x} - \frac{1}{2}\right) (c\beta_0 + c\beta_1 \overline{x}) - \Omega \overline{x}_{\phi_1} (\beta_0 + \beta_1 \overline{x})}{(\beta_0 + \beta_1 \overline{x})^4} \tag{4.31}$$

Recalling that for our candidate point holds $\Omega = 0$ and $\overline{x} = \frac{1}{2}$, many terms of the above equation simplify, and we are left with:

$$\frac{\partial^2 \widehat{S}}{\partial \phi_1^2} = \frac{\overline{x}_{\phi_1} \left[2c\beta_0 + c\beta_1 \left(\overline{x} + \frac{1}{2}\right)\right]}{(\beta_0 + \beta_1 \overline{x})^2}, \tag{4.32}$$

to be evaluated in $\overline{x} = \frac{1}{2}$. In Eq. (4.32), all terms in bracket are always positive, so that $\text{sign}\left(\frac{\partial^2 \widehat{S}}{\partial \phi_1^2}\right) = \text{sign}\,(\overline{x}_{\phi_1})$. However, increasing the value of ϕ_1 means increasing selection pressure on pathogens with higher trait value x, thus decreasing its average quantity. Therefore, it follows that $\overline{x}_{\phi_1} < 0$, and the desired condition on the second derivative of $\widehat{S}$ (Eq. (4.27)) is satisfied.

By setting the definition of Ω Eq. (4.24) to zero, I finally obtain the value of the optimal type ϕ_1^{opt} as function of the pesticide application rate (as well as of the other parameters):

$$\phi_1^{\text{opt}} = \frac{2}{2\beta_0 + \beta_1} \left[\frac{\beta_1\,(\delta + \nu_0) - \beta_0 \nu_1}{c} - \beta_1\right] \tag{4.33}$$

With respect to Figs. 4.4 and 4.6, the above equation corresponds to the curves separating the *low* and *high* states in the (ϕ_1, c) phase diagrams, for which $\Omega = 0$. The

effect of each parameter on ϕ_1^{opt} is summarised in Table 4.2. For instance, the impact of harvesting rate δ and of baseline virulence ν_0 are mediated by the trait-dependent transmission coefficient β_1. Therefore, one should expect such parameters to be uninfluential, in absence of transmission heterogeneity. Overall, Eq. (4.33) shows that the optimal pesticide's degree of specialisation ϕ^{opt} is a decreasing function of application rate c, so that extremely specialised pesticide types will perform better for low c.

Table 4.2: **Effect of the parameters on the optimal pesticide choice** ϕ_1^{opt}. The symbol $\uparrow$ ($\downarrow$) indicates that an increase in the parameter in question leads to an increase (decrease) of ϕ_1^{opt}.

Parameter	**Effect on** ϕ_1^{opt}
β_0	$\uparrow$ if $(\delta + \nu_0 + \nu_1/2 - c) > 0$ and $\downarrow$ otherwise
β_1	$\uparrow$ if $(\delta + \nu_0 + \nu_1/2 - c) < 0$ and $\downarrow$ otherwise
c	$\uparrow$ if $(\beta_0\nu_1 - \beta_1\delta - \beta_1\nu_0) > 0$ and $\downarrow$ otherwise
ν_0	$\uparrow$ always
ν_1	$\downarrow$ always
δ	$\downarrow$ always

4.4. Discussion and conclusions

Theoretical works treating trait-structured populations typically aim at deriving equations that characterise the evolutionary state of the system, namely the population's average virulence (Day and Gandon, 2006; Day and Proulx, 2004; Day et al., 2020). Instead, my approach highlights the environmental and economic implications of evolutionary adaptation by framing the problem in the context of pest management: that is, understanding how the pesticide's dependence on the heterogeneous trait relates to its application rate, with the aim of maximising the amount of yield at equilibrium for a given quantity of pesticide deployment.

I have considered a pathogen expressing continuous levels of disease-induced mortality

and infection transmission (Eqs. (4.15)-(4.16)), and a pesticide exerting an eradicant action that can be either positively or negatively correlated with such traits (Eq. (4.17) and Fig. 4.2), depending on the chosen type. I have shown that, in absence of pesticide treatment, the infected population may adapt towards either a high virulence-high transmission or a low virulence-low transmission state, depending on the ecological parameters, and on the trait-dependent contributions to the epidemiological traits. I have shown that, due to its heterogeneous selection pressure, the use of pesticides with trait-dependent sensitivity may induce a transition in the pathogen trait distribution, depending on pesticide type ϕ_1 and application rate c (panels B and D of Fig. 4.4, panels B and C of Fig. 4.6). Pesticide sensitivity has been treated as a potentially continuous control parameter; however, focusing on only few classes (as I have done in Fig. 4.7) is enough to provide significant guidance, since in practice there will only be a limited number of choices on the market.

Despite increasing pesticide application rate always leading to an absolute gain in yield, such gain will eventually saturate as a consequence of this transition, if improper pesticide types are used (Fig. 4.7). Finally, I have shown that the optimal choice of pesticide has a non trivial relation with the application rate (Eq. (4.33)): as a general rule, my results suggest that very specialised pesticides, exhibiting a strong (positive or negative) degree of correlation, should be employed at low application rates; instead, generalist pesticides, with a more uniform action over the trait space, are likely to perform better at high application rates.

In terms of multi-criteria optimisation analysis (Kennedy et al., 2008), Fig. 4.7 shows that maximising yield ($\widehat{S}/\widehat{S}_0$) and minimising pesticide application (c) are conflicting objectives. As a consequence, one can identify the Pareto-efficient solutions to our control strategy, highlighted by the solid curves. Choosing a different combination of the control parameters (c, ϕ_1) will necessarily worsen the outcome (dashed curves), by either decreasing the amount of yield, or increasing the costs related to pesticide application.

Validating the results herein presented will require the measurement of the trait-

dependent epidemiological functions, for specific pathogen-pesticide systems. This achievement depends on the identification of heterogeneous phenotypic traits, and of their chemical interaction with the pesticide. Examples of potential candidate traits in fungi are the level of expression of the virulence-associated adhesin *Epa1* (Halliwell et al., 2012; Steels et al., 2000), or drug transporters responsible for fungicide resistance (De Waard et al., 2006). Furthermore, many other genes controlling virulence may reveal heterogeneous levels of expressions, such as *CPS1* in the corn fungus *Cochliobolus heterostrophus* (Lu et al., 2003) or necrotrophic effectors in the wheat fungus *Parastagonospora nodorum* (Lin et al., 2017), and hence become potential targets for heterogeneous pesticide action. Targeting virulence is considered a promising strategy for the development of antifungal drugs (Gauwerky et al., 2009), and this work may help to identify the optimal type of pesticide according to the biological and environmental conditions of the considered system. Several plant bacteria are united by the use of phytotoxins as virulence factors (Pontes et al., 2020): for instance, *Candidatus* Liberibacter spp. (affecting different species of citrus), *Erwinia amylovora* (the Fire Blight infesting apple and pear orchards), *Xanthomonas* spp. (Black Rot disease affecting *Brassica* crops) are among the most destructive pathogens, in terms of agricultural loss (Mansfield et al., 2012). Potential chemical strategies based on the inhibition of phytotoxin production (Garland et al., 2017), or acting on virulence-related gene regulators (Yang et al., 2011), may be implemented in pesticide design in order to develop a spectrum of trait-dependent chemical treatments. Combining such experimental development with such theoretical methods of investigation, may allow us to harness heterogeneity in pathogen populations - which is almost always considered to be a key difficulty in management, by allowing evolution of resistance to chemical controls - to our advantage.

5. Conclusions and Research Perspectives

I conclude with outlining two main future research perspectives: a first line of research would spontaneously arise by merging the problems tackled independently in Chapters 3 and 4; a second line consists in proposing further applications of the RME in the field of evolutionary epidemiology, and a potential general framework of trait-dependent control strategies.

5.1. Accounting for Fittest/Flattest duality in evolutionary epidemiology models

In Chapter 3, I have shown that degenerate fitness landscapes trigger a dual fittest/-flattest behaviour between full trait and marginal fitness distributions. Acknowledging this duality can help improve the accuracy of models in the field of evolutionary epidemiology, such as the one analysed in Chapter 4, where the information on the state of the distributions can be used to design treatment policies. As a result, the most effective interventions might not be those that focus on the extremes of the sole fitness-related traits.

For example, in a pathogen population, suppose that x quantifies the resistance to a drug or antibiotic, so that larger x confers higher fitness to its carriers. Then, one

might expect the population to be dominated by individuals with highest resistance (*i.e.* optimal fitness), and a therapy would be developed to counter fittest-like distributions, hence maximising the intervention on the traits carrying the maximal resistance value. However, if such a selective trait is entwined with another, neutral one (*i.e.* not affecting the resistance) via a degeneracy-fitness trade-off, then the distribution will very likely be dominated by individuals with sub-optimal resistance, and the therapy would erroneously target non-redundant traits, with the possibility of unwittingly helping sub-optimal strains to mutate and become fitter.

On the other hand, suppose that an experimentalist measures the growth rates in a rapidly mutant population as a function of x, and obtains a profile similar to panels **e-f** of Fig. 3.3, with a peak in the distribution at an intermediate value $x = \tilde{x}$ with $0 < \tilde{x} < 1$. Then they might erroneously conclude that $\tilde{x}$ confers the optimal fitness value, whereas, in fact, the trait $\tilde{x}$ dominates the population due to its degeneracy, rather than due to a selective advantage. In the 'worst case', by confusing a degeneracy-dominated fitness profile with a one-dimensional survival-of-the-fittest distribution, one would infer a direction of selection opposite to the true one, and conclude that trait $x = 0$ has optimal fitness.

5.2. Generalising the study of trait-dependent control strategies

Despite the analytical derivations presented in Chapter 4 relying on many simplifying assumptions, it highlights the qualitative role of the various ecological interactions, and it provides a starting point for the introduction of further elements of complexity. For example, the effects of nonlinearities in the Transmission-Virulence trade-off (Bolzoni and De Leo, 2013; Pugliese, 2002) can be straightforwardly analysed numerically. The analysis has been carried out using and underpinning model with an SIS-type dynam-

ics, although it can be straightforwardly extended to other epidemiological models, potentially including explicit vital dynamics of the pathogen (Gilligan, 2002; Madden et al., 2000). For instance, in SIR-type models, one may want to calculate optimal curves based on different quantities (*e.g.* $S+R$). Particularly, we note that an SI-type model, typically used for those diseases that do not allow for recovery, would preserve the above results, as far as the quantity of interest is the number of susceptible individuals. However, as the functional form of host demography may have a significant impact on the population composition at equilibrium (Cunniffe and Gilligan, 2010), the optimal pesticide curves may depend on the host growth function as well.

Modelling pesticide application, I have deliberately focused on the eradicant effect and neglected protectant contributions (Hall et al., 2007). The latter might be introduced by relaxing the form of the TV trade-off (Fig. 4.2, panel B): a trait-dependent protectant effect may modify or break the monotonicity of the transmission function, thus opening the possibility of choices significantly different from the linear one. Different transmission functions may also emerge as a consequence of physiological alterations of hosts' level of activity, in the case of animal (and human) systems, and of intervention policies in the context of human disease modelling (quarantine, contact tracing, etc...).

The framework herein presented might also be relevant to study the optimisation of inevitably imperfect treatments (Walter and Lion, 2021), such as a potential eradication-protection trade-off: indeed, due to its inhibitory action on transmission events, an investment in the protectant contribution is expected to be efficient whenever the infected population is in a high-transmission state. However, if such investment is paid for by a reduced eradicant effect, it is not obvious how the pathogen would adapt to such intervention; hence, the importance of a tool able to predict the trait distribution. Performing a similar analysis, one might be able to compute the optimal balance between the two actions, and to relate this choice to the ecological interactions at play.

Ultimately, the potential of evolutionary epidemiology goes beyond agricultural practice, which here has been chosen in order to move within a well established frame. The

combination of analytical and numerical investigation of RME equations has a certain degree of flexibility that should be exploited as much as possible to address control strategy problems. The hope is that in the future, the models herein presented will be considered as instantiations of a general, mathematical theory of trait-dependent intervention.

A. Appendix

A.1. Numerical codes

A.1.1. Agent-based selection-mutation dynamics on redundant fitness landscapes

In the following, I report the Processing code employed for the agent-based dynamics of the asymmetric degenerate fitness landscape, as detailed in Subsection 3.2.3. The codes employed for the non-degenerate and the symmetric landscapes are analogous, upon replacement of the corresponding trait space.

```
// Agent based simulation of the selection-mutation dynamics on two
   dimensional asymmetric redundant fitness landscape
// Individuals have two traits: x is the selective trait; y is the neutral
   trait
// Fitness is linearly proportional to x
// The phenotype space T(x,y) is bounded by the profile beta(x)=1-x
   mimicking the degeneracy-selection trade-off
// T = { (x,y) | 0 <= x <= 1 ; 0 <= y <= 1-x }

// Parameters

int RandomNumberSeed=2;              // set random number seed
```

```
float mu=1;                          // mutation event rate
float gamma=1;                       // competition event rate
float tot_rate=mu+gamma;             // total events rate
float Mutation=0.04;                 // width mutation step
int L=100000;                        // population size
float w=0.004;                       // selection pressure
int bin=50;                          // number of bins population histogram
int time_idx=0;                      // initialise time
int time_max=10000;                   // number of time steps
int pre_itr_max=2000;                // number of transient iterations

// Auxiliary arrays and variables

int[] pop_hist=new int[bin];               // not normalised histogram of
   fitness-related phenotype trait x
float[] fitness_hist=new float[bin];       // normalised histogram of
   fitness-related phenotype trait x
float[] avg_x=new float[bin];              // temporal vector of average
   phenotype trait x
Table table,mean_x,hist_x;
String lbl_r,lbl_c;
float avg;

// Define directory and name of the data files

// here put the address of the output data files (optional)
String address="";

// temporal trajectory of average trait x
String filename_avgx= address + day() + "-" + month() + "-" + year() + "-"
```

```
    + hour() + "-" + minute() + "_avgx.csv";

// temporal average of trait x distribution
String filename_hist= address + day() + "-" + month() + "-" + year() + "-"
    + hour() + "-" + minute() + "_hist.csv";

// txt file printing parameters used
PrintWriter parameters;

// Define new class Player

class Player{
  float x;      // selective trait
  float y;      // neutral trait
  Player (float x_, float y_){
  x=x_;
  x=x_;
}

// Define Mutation Event

  void InheritFromMut(Player parent){
    float xtemp=parent.x;
    float ytemp=parent.y;
    p=parent.x+random(-Mutation,+Mutation); // mutate trait x of random
        quantity
    y=parent.y+random(-Mutation,+Mutation); // mutate trait y of random
        quantity
    if((x<0) || (x>1) || (y<0) || (y>1-x)) {x=xtemp; y=ytemp;} // if
        mutation leads outside boundary then reject
```

```
  }

// Define Asexual reproduction without mutation

  void InheritFrom(Player parent){
    xparent.x;
    y=parent.y;
  }
}

// Define population of players
Player[] player;

// Initialisation of the system

void setup(){
  int i,l,index;
  float x0,y0;
  randomSeed(RandomNumberSeed);
  for(l=0;l<bin; l++){pop_hist[l]=0; fitness_hist[l]=float(0);} //
      Initialise histograms


  parameters = createWriter(address + day() + "-" + month() + "-" + year()
      + "-" + hour() + "-" + minute() + "_parameters.txt");
  table = new Table();
  hist_p = new Table();
  for(i=0;i<bin;i++){
  String lbl=str(i);
  table.addColumn(lbl, Table.FLOAT);
```

```
  hist_x.addColumn(lbl, Table.FLOAT);
  }
  mean_x = new Table();
  mean_x.addColumn("<x>", Table.FLOAT);

// Initialise population with randomly uniform distributed phenotypes in
    the Adaptive Space and update histogram

  player =new Player[L];
  for (i=0;i<L;i++){
    player[i]= new Player (x0=random(1.0), y0=random(1-x0));
    index=get_index(player[i].x);
    pop_hist[index]++;
  }
}

// Runs the algorithm

void draw(){

  for (int pre_itr=0;pre_itr<pre_itr_max;pre_itr++) dynamics(); //
      transient window

  while(time_idx<time_max){
    dynamics();
    update_histogram();
    update_statistics();
    time_idx++;
    println(time_idx);
  }
```

```
  // Finally, the averages over time are computed and the data are saved

  compute_temporal_average();

  // Save tables data and parameters.txt file

  saveTable(mean_p,filename_avgx);
  saveTable(hist_x,filename_hist);
  parameters.println("RandomNumberSeed = " + str(RandomNumberSeed));
  parameters.println("mu = " + str(mu));
  parameters.println("gamma = " + str(gamma));
  parameters.println("Mutation = " + str(Mutation));
  parameters.println("w = " + str(w));
  parameters.println("bin = " + str(bin));
  parameters.println("n_iterations = " + str(n_iterations));
  parameters.println("time_max = " + str(L));
  parameters.println("pre_itr_max = " + str(pre_itr_max));
  parameters.close();
  exit();
}


// Define dynamics

void dynamics(){
  int i,i1,index;
  float r1;
  for (int repeat=1; repeat<=L; repeat++){ // events are repeated L times
    r1=random(1.0);
```

```
i=int(random(float(L)));              // a focal player i is sampled
index=get_index(player[i].x);
if(r1<=mu/tot_rate){                  // i mutates with probability
    mu/tot_rate
  pop_hist[index]--;
  player[i].InheritFromMut(player[i]);
  index=get_index(player[i].p);
  pop_hist[index]++;
}
else{                                 // otherwise i competes with another
    random player i1
  i1=int(random(float(L)));
  while(i1==i) {i1=int(random(float(L)));}

  // Player i1 wins the competition and reproduces with probability
     proportional to the difference
  // between their fitness and i's

  if(random(1.0)<=(1+w*(player[i1].x-player[i].x))/2){ // probability
      i1 wins
    pop_hist[index]--;
    player[i].InheritFrom(player[i1]);  // traits player i become those
       of player i1
    index=get_index(player[i1].x);
    pop_hist[index]++;
  }

  // Otherwise player i wins the competition and i1 becomes i

  else{
```

```
        pop_hist[index]++;
        index=get_index(player[i1].x);
        pop_hist[index]--;
        player[i1].InheritFrom(player[i]);
      }
    }
  }
}

// updates histogram at the end of each timestep

void update_histogram(){
  int i;
  for(i=0;i<bin;i++){
    fitness_hist[i]=(float(pop_hist[i])/float(L))*bin;
  }
  TableRow row = table.addRow();
  for(i=0;i<bin;i++){
    String lbl=str(i);
    row.setFloat(lbl, fitness_hist[i]);
  }
}

// Updates average trait at the end of each timestep

void update_statistics() {
  int i;
  float average_x=0;
  for(i=0; i<L; i++) {average_x+= (player[i].x)/L;}
  TableRow row = mean_x.addRow();
```

```
  row.setFloat("<x>", average_x);
}

// Auxiliary function getting index of histogram

int get_index(float x){
  int idx;
  idx=int(x*bin);
  if(idx==bin) idx--;
  return idx;
}

// Finally, computes average over time of histogram

void compute_temporal_average() {
 int i,j;
 int lines=table.getRowCount();
  for(j=0; j<bin; j++){
    avg=float(0);
    for(i=0;i<lines;i++){
      avg+=table.getFloat(i,str(j));
    }
    avg_x[j]=avg/float(lines);
  }
  TableRow row = hist_x.addRow();
  for(i=0;i<bin;i++){
    row.setFloat(str(i), avg_x[i]);
  }
}
```

A.1.2. Agent-based simulation of the SISx dynamics

In the following, I report the Python code employed to simulate the agent-based SISx dynamics, as detailed in Subsection 4.2.5. The code is also provided with the semi-analytical part giving the deterministic prediction for the trait distribution, based on the self-consistent method (see Subsection 2.2.6).

```
import numpy as np
import random
from scipy import stats
import matplotlib.pyplot as plt

# Parameters

I_init=1000              # initialise total I hosts
S_init=1000              # initalise total S hosts
n_iterations=3000        # number of iterations
tau=0.0001               # timestep
b0=0.0001                # baseline infection rate
b1=0.0001                # strain-dependent transmission contribution
theta=300                # replanting rate
d=0.06                   # harvesting rate
mu_step=0.02             # random mutation step
mu=1                     # mutation rate
c=0.1                    # pesticide application rate
nu0=0.1                  # baseline virulence rate
nu1=0.1                  # strain-dependent virulence contribution
phi1=-1                  # pesticide type, must be -2 <= phi1 <= 2

name_dataset = "name_dataset"
```

```
# compound constants

mu_diff=mu/6*mu_step**2  # mutation diffusion coefficient
phi11=1-phi1/2           # normalisation factor for pesticide type

# Predictions of the deterministic theory

from scipy.optimize import fsolve
import math
from scipy.special import airy, jv, iv
from numpy import sqrt, where
import scipy.integrate as integrate

def Ai(x):
    (ai, ai_prime, bi, bi_prime) = airy(x)
    return ai

def Bi(x):
    (ai, ai_prime, bi, bi_prime) = airy(x)
    return bi

def Aip(x):
    (ai, ai_prime, bi, bi_prime) = airy(x)
    return ai_prime

def Bip(x):
    (ai, ai_prime, bi, bi_prime) = airy(x)
    return bi_prime

def find_avg_vir_positive_Omega(p):
```

```
    e=1/3;
    delta0=(b1*(d+nu0)-b0*nu1-b0*c*phi1+b1*c*phi11)/(mu_diff*(b1*p+b0))
    delta=abs(delta0)
    C=-(Aip(p*delta**e)/Bip(p*delta**e))
    C1, C1err =(integrate.quad(lambda z:
        (Ai((p-z)*delta**(1/3))+C*Bi((p-z)*delta**(1/3))),0,1))
    avg, avgerr = integrate.quad(lambda z:
        C1**(-1)*(z*(Ai((p-z)*delta**(1/3))+C*Bi((p-z)*delta**(1/3)))),0,1)
    return avg-p

def find_avg_vir_negative_Omega(p):
    e=1/3;
    delta0=(b1*(d+nu0)-b0*nu1-b0*c*phi1+b1*c*phi11)/(mu_diff*(b1*(1-p)+b0))
    delta=abs(delta0)
    C=-(Aip(p*delta**e)/Bip(p*delta**e))
    C1, C1err =(integrate.quad(lambda z:
        (Ai((p-z)*delta**(1/3))+C*Bi((p-z)*delta**(1/3))),0,1))
    avg, avgerr = integrate.quad(lambda z:
        C1**(-1)*(z*(Ai((p-z)*delta**(1/3))+C*Bi((p-z)*delta**(1/3)))),0,1)
    return avg-p

Omega = (b1*(d+nu0)-b0*nu1-b0*c*phi1+b1*c*phi11)

# Average strain value at endemic equilibrium

if Omega >=0:
    avg_x = fsolve(find_avg_vir_positive_Omega,1)
else:
    avg_x = 1 - fsolve(find_avg_vir_negative_Omega,1)
```

```
# Average virulence, transmission and sensitivity at endemic equilibrium

avg_vir=nu0+nu1*avg_x
avg_tra=b0+b1*avg_x
avg_sen=phi11+phi1*avg_x

# Total number of susceptible and infected hosts at equilibrium

Seq= min(theta/d, (d+avg_vir+c*avg_sen)/avg_tra)
Ieq = max(0, (theta - d*Seq)/(d+avg_vir))

# Print equilibrium state

if Ieq == 0:
    avg_x=0
    print("Disease extinction - Seq = {}".format(theta/d))
else:
    print("S_eq = {}, I_eq = {}, average_trait = {}, Omega = {},
        ".format(Seq,Ieq,avg_x,Omega))

name_parameters_file = name_dataset + "_parameters" + ".txt"
parameters = open(name_parameters_file, "w")
parameters.write("I_init = " + str(I_init) + "\n")
parameters.write("S_init = " + str(S_init) + "\n")
parameters.write("n_iterations = " + str(n_iterations) + "\n")
parameters.write("tau = " + str(tau) + "\n")
parameters.write("b0 = " + str(b0) + "\n")
parameters.write("b1 = " + str(b1) + "\n")
parameters.write("d = " + str(d) + "\n")
parameters.write("mu_step = " + str(mu_step) + "\n")
```

```
parameters.write("mu = " + str(mu) + "\n")
parameters.write("theta = " + str(theta) + "\n")
parameters.write("c = " + str(c) + "\n")
parameters.write("nu0 = " + str(nu0) + "\n")
parameters.write("nu1 = " + str(nu1) + "\n")
parameters.write("phi1 = " + str(phi1))
parameters.close()

# Stochastic processes

def Mutation_event(x,y):          # Mutation event
    r1=random.uniform(0,1);
    rate=tau*mu*x.shape[0]
    if r1 <= rate:
        idx=random.randint(0,x.shape[0]-1)
        old_v=x[idx]
        x[idx]+=random.uniform(-mu_step,+mu_step)
        if x[idx] > 1 or x[idx] < 0:
            x[idx]=old_v
    return x, y

def Infection_event(x,y):         # Infection event
    r1=random.uniform(0,1)
    idx=random.randint(0,x.shape[0]-1)
    rate=tau*(b0+b1*x[idx])*x.shape[0]*y
    if r1 <= rate:
        y-=1
        x=np.append(x,x[idx])
    return x, y
```

```
def Death_I_event(x,y):          # Spontaneous death of I event
    rate=tau*d*x.shape[0]
    r1=random.uniform(0,1)
    if r1 <= rate:
        idx=random.randint(0,x.shape[0]-1)
        x = np.delete(x, idx)
    return x, y

def Virulence_event(x,y):        # Death of I by virulence event
    r1=random.uniform(0,1)
    idx=random.randint(0,x.shape[0]-1)
    rate=tau*(nu0+nu1*x[idx])*x.shape[0]
    if r1 <= rate:
        x = np.delete(x, idx)
    return x, y

def Birth_S_event(x,y):          # Replanting of S event
    rate=tau*theta
    r1=random.uniform(0,1)
    if r1 <= rate:
        y+=1
    return x, y

def Death_S_event(x,y):          # Spontaneous death of S event
    rate=tau*d*y
    r1=random.uniform(0,1)
    if r1 <= rate:
        y-=1
    return x, y
```

```
def Eradication_event(x,y):      # Eradication of I event
    r1=random.uniform(0,1)
    idx=random.randint(0,x.shape[0]-1)
    rate=tau*c*(1-phi1/2+phi1*x[idx])*x.shape[0]
    if r1 <= rate:
        x = np.delete(x, idx)
        y+=1
    return x, y

# Initialise system

I=np.zeros(I_init,dtype=float)
S=S_init
data=np.zeros([n_iterations,3])
datahist=np.zeros([n_iterations,10])
for i in range(I_init):
    I[i]=random.uniform(0,1)

# Agent-based simulation

for i in range(0,n_iterations):
    N_tot=I.shape[0]+S
    print(i)
    for j in range(0,N_tot):
        I, S = Birth_S_event(I,S)
        I, S = Death_I_event(I,S)
        I, S = Mutation_event(I,S)
        I, S = Infection_event(I,S)
        I, S = Virulence_event(I,S)
        I, S = Death_S_event(I,S)
```

```
        I, S = Eradication_event(I,S)


    data[i,0]=I.shape[0]          # Total number of I hosts at time-step i
    data[i,1]=S                   # Total number of S hosts at time-step i
    data[i,2]=np.mean(I)          # Average strain value v at time-step


# Plot temporal trajectories

plt.figure(1)
plt.plot(data[:,0],'r')                    # Temporal trajectory I hosts
plt.plot(data[:,1],'b')                    # Temporal trajectory S hosts
plt.hlines(Ieq,0,n_iterations,'r','--')    # Equilibrium I deterministic
    theory
plt.hlines(Seq,0,n_iterations,'b','--')    # Equilibrium S deterministic
    theory
plt.xlabel("timestep")
plt.ylabel("number hosts")
plt.legend(['Infected hosts', 'Susceptible hosts',])

plt.figure(2)
plt.plot(data[:,2],'k')                     # Temporal trajectory average
    strain value v
plt.hlines(avg_x,0,n_iterations,'k','--')  # Equilibrium average trait x
    determistic theory
plt.xlabel("timestep")
plt.ylabel("average trait")

# Save data
```

```
np.savetxt(name_dataset + ".csv", data, delimiter=",")
data_eq=np.array([Ieq,Seq,avg_x])
np.savetxt(name_dataset + "_eq" + ".csv",data_eq,delimiter=",")
```

A.2. The method of the generating function

Here I apply the method of the generating function to derive the Fokker-Plank equation from the master equation. I define the generating function $\zeta(h_A, t)$ associated to the master equation as:

$$\zeta(h_A, t) = \sum_{N_A} e^{N_A h_A} P(N_A, t), \tag{A.1}$$

where $h_A < 0$ is the variable conjugate to N_A. By construction, the following important relation holds:

$$\frac{\partial \zeta(h_A, t)}{\partial h_A} = \zeta' = \sum_{N_A} N_A e^{N_A h_A} P(N_A, t), \tag{A.2}$$

where the prime notation refers to the derivative with respect to h_A. In order to derive the equation describing the temporal evolution of $\zeta(h_A, t)$, I multiply both sides of Eq. (2.16) by the term $e^{N_A h_A}$, and sum over N_A:

$$\begin{aligned} &\sum_{N_A} e^{N_A h_A} \frac{\partial P(N_A, t)}{\partial t} = \frac{\partial \zeta(h_A, t)}{\partial t} = \\ &\sum_{N_A} e^{N_A h_A} T^+(N_A - 1) P(N_A - 1) - \sum_{N_A} e^{N_A h_A} T^+(N_A) P(N_A) r \\ &+ \sum_{N_A} e^{N_A h_A} T^-(N_A + 1) P(N_A + 1) - \sum_{N_A} e^{N_A h_A} T^-(N_A) P(N_A). \end{aligned} \tag{A.3}$$

By rearranging the sums of the right-hand side, I obtain:

$$\frac{\partial \zeta(h_A, t)}{\partial t} = \sum_{N_A} \left(e^{h_A} - 1\right) T^+(N_A) e^{N_A h_A} P(N_A) + \sum_{N_A} \left(e^{-h_A} - 1\right) T^-(N_A) e^{N_A h_A} P(N_A). \tag{A.4}$$

Recalling the property Eq. (A.2), I obtain the equation for temporal evolution of ζ in h_A and t:

$$\begin{aligned}\frac{\partial\zeta(h_A,t)}{\partial t} = &\left(e^{h_A}-1\right)\left[\gamma\left(1+\omega\right)\left(\frac{\zeta'}{N}-\frac{\zeta''}{N^2}\right)+\mu\left(\zeta-\frac{\zeta'}{N}\right)\right]\\ &+\left(e^{-h_A}-1\right)\left[\gamma\left(1-\omega\right)\left(\frac{\zeta'}{N}-\frac{\zeta''}{N^2}\right)+\mu\frac{\zeta'}{N}\right].\end{aligned} \tag{A.5}$$

Next, I assume the existence of a small parameter $\epsilon \to 0$, and introduce the rescaled conjugated variable $\epsilon s_A = h_A$. Performing a Taylor expansion with respect to ϵ on the exponential functions, I obtain:

$$\begin{aligned}\frac{\partial\zeta(s_A,t)}{\partial t} = &\left(1+\epsilon s_A+\frac{1}{2!}s_A^2+\cdots-1\right)\left[\gamma\left(1+\omega\right)\left(\frac{\zeta'}{\epsilon N}-\frac{\zeta''}{\epsilon^2N^2}\right)+\mu\left(\zeta-\frac{\zeta'}{\epsilon N}\right)\right]\\ &+\left(1-\epsilon s_A+\frac{1}{2!}S^2+\cdots-1\right)\left[\gamma\left(1-\omega\right)\left(\frac{\zeta'}{\epsilon N}-\frac{\zeta''}{\epsilon^2N^2}\right)+\mu\frac{\zeta'}{\epsilon N}\right],\end{aligned} \tag{A.6}$$

where now the prime notation denotes the derivative with respect to the rescaled variable s_A. Truncating the expansion at second order and collecting the terms of same order in s_A, I obtain:

$$\begin{aligned}\frac{\partial\zeta(s_A,t)}{\partial t} =&s_A\left[\frac{2\gamma\omega}{N}\left(\zeta'-\frac{\zeta''}{\epsilon N}\right)+\mu\left(\epsilon\zeta-\frac{2}{N}\zeta'\right)\right]\\ &+\frac{1}{2}s_A^2\left[\frac{2\gamma}{N}\left(\epsilon\zeta'-\frac{\zeta'}{N}\right)+\epsilon^2\mu\zeta\right].\end{aligned} \tag{A.7}$$

Equation (A.7) allows to derive the diffusion approximation for various regimes, corresponding to different interpretations of the scaling parameter ϵ. The usual system size expansion (equivalent to the Kramers-Moyal approach) is recovered by setting

$\epsilon = \frac{1}{N}$. In this case, Eq. (A.7) becomes:

$$\begin{aligned}\frac{\partial \zeta(s_A,t)}{\partial t} =& \frac{1}{N} s_A \left[2\gamma\omega\left(\zeta' - \zeta''\right) + \mu\left(\zeta - 2\zeta'\right)\right] \\ &+ \frac{1}{2N^2} s_A^2 \left[2\gamma\left(\zeta' - \zeta'\right) + \mu\zeta\right].\end{aligned} \tag{A.8}$$

Introducing the rescaled time $N\tau = t$, the rescaled continuous variable $n_A = \frac{N_A}{N}$, and performing the backward transformation on $\zeta(s_A, t)$, I finally get the Fokker-Planck equation for the density probability $P(n_A, \tau)$:

$$\begin{aligned}\frac{\partial P(n_A,\tau)}{\partial \tau} =& -\frac{\partial}{\partial n_A}\left\{\left[2\gamma\omega n_A\left(1-n_A\right) + \mu\left(1-2n_A\right)\right] P(n_A,\tau)\right\} \\ &+ \frac{1}{2N}\frac{\partial^2}{\partial n_A^2}\left\{\left[2\gamma n_A\left(1-n_A\right) + \mu\right] P(n_A,\tau)\right\}.\end{aligned} \tag{A.9}$$

It is customary to recast the above Fokker-Plank equation in the form of a continuity equation:

$$\frac{\partial P(n_A,\tau)}{\partial \tau} = -\nabla J(n_A,\tau), \tag{A.10}$$

where $J(n_A, \tau)$ is the probability current:

$$J(n_A,\tau) = a(n_A)P(n_A,\tau) - \frac{1}{2}\frac{\partial}{\partial n_A} b(n_A)P(n_A,\tau), \tag{A.11}$$

with:

$$\begin{cases} a(n_A) = 2\gamma\omega n_A\left(1-n_A\right) + \mu\left(1-2n_A\right) \\ b(n_A) = \frac{1}{N}\left[2\gamma n_A\left(1-n_A\right) + \mu\right], \end{cases} \tag{A.12}$$

as shown in Subsection 2.1.5.

A.3. Spectral method

Given a two-dimensional trait space $\mathcal{T}_2$ and the trait distribution $n(x, y)$ solution of the sRME Eq. (3.10), the rationale of the spectral method is to look for a solution of the form:

$$n(x, y) = \sum_{i,j} a_{i,j} e_{i,j}(x, y), \tag{A.13}$$

where the $e_{i,j}(x, y)$ are the eigenfunctions of the Helmholtz problem with Neuman boundary conditions, on trait space considered. However, the number of two-dimensional domains for which such eigenfunctions are known is limited. Therefore, in order to proceed with analytical calculations, one has to choose particular shapes of the trait space.

Asymmetric landscape

For the asymmetric landscape $\mathcal{T}_2^{\mathrm{a}} = \{0 \leq x \leq 1, 0 \leq y \leq \mathcal{B}(x)\}$, with linear boundary profile $\mathcal{B}(x) = 1 - x$, the trait space becomes a right triangle. The Helmoholtz problem with Neumann boundary conditions reads:

$$\begin{cases} \nabla^2 e_{i,j}(x, y) = \lambda_{i,j}\, e_{i,j}(x, y) \\ \frac{\partial e_{i,j}(x,y)}{\partial x} \,|_{x=0} = \frac{\partial e_{i,j}(x,y)}{\partial y} \,|_{y=0} = \frac{\partial e_{i,j}(x,y)}{\partial x} + \frac{\partial e_{i,j}(x,y)}{\partial y} \,|_{y=1-x} = 0. \end{cases} \tag{A.14}$$

The above problem is solved by Prager's method (Damle and Peterson, 2010): first, the eigenfunctions corresponding to the same problem on the square domain are found; then these functions are "folded" around the diagonal with a linear transformation.

The resulting normalised eigenfunctions and relative eigenvalues are:

$$\begin{cases} e_{0,0} = 2 \\ e_{i,j}(x,y) = \mathcal{Z}_{i,j}\big[\cos(i\pi x)\,\cos(j\pi y) + (-1)^{i+j}\,\cos(i\pi y)\,\cos(j\pi x)\big] \quad \forall i,j \neq 0 \\ \lambda_{i,j} = -\pi^2\,(i^2+j^2)\,, \end{cases} \tag{A.15}$$

with $\mathcal{Z}_{i,j} = \sqrt{2} + \left(2-\sqrt{2}\right)\delta_{i,j} + \left(2-\sqrt{2}\right)\delta_{j,0}$ constant of normalisation. The above eigenfunctions have the same properties:

$$\begin{cases} \int_0^1 \int_0^{1-x} e_{i,j}\, e_{k,l}\, dxdy = \delta_{i,k}\,\delta_{j,l} & \textit{orthonormality} \\ e_{i,j}(x,y) = (-1)^{i+j}\, e_{j,i}(x,y) & \textit{symmetry} \\ \int_0^1 \int_0^{1-x} e_{i,j}(x,y)\, dxdy = 0 \quad \forall\, i,j \neq 0. & \end{cases} \tag{A.16}$$

Due to the symmetry property, only half of the $\{e_{i,j}\}$ are needed to create a complete orthonormal basis for L^2. Hence, the expansion reads:

$$n(x,y) = \sum_{i=1}^{+\infty} \sum_{j=0}^{i} a_{i,j} e_{i,j}(x,y). \tag{A.17}$$

Combining the normalisation constraint on the solution with the last property in Eq. (A.16), we get:

$$\int_0^1 \int_0^{1-x} n(x,y)\, dxdy = a_{0,0} + 0 + \cdots + 0 = 1. \tag{A.18}$$

Hence, the zero coefficient of the expansion is $a_{0,0} = 1$. In order to find the remaining coefficients, I insert the expansion Eq. (A.17) into Eq. (3.10), then I multiply by $e_{k,l}(x,y)$, and integrate over the triangle domain. Using the orthonormalisation

condition and rearranging the terms, we get:

$$\left(\lambda_{k,l} - \delta\phi + \delta\langle\, F(x)\,\rangle_{k,l;k,l}\right) a_{k,l} \;+\; \delta \sum_{i\neq k}^{+\infty} \sum_{j\neq l}^{i} a_{i,j}\, \langle\, F(x)\,\rangle_{i,j;k,l} = -\delta\, \langle\, F(x)\,\rangle_{0,0;k,l}, \tag{A.19}$$

where the notation $\langle\, \cdot\,\rangle_{i,j;k,l}$ indicates the average over $e_{i,j}(x,y)\, e_{k,l}(x,y)$, *e.g.*:

$$\langle\, x\,\rangle_{i,j;k,l} = \int_0^1 \int_0^{\mathcal{B}(x)} x\, e_{i,j}(x,y)\, e_{k,l}(x,y)\, dxdy. \tag{A.20}$$

The Eq. (A.19) represents an infinite system of linear equations for the unknown coefficients $\{a_{i,j}\}$ (I remind that at this stage the coefficients still depend on the average fitness ϕ). In order to solve the problem, I truncate the system to the first M eigenfunctions, then solve the linear problem with MATLAB's function *linsolve*(). At this point, I have found the M $\phi-$dependent coefficients $a^{\phi}_{i,j}$ of the spectral expansion. Finally, the solution is closed by solving numerically the self-consistent condition on the average fitness Eq. (3.11).

Symmetric landscape

In the symmetric case, the dynamics takes place in the trait space $\mathcal{T}_2^{\mathrm{s}} = \{x, y \mid x^2 + y^2 \leq 1\}$, that is a disk of radius 1. The eigenfunctions of the Helmholtz eigenfunctions on the disk with Neumann boundary conditions are given by:

$$e_k(r) = J_0\left(\beta_{0,k}\, r\right), \tag{A.21}$$

where J_0 is the Bessel function of first kind for order zero, and $\beta_{0,k}$ is the positive k^{th} root of the first derivative J_0' (Grebenkov and Nguyen, 2013). The radial function

$R(r)$ is then written as:

$$R(r) = \sum_k c_k \, J_0 \left(\beta_{0,k} \, r \right), \tag{A.22}$$

where c_k is the k-th coefficient of the expansion- Again, it is straightforward to show that the first coefficient $c_0 = 2$ is fixed by the normalisation constraint. Substituting Eq. (A.22) into Eq. (3.21) and exploiting the orthonormalisation properties of the eigenfunctions (Bowman, 2012), I obtain the linear system of equations for the other coefficients $\{c_k\}$ of the expansion:

$$c_l \left(-\delta \, \phi - \beta_l^2 \right) \frac{J_0(\beta_l)^2}{2} + \delta \sum_{k=1}^{+\infty} c_k \, \langle \, F(r) \, \rangle_{k,l} = 0, \tag{A.23}$$

with:

$$\langle \, F(r) \, \rangle_{k,l} = \int_0^1 F(r) \, J_0 \left(\beta_k r \right) \, J_0 \left(\beta_l r \right) \, r \, dr. \tag{A.24}$$

Similarly to the asymmetric case, Eq. (A.23) represents an infinite system of linear equations for the unknown coefficients $a_{i,j}$ of the spectral solution Eq. (A.22). truncating the system of equations to a finite number of terms, one first solves the above linear problem with standard numerical routines, then finds ϕ solving the self-consistent condition on the average fitness. The system is solved likewise the asymmetric case: I truncate the system to the first M eigenfunctions, and find the M $\phi-$dependent coefficients $a_{i,j}^{\phi}$ with MATLAB's function *linsolve*(). Finally, I close the solution by numerically solving the self-consistent condition on the average fitness Eq. (3.22).

A.4. Total rate of reaction for trait-structured Gillespie algorithm

Recall that the microscopic dynamics is given by mutation events occurring at rate μ per individual, and by competition events occurring at rate γ per pair of individuals. Consider a focal phenotype $\underline{\mathbf{x}}$. Following the formalism of transition rates presented in

Subsection 2.1.4, the rate at which individuals with phenotype $\underline{\mathbf{x}}$ mutate is proportional to $\mu n(\underline{\mathbf{x}})$, and the total rate of mutation events is then obtained integrating over all possible focal phenotypes, that is:

$$\int_0^1 \mu n(\underline{\mathbf{x}}) d\underline{\mathbf{x}} = \mu \tag{A.25}$$

(remember that $\int_{\mathcal{T}} n(\underline{\mathbf{x}}) d\underline{\mathbf{x}} = 1$ due to normalisation). Concomitantly, the rate at which individuals with the focal phenotype $\underline{\mathbf{x}}$ compete with another phenotype $\underline{\mathbf{x}}'$ is proportional to $\gamma n(\underline{\mathbf{x}}) n(\underline{\mathbf{x}}')$; the total rate at which individuals with focal phenotype compete is obtained integrating over all other competing phenotypes $\underline{\mathbf{x}}'$, that is:

$$\int_0^1 \gamma n(\underline{\mathbf{x}}) n(\underline{\mathbf{x}}') d\underline{\mathbf{x}}' = \gamma n(\underline{\mathbf{x}}). \tag{A.26}$$

Finally, the total rate of competition events is again obtained integrating over all possible focal phenotypes, that is:

$$\int_0^1 \gamma n(\underline{\mathbf{x}}) d\underline{\mathbf{x}} = \gamma. \tag{A.27}$$

Therefore, the total reaction rate r_{tot} of events is fixed and equal to $r_{\text{tot}} = \mu + \gamma$.

A.5. Marginal fitness distribution in the weak selection limit for asymmetric landscape

For the asymmetric landscape with triangular shape and linear fitness function, it is possible to obtain a closed analytical approximation of the marginal fitness distribution $\mathcal{N}^a(f)$, based on a linear perturbation expansion on δ. For small values of δ (known as the weak selection limit), I assume that the trait distribution is given by a perturbation of the neutral solution. Starting from the spectral form Eq. (A.13), I assume the

coefficients $a_{i,j}$ of the expansion to be of first order in δ:

$$a_{i,j} = O(\delta), \quad \forall i,j \neq 0. \tag{A.28}$$

Inserting this assumption into the system Eq. (A.19) and retaining only the terms of first order in δ, I get:

$$a_{i,j} = -\delta \frac{\langle x \rangle_{0,0;i,j}}{\lambda_{i,j}}, \tag{A.29}$$

with $\lambda_{i,j}$ being the eigenvalues Eq. (A.15) and $\langle x \rangle_{0,0;i,j}$ the averages according to notation Eq. (A.20). Computing the values of the averages for the linear fitness function $F(x) = x$, and of the eigenvalues one obtains:

$$n(x,y) = 2 + \delta\Big\{ -4 \sum_{k=1}^{+\infty} \frac{1}{k^4\pi^4} e_{k,0}(x,y) + 4 \sum_{k=1}^{+\infty} \frac{(-1)^k}{k^4\pi^4} e_{k,k}(x,y) \Big\} + O(\delta^2) = \tag{A.30}$$

$$2 + \delta\Big\{ -4 \sum_{k=1}^{+\infty} \frac{1}{k^4\pi^4} \left[\cos(k\pi x) + (-1)^k \cos(k\pi y) \right] + 4 \sum_{k=1}^{+\infty} \frac{(-1)^k}{k^4\pi^4} \cos(k\pi x)\cos(k\pi y) \Big\} + O(\delta^2).$$

Integrating Eq. (A.30) over the neutral variable y and replacing the selective variable x with its fitness value f (recall that $f = x$), I obtain the marginal fitness distribution $\mathcal{N}^a(f)$:

$$\begin{aligned} \mathcal{N}^a(f) =& 2(1-f) + \delta\Big\{ -4(1-f) \sum_{k=1}^{+\infty} \frac{1}{k^4\pi^4} \cos(k\pi f) + \\ &+ 4 \sum_{k=1}^{+\infty} \frac{1}{k^5\pi^5} \sin(k\pi f) - 4 \sum_{k=1}^{+\infty} \frac{1}{k^5\pi^5} \cos(k\pi f)\sin(k\pi f) \Big\} + O(\delta^2). \end{aligned} \tag{A.31}$$

Using the properties of the trigonometric functions, the sums appearing in Eq. (A.31) can be evaluated in terms of Bernoulli polynomials (Gradshteyn and Ryzhik, 2014). Finally, I obtain:

$$\mathcal{N}^a(f) = \mathcal{N}^0(f) + \delta \mathcal{N}^{\,\mathrm{I}}(f) + O\left(\delta^2\right), \tag{A.32}$$

with:

$$\begin{cases} \mathcal{N}^0(f) = 2(1-f) \\ \mathcal{N}^{\,\mathrm{I}}(f) = \left\{ \frac{4}{3}(1-f)B_4(\frac{f}{2}) - \frac{8}{15}B_5(\frac{f}{2}) + \frac{4}{15}B_5(f) \right\}, \end{cases} \tag{A.33}$$

where $B_k(z)$ is the k^{th}-order Bernoulli polynomial of the variable z. Equation (A.32) is composed of two terms: the first term $\mathcal{N}_0^a(f)$ is the purely neutral contribution, corresponding to the monotonically decreasing linear profile; the second term $\mathcal{N}_{\mathrm{I}}^a(f)$ is the first order correction to the neutral profile, with respect to δ. The average fitness ϕ_{pert} predicted by the perturbative solution is given by:

$$\begin{aligned} \phi_{\text{pert}} &= \int_0^1 x \left\{ \mathcal{N}^0(f) + \delta \mathcal{N}^{\,\mathrm{I}}(f) \right\} + O\left(\delta^2\right) \\ &= \frac{1}{3} + \frac{1}{189}\,\delta + O\left(\delta^2\right). \end{aligned} \tag{A.34}$$

Equation (A.32) can be used to estimate the threshold value δ at which the intermediate maximum appears in the marginal fitness distribution. The first derivative of Eq. (A.32) reads:

$$\frac{\partial \mathcal{N}^a(f)}{\partial f} = -2 + \frac{1}{90}\delta \Big\{ 75f^4 - 60f^3 - 90f^2 + 60f + 4 \Big\}. \tag{A.35}$$

A local maximum exists whenever $\frac{\partial \mathcal{N}^a(f)}{\partial f} = 0$, that is whenever the following condition is satisfied:

$$75f^4 - 60f^3 - 90f^2 + 60f + 4 = \frac{180}{\delta}, \tag{A.36}$$

which is treated by graphical comparison in Fig. A.1. The minimum value of δ for which the lines $y = \frac{180}{\delta}$ and $y = 75f^4 - 60f^3 - 90f^2 + 60f$ intersect, correspond to the local maximum of the latter. The local maximum is located at $x = \frac{\sqrt{6}-1}{5}$ and has value of $\simeq 12.9$. Hence, the threshold value δ_{th} predicted by the perturbative approximation is:

$$\delta_{\text{th}} = \frac{180}{12.9} \simeq 13.95. \tag{A.37}$$

Below $\delta_{\rm th}$, there is no solution to Eq. (A.36), and the marginal fitness distribution $\mathcal{N}^a(f)$ is monotonically decreasing (corresponding to the *redundancy-dominated* regime). Above $\delta_{\rm th}$, the condition Eq. (A.36) has two solutions, indicating the presence of a new pair of local maximum and minimum. This estimation is consistent with the diagram of extrema positions obtained using the exact spectral solution (Fig. 4 of main text). The perturbative solution also gives a good estimation of the average fitness ϕ, up to $\delta \simeq 30$ (left panel Fig. A.2), that is when the linear prediction given by Eq. (A.34) is accurate. For large values of δ, second order contributions due to selection become important and the perturbative solution fails. Indeed, in the right panel of Fig. A.2 we can see that spectral (solid lines) and perturbative (dashed lines) profiles of the marginal fitness distributions agree almost perfectly for small δ (black line $\delta = 10$ case), and are qualitative consistent for intermediate values (black line $\delta = 30$ case). However, for higher values the approximation breaks down and also stops having biological value, as the distribution attains forbidden negative values (blue line $\delta = 50$ case).

A.6. Analytical solution of SISx trait distribution

Recall that under the choice of linear trait-dependent epidemiological trait functions (Eqs. (4.15)-(4.17)), the sRME for the stationary trait distribution is:

$$\mu\nabla^2\,\widehat{i(x)} + \frac{\Omega}{\beta_0+\beta_1\overline{x}}\,\widehat{i(x)}\,[x-\overline{x}] = 0, \tag{A.38}$$

with

$$\Omega = \beta_1\,(\delta+\nu_0) - \beta_0\nu_1 + c\,[\beta_1 - \beta_1\phi_1/2 - \beta_0\phi_1]\,. \tag{A.39}$$

If $\Omega > 0$, performing the transformation of variable $z = \sqrt[3]{\frac{\Omega}{\mu[\beta_0+\beta_1 x]}}\,(\overline{x}-x)$, the sRME becomes:

$$\frac{d^{\,2}\,i(z)}{d\,z^{\,2}} \;-\; z\,n(z) = 0, \tag{A.40}$$

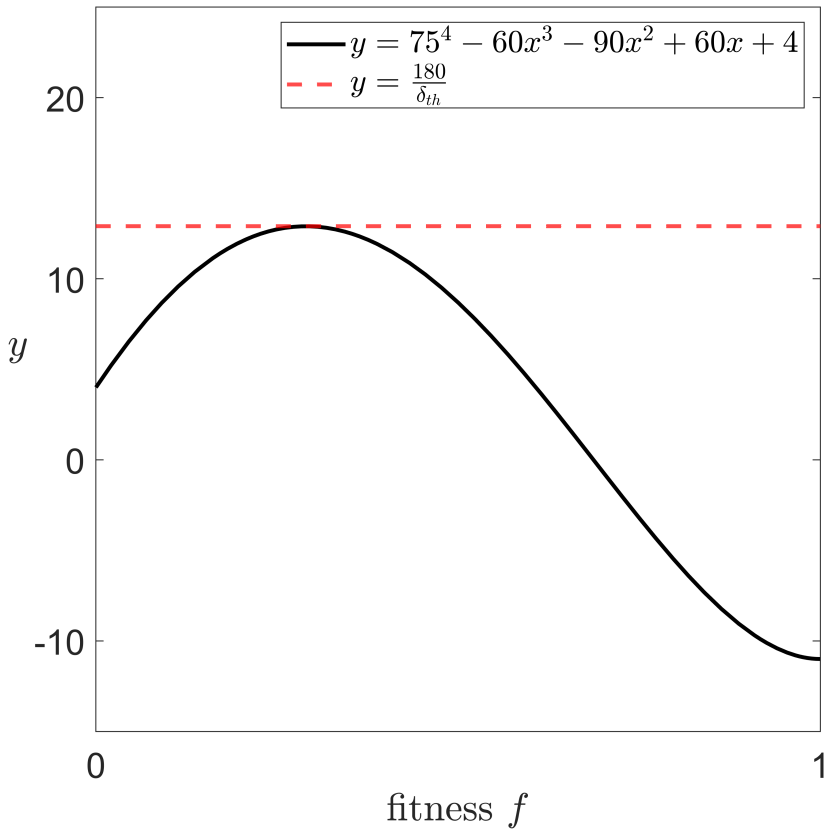

Figure A.1: **Perturbative estimation of the threshold value δ_{th}.** The intersection between the left-hand side (black line) of Eq. (A.36) and horizontal lines gives the position of the local maxima and minima of the marginal fitness profiles, under the perturbative approach. The value of δ for which they intersect for the first time corresponds to the threshold value δ_{th} (red dashed line) predicted by the perturbative approach. Below δ_{th}, there is no intersection, hence no local extrema are present in the interior of the genomic space. Above δ_{th}, horizontal lines intersect twice the black line, identifying a pair of local maxima and minima, in agreement with the behaviour of the spectral solutions.

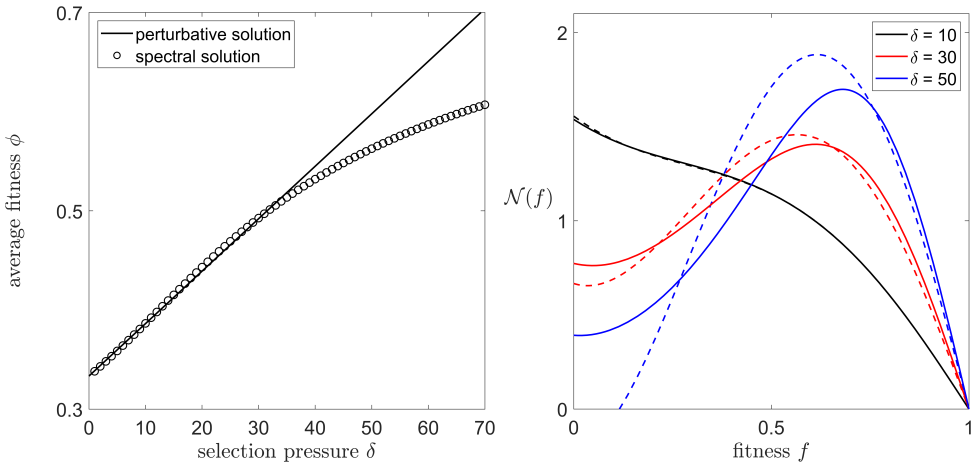

Figure A.2: **Perturbative *versus* spectral predictions.** Left panel: Comparison between perturbative (black line) and spectral (circles) estimation of the average fitness ϕ, at the varying of δ, in the case of asymmetric landscape. The perturbative solution gives a good estimate up to $\delta \simeq 30$. Right panel: Comparison between perturbative (dashed lines) and spectral (solid lines) profiles of the marginal fitness distribution. As we can see, the perturbative solution works very well for small δ (black lines), that is in the *degeneracy-dominated* regime. For intermediate values of δ (red lines), the two profiles start diverging, yet the perturbative one still captures the qualitative behaviour. For large values of δ (blue lines), the perturbative approximation breaks down, giving negative non-biological profiles.

which is an Airy differential equation such as that analysed in Chapter 2. The solution is then a linear combination of the Airy functions of first and second kind which, back in the original variable, reads:

$$\widehat{i_{\overline{x}}(x)} = \mathcal{Z}\Big\{\mathrm{Ai}\left[\gamma\left(\overline{x}-x\right)\right] + \mathcal{C}\,\mathrm{Bi}\left[\gamma\left(\overline{x}-x\right)\right]\Big\}, \quad \gamma = \sqrt[3]{\frac{|\Omega|}{\mu\left(\beta_0+\beta_1\overline{x}\right)}}, \tag{A.41}$$

with $\mathcal{Z}$ and $\mathcal{C}$ constants of integration given by (prime notation indicates the x derivative):

$$\mathcal{C} = -\frac{\mathrm{Ai}'\left(\gamma\overline{x}\right)}{\mathrm{Bi}'\left(\gamma\overline{x}\right)} \tag{A.42.a}$$

$$\mathcal{Z}^{-1} = \int_{\mathcal{T}} \mathrm{Ai}\left[\gamma\left(\overline{x}-x\right)\right] + \mathcal{C}\,\mathrm{Bi}\left[\gamma\left(\overline{x}-x\right)\right]\,dx \tag{A.42.b}$$

Equation (A.41) represents the $\overline{x}$-family of solutions to Eq. (A.38). The correct solution can be identified self-consistently by solving the constraint related to the average quantity:

$$\overline{x} = \int_{\mathcal{T}} x\,\widehat{i_{\overline{x}}(x)}\,dx. \tag{A.43}$$

This last step can be performed numerically by means of standard routines such as MATLAB or Python's *fsolve*() function. If $\Omega < 0$, equivalent solutions to Eq. (A.38) can be found upon replacing x with $(1-x)$.

Bibliography

Abramowitz, M. and Stegun, I. (1964). *Handbook of mathematical functions: with formulas, graphs, and mathematical tables*, volume 55. Courier Corporation.

Aguirre, J., Buldú, J. M., and Manrubia, S. C. (2009). Evolutionary dynamics on networks of selectively neutral genotypes: Effects of topology and sequence stability. *Physical Review E*, 80(6):066112.

Ahnert, S. E. (2017). Structural properties of genotype–phenotype maps. *Journal of The Royal Society Interface*, 14(132):20170275.

Alfaro, M. and Carles, R. (2017). Replicator-mutator equations with quadratic fitness. *Proceedings of the American Mathematical Society*, 145(12):5315–5327.

Alfaro, M. and Veruete, M. (2019). Evolutionary branching via replicator–mutator equations. *Journal of Dynamics and Differential Equations*, 31(4):2029–2052.

Alizon, S., Hurford, A., Mideo, N., and Van Baalen, M. (2009). Virulence evolution and the trade-off hypothesis: history, current state of affairs and the future. *Journal of evolutionary biology*, 22(2):245–259.

Alves, D. and Fontanari, J. F. (1998). Error threshold in finite populations. *Physical review E*, 57(6):7008.

Amicone, M. and Gordo, I. (2020). Molecular signatures of resource competition: clonal interference drives the emergence of ecotypes. *bioRxiv*.

Anderson, R. M. and May, R. M. (1981). The population dynamics of microparasites and their invertebrate hosts. *Philosophical Transactions of the Royal Society of London. B, Biological Sciences*, 291(1054):451–524.

Avery, S. V. (2006). Microbial cell individuality and the underlying sources of heterogeneity. *Nature Reviews Microbiology*, 4(8):577–587.

Baake, E. and Wagner, H. (2001). Mutation–selection models solved exactly with methods of statistical mechanics. *Genetics Research*, 78(1):93–117.

Balázsi, G., van Oudenaarden, A., and Collins, J. J. (2011). Cellular decision making and biological noise: from microbes to mammals. *Cell*, 144(6):910–925.

Barghi, N., Hermisson, J., and Schlötterer, C. (2020). Polygenic adaptation: a unifying framework to understand positive selection. *Nature Reviews Genetics*, pages 1–13.

Barton, N. H. and Coe, J. (2009). On the application of statistical physics to evolutionary biology. *Journal of theoretical biology*, 259(2):317–324.

Beardmore, R. E., Gudelj, I., Lipson, D. A., and Hurst, L. D. (2011). Metabolic trade-offs and the maintenance of the fittest and the flattest. *Nature*, 472(7343):342.

Begg, G. S., Cook, S. M., Dye, R., Ferrante, M., Franck, P., Lavigne, C., Lövei, G. L., Mansion-Vaquie, A., Pell, J. K., Petit, S., Quesada, N., Ricci, B., Wratten, S. D., and Birch, A. N. E. (2017). A functional overview of conservation biological control. *Crop Protection*, 97:145–158.

Begon, M., Bennett, M., Bowers, R. G., French, N. P., Hazel, S., and Turner, J. (2002). A clarification of transmission terms in host-microparasite models: numbers, densities and areas. *Epidemiology & Infection*, 129(1):147–153.

Biancalani, T. (2014). *The Influence of Demographic Stochasticity on Population Dynamics: A Mathematical Study of Noise-Induced Bistable States and Stochastic Patterns*. Springer.

Blythe, R. A. and McKane, A. J. (2007). Stochastic models of evolution in genetics, ecology and linguistics. *Journal of Statistical Mechanics: Theory and Experiment*, 2007(07):P07018.

Boccabella, A., Natalini, R., and Pareschi, L. (2011). On a continuous mixed strategies model for evolutionary game theory. *Kinetic & Related Models*, 4(1):187.

Bolzoni, L. and De Leo, G. A. (2013). Unexpected consequences of culling on the eradication of wildlife diseases: the role of virulence evolution. *The American Naturalist*, 181(3):301–313.

Bomze, I. M. and Burger, R. (1995). Stability by mutation in evolutionary games. *Games and Economic Behavior*, 11(2):146–172.

Bonduriansky, R. and Day, T. (2009). Nongenetic inheritance and its evolutionary implications. *Annual Review of Ecology, Evolution, and Systematics*, 40:103–125.

Bonduriansky, R. and Day, T. (2019). Extended heredity: A new understanding of inheritance and evolution.

Bowman, F. (2012). *Introduction to Bessel functions*. Courier Corporation.

Bu, R. et al. (1988). Mutation-selection balance and continuum-of-alleles models. *Mathematical biosciences*, 91(1):67–83.

Bull, J. J. (1994). Virulence. *Evolution*, 48(5):1423–1437.

Bürger, R. (1986). On the maintenance of genetic variation: global analysis of kimura's continuum-of-alleles model. *Journal of mathematical biology*, 24(3):341–351.

Callahan, H. S., Pigliucci, M., and Schlichting, C. D. (1997). Developmental phenotypic plasticity: where ecology and evolution meet molecular biology. *Bioessays*, 19(6):519–525.

Carja, O. and Plotkin, J. B. (2017). The evolutionary advantage of heritable phenotypic heterogeneity. *Scientific reports*, 7(1):1–12.

Carvalho, F. P. (2017). Pesticides, environment, and food safety. *Food and Energy Security*, 6(2):48–60.

Castle, M. D. and Gilligan, C. A. (2012). An epidemiological framework for modelling fungicide dynamics and control. *PLoS One*, 7(8):e40941.

Chisholm, R. H., Lorenzi, T., Lorz, A., Larsen, A. K., de Almeida, L. N., Escargueil, A., and Clairambault, J. (2015). Emergence of drug tolerance in cancer cell populations: an evolutionary outcome of selection, nongenetic instability, and stress-induced adaptation. *Cancer research*, 75(6):930–939.

Ciliberti, S., Martin, O. C., and Wagner, A. (2007a). Innovation and robustness in complex regulatory gene networks. *Proceedings of the National Academy of Sciences*, 104(34):13591–13596.

Ciliberti, S., Martin, O. C., and Wagner, A. (2007b). Robustness can evolve gradually in complex regulatory gene networks with varying topology. *PLoS computational biology*, 3(2):e15.

Codoner, F. M., Darós, J.-A., Solé, R. V., and Elena, S. F. (2006). The fittest versus the flattest: experimental confirmation of the quasispecies effect with subviral pathogens. *PLoS pathogens*, 2(12):e136.

Cunniffe, N. J. and Gilligan, C. A. (2010). Invasion, persistence and control in epidemic models for plant pathogens: the effect of host demography. *Journal of the Royal Society Interface*, 7(44):439–451.

Damle, A. and Peterson, G. C. (2010). Understanding the eigenstructure of various triangles. *SIAM Undergraduate Research Online*, 3(1):187–208.

Day, T. (2005). 13— modelling the ecological context of evolutionary change: Déjà vu or something new? *Ecological paradigms lost: routes of theory change*, page 273.

Day, T. and Gandon, S. (2006). Insights from price's equation into evolutionary. *Disease evolution: models, concepts, and data analyses*, 71:23.

Day, T., Parsons, T., Lambert, A., and Gandon, S. (2020). The price equation and evolutionary epidemiology. *Philosophical Transactions of the Royal Society B*, 375(1797):20190357.

Day, T. and Proulx, S. R. (2004). A general theory for the evolutionary dynamics of virulence. *The American Naturalist*, 163(4):E40–E63.

De Martino, A., Gueudré, T., and Miotto, M. (2019). Exploration-exploitation tradeoffs dictate the optimal distributions of phenotypes for populations subject to fitness fluctuations. *Physical Review E*, 99(1):012417.

De Martino, D., Capuani, F., and De Martino, A. (2016). Growth against entropy in bacterial metabolism: the phenotypic trade-off behind empirical growth rate distributions in e. coli. *Physical biology*, 13(3):036005.

De Visser, J. A. G. and Krug, J. (2014). Empirical fitness landscapes and the predictability of evolution. *Nature Reviews Genetics*, 15(7):480–490.

De Waard, M. A., Andrade, A. C., Hayashi, K., Schoonbeek, H.-j., Stergiopoulos, I., and Zwiers, L.-H. (2006). Impact of fungal drug transporters on fungicide sensitivity, multidrug resistance and virulence. *Pest Management Science: formerly Pesticide Science*, 62(3):195–207.

Débarre, F., Lenormand, T., and Gandon, S. (2009). Evolutionary epidemiology of drug-resistance in space. *PLoS Comput Biol*, 5(4):e1000337.

DeJong-Lambert, W. (2012). *The Cold War politics of genetic research: An introduction to the Lysenko affair*, volume 32. Springer Science & Business Media.

Dieckmann, U., Metz, J. A., and Sabelis, M. W. (2005). *Adaptive dynamics of infectious diseases: in pursuit of virulence management*. Number 2. Cambridge University Press.

Doebeli, M., Ispolatov, Y., and Simon, B. (2017). Point of view: Towards a mechanistic foundation of evolutionary theory. *Elife*, 6:e23804.

Domingo, E., Sheldon, J., and Perales, C. (2012). Viral quasispecies evolution. *Microbiology and Molecular Biology Reviews*, 76(2):159–216.

Draghi, J. A., Parsons, T. L., Wagner, G. P., and Plotkin, J. B. (2010). Mutational robustness can facilitate adaptation. *Nature*, 463(7279):353.

Dudley, N. and Alexander, S. (2017). Agriculture and biodiversity: a review. *Biodiversity*, 18(2-3):45–49.

Dutta, A., Croll, D., McDonald, B. A., and Barrett, L. G. (2020). Maintenance of variation in virulence and reproduction in populations of an agricultural plant pathogen. *bioRxiv*.

Eigen, M., McCaskill, J., and Schuster, P. (1988). Molecular quasi-species. *The Journal of Physical Chemistry*, 92(24):6881–6891.

Eigen, M. and Schuster, P. (1977). A principle of natural self-organization. *Naturwissenschaften*, 64(11):541–565.

Elderfield, J. A., Lopez-Ruiz, F. J., van den Bosch, F., and Cunniffe, N. J. (2018). Using epidemiological principles to explain fungicide resistance management tactics: Why do mixtures outperform alternations? *Phytopathology*, 108(7):803–817.

Evans, R. (2018). Pay-off scarcity causes evolution of risk-aversion and extreme altruism. *Scientific reports*, 8(1):1–10.

Fisher, R. A. (1958). *The genetical theory of natural selection.* .

Fontana, W. (2006). The topology of the possible. In *Understanding Change*, pages 67–84. Springer.

Forster, G. A. and Gilligan, C. A. (2007a). Optimizing the control of disease infestations at the landscape scale. *Proceedings of the National Academy of Sciences*, 104(12):4984–4989.

Forster, G. A. and Gilligan, C. A. (2007b). Optimizing the control of disease infestations at the landscape scale. *Proceedings of the National Academy of Sciences of the United States of America*, 104(12):4984–4989.

Froissart, R., Doumayrou, J., Vuillaume, F., Alizon, S., and Michalakis, Y. (2010). The virulence–transmission trade-off in vector-borne plant viruses: a review of (non-) existing studies. *Philosophical Transactions of the Royal Society B: Biological Sciences*, 365(1548):1907–1918.

Galvani, A. P. (2003). Epidemiology meets evolutionary ecology. *Trends in Ecology & Evolution*, 18(3):132–139.

Gandon, S., Mackinnon, M. J., Nee, S., and Read, A. F. (2001). Imperfect vaccines and the evolution of pathogen virulence. *Nature*, 414(6865):751–756.

Gardiner, C. W. et al. (1985). *Handbook of stochastic methods*, volume 3. springer Berlin.

Garland, M., Loscher, S., and Bogyo, M. (2017). Chemical strategies to target bacterial virulence. *Chemical Reviews*, 117(5):4422–4461.

Gauwerky, K., Borelli, C., and Korting, H. C. (2009). Targeting virulence: a new paradigm for antifungals. *Drug discovery today*, 14(3-4):214–222.

Gavrilets, S. (2010). High-dimensional fitness landscapes and speciation. *Evolution: the extended synthesis*, pages 45–79.

Gerland, U. and Hwa, T. (2002). On the selection and evolution of regulatory dna motifs. *Journal of molecular evolution*, 55(4):386–400.

Gil, M.-E., Hamel, F., Martin, G., and Roques, L. (2019). Dynamics of fitness distributions in the presence of a phenotypic optimum: an integro-differential approach. *Nonlinearity*, 32(10):3485.

Gillespie, D. T. (1976). A general method for numerically simulating the stochastic time evolution of coupled chemical reactions. *Journal of computational physics*, 22(4):403–434.

Gillespie, D. T. (1977). Exact stochastic simulation of coupled chemical reactions. *The journal of physical chemistry*, 81(25):2340–2361.

Gilligan, C. A. (2002). An epidemiological framework for disease management.

Gilligan, C. A. (2008). Sustainable agriculture and plant diseases: an epidemiological perspective. *Philosophical Transactions of the Royal Society B: Biological Sciences*, 363(1492):741–759.

Gilligan, C. A. C. and van den Bosch, F. (2008). Epidemiological Models for Invasion and Persistence of Pathogens. *Annual Review of Phytopathology*, 46(1):385–418.

González, R., Butković, A., and Elena, S. F. (2019). Role of host genetic diversity for susceptibility-to-infection in the evolution of virulence of a plant virus. *Virus evolution*, 5(2):vez024.

Gradshteyn, I. S. and Ryzhik, I. M. (2014). *Table of integrals, series, and products*. Academic press.

Grebenkov, D. S. and Nguyen, B.-T. (2013). Geometrical structure of laplacian eigenfunctions. *siam REVIEW*, 55(4):601–667.

Greenbury, S. F., Schaper, S., Ahnert, S. E., and Louis, A. A. (2016). Genetic correlations greatly increase mutational robustness and can both reduce and enhance evolvability. *PLoS computational biology*, 12(3):e1004773.

Gudelj, I., Coman, C. D., and Beardmore, R. E. (2006). Classifying the role of tradeoffs in the evolutionary diversity of pathogens. *Proceedings of the Royal Society A: Mathematical, Physical and Engineering Sciences*, 462(2065):97–116.

Gupta, D., Garlaschi, S., Suweis, S., Azaele, S., and Maritan, A. (2021). An effective resource-competition model for species coexistence.

Hall, R. J., Gubbins, S., and Gilligan, C. A. (2007). Evaluating the performance of chemical control in the presence of resistant pathogens. *Bulletin of mathematical biology*, 69(2):525–537.

Halliwell, S. C., Smith, M. C., Muston, P., Holland, S. L., and Avery, S. V. (2012). Heterogeneous expression of the virulence-related adhesin epa1 between individual cells and strains of the pathogen candida glabrata. *Eukaryotic cell*, 11(2):141–150.

Hethcote, H. W. (2000). The mathematics of infectious diseases. *SIAM review*, 42(4):599–653.

Hewitt, S. K., Foster, D. S., Dyer, P. S., and Avery, S. V. (2016). Phenotypic heterogeneity in fungi: importance and methodology. *Fungal Biology Reviews*, 30(4):176–184.

Hofbauer, J., Sigmund, K., et al. (1998). *Evolutionary games and population dynamics*. Cambridge university press.

Huang, S. (2009). Non-genetic heterogeneity of cells in development: more than just noise. *Development*, 136(23):3853–3862.

Iwasa, Y. (1988). Free fitness that always increases in evolution. *Journal of Theoretical Biology*, 135(3):265–281.

Jablonka, E. and Lamb, M. J. (2014). *Evolution in four dimensions, revised edition: Genetic, epigenetic, behavioral, and symbolic variation in the history of life*. MIT press.

Jain, N. and Fries, B. C. (2009). Antigenic and phenotypic variations in fungi. *Cellular microbiology*, 11(12):1716–1723.

Jørgensen, L. N., van den Bosch, F., Oliver, R., Heick, T., and Paveley, N. (2017). Targeting Fungicide Inputs According to Need. *Annual Review of Phytopathology*, 55(1):181–203.

Kaern, M., Elston, T. C., Blake, W. J., and Collins, J. J. (2005). Stochasticity in gene expression: from theories to phenotypes. *Nature Reviews Genetics*, 6(6):451–464.

Kaneko, K. (2007). Evolution of robustness to noise and mutation in gene expression dynamics. *PLoS one*, 2(5):e434.

Kennedy, M. C., Ford, E. D., Singleton, P., Finney, M., and Agee, J. K. (2008). Informed multi-objective decision-making in environmental management using pareto optimality. *Journal of Applied Ecology*, 45(1):181–192.

Kermack, W. O. and McKendrick, A. G. (1927). A contribution to the mathematical theory of epidemics. *Proceedings of the royal society of london. Series A, Containing papers of a mathematical and physical character*, 115(772):700–721.

Khatri, B. (2018a). Survival of the frequent at finite population size and mutation rate: filing the gap between quasispecies and monomorphic regimes.

Khatri, B. S. (2018b). Survival of the frequent at finite population size and mutation rate: filing the gap between quasispecies and monomorphic regimes. *BioRxiv*, page 375147.

Khatri, B. S. and Goldstein, R. A. (2015). A coarse-grained biophysical model of sequence evolution and the population size dependence of the speciation rate. *Journal of theoretical biology*, 378:56–64.

Khatri, B. S. and Goldstein, R. A. (2019). Biophysics and population size constrains speciation in an evolutionary model of developmental system drift. *PLoS computational biology*, 15(7):e1007177.

Kimura, M. (1965). A stochastic model concerning the maintenance of genetic variability in quantitative characters. *Proceedings of the National Academy of Sciences of the United States of America*, 54(3):731.

Kimura, M. (1968). Genetic variability maintained in a finite population due to mutational production of neutral and nearly neutral isoalleles. *Genetics research*, 11(3):247–270.

Kimura, M. et al. (1968). Evolutionary rate at the molecular level. *Nature*, 217(5129):624–626.

Kingman, J. (1977). On the properties of bilinear models for the balance between genetic mutation and selection. In *Mathematical Proceedings of the Cambridge Philosophical Society*, volume 81, pages 443–453. Cambridge University Press.

Kingman, J. F. (1978). A simple model for the balance between selection and mutation. *Journal of Applied Probability*, 15(1):1–12.

Klumpp, S. and Hwa, T. (2014). Bacterial growth: global effects on gene expression, growth feedback and proteome partition. *Current opinion in biotechnology*, 28:96–102.

Korobeinikov, A. (2018). Immune response and within-host viral evolution: immune response can accelerate evolution. *Journal of theoretical biology*, 456:74–83.

Korobeinikov, A. and Dempsey, C. (2014). A continuous phenotype space model of rna virus evolution within a host. *Mathematical Biosciences & Engineering*, 11(4):919.

Korobeinikov, A. and Wake, G. C. (2002). Lyapunov functions and global stability for sir, sirs, and sis epidemiological models. *Applied Mathematics Letters*, 15(8):955–960.

Laine, A.-L. and Barrès, B. (2013). Epidemiological and evolutionary consequences of life-history trade-offs in pathogens. *Plant Pathology*, 62:96–105.

Lamichhane, J. R., Dachbrodt-Saaydeh, S., Kudsk, P., and Messéan, A. (2016). Conventional Pesticides in Agriculture: Benefits Versus Risks. *Plant Disease*, 100(1):10–24.

Laxminarayan, R. (2010). *Battling resistance to antibiotics and pesticides: an economic approach*. Routledge.

Lechenet, M., Dessaint, F., Py, G., Makowski, D., and Munier-Jolain, N. (2017). Reducing pesticide use while preserving crop productivity and profitability on arable farms. *Nature Plants*, 3(March):1–6.

Lin, S.-Y. et al. (2017). The study of transcriptional regulation of necrotrophic effector genes toxa and tox3 in the wheat pathogen parastagonospora nodorum.

Lipsitch, M., Herre, E. A., and Nowak, M. A. (1995). Host population structure and the evolution of virulence: a "law of diminishing returns". *Evolution*, 49(4):743–748.

Lorenzi, T., Chisholm, R. H., and Clairambault, J. (2016). Tracking the evolution of cancer cell populations through the mathematical lens of phenotype-structured equations. *Biology direct*, 11(1):43.

Lorenzi, T., Pugliese, A., Sensi, M., and Zardini, A. (2020). Evolutionary dynamics in an si epidemic model with phenotype-structured susceptible compartment. *arXiv preprint arXiv:2010.10443*.

Lorz, A., Lorenzi, T., Hochberg, M. E., Clairambault, J., and Perthame, B. (2013). Populational adaptive evolution, chemotherapeutic resistance and multiple anti-cancer therapies. *ESAIM: Mathematical Modelling and Numerical Analysis*, 47(2):377–399.

Lu, S.-W., Kroken, S., Lee, B.-N., Robbertse, B., Churchill, A. C., Yoder, O., and Turgeon, B. G. (2003). A novel class of gene controlling virulence in plant pathogenic ascomycete fungi. *Proceedings of the National Academy of Sciences*, 100(10):5980–5985.

MacArthur, R. (1970). Species packing and competitive equilibrium for many species. *Theoretical population biology*, 1(1):1–11.

Madden, L., Jeger, M., and Van den Bosch, F. (2000). A theoretical assessment of the effects of vector-virus transmission mechanism on plant virus disease epidemics. *Phytopathology*, 90(6):576–594.

Manrubia, S., Cuesta, J. A., Aguirre, J., Ahnert, S. E., Altenberg, L., Cano, A. V., Catalán, P., Diaz-Uriarte, R., Elena, S. F., García-Martín, J. A., et al. (2020). From genotypes to organisms: State-of-the-art and perspectives of a cornerstone in evolutionary dynamics. *arXiv preprint arXiv:2002.00363*.

Manrubia, S., Cuesta, J. A., Aguirre, J., Ahnert, S. E., Altenberg, L., Cano, A. V., Catalán, P., Diaz-Uriarte, R., Elena, S. F., García-Martín, J. A., et al. (2021). From genotypes to organisms: State-of-the-art and perspectives of a cornerstone in evolutionary dynamics. *Physics of Life Reviews*.

Mansfield, J., Genin, S., Magori, S., Citovsky, V., Sriariyanum, M., Ronald, P., Dow, M., Verdier, V., Beer, S. V., Machado, M. A., et al. (2012). Top 10 plant pathogenic bacteria in molecular plant pathology. *Molecular plant pathology*, 13(6):614–629.

Marchi, J., Lässig, M., Walczak, A. M., and Mora, T. (2021). Antigenic waves of virus-immune co-evolution. *arXiv preprint arXiv:2102.10441*.

Mbah, M. L. N., Forster, G. A., Wesseler, J. H., and Gilligan, C. A. (2010). Economically optimal timing for crop disease control under uncertainty: an options approach. *Journal of the Royal Society Interface*, 7(51):1421–1428.

McAdams, H. H. and Arkin, A. (1997). Stochastic mechanisms in gene expression. *Proceedings of the National Academy of Sciences*, 94(3):814–819.

McGhee, G. R. (2006). *The geometry of evolution: adaptive landscapes and theoretical morphospaces*. Cambridge University Press.

Medina-Pastor, P. and Triacchini, G. (2020). The 2018 european union report on pesticide residues in food. *EFSA Journal*, 18(4):1–103.

Miele, L., Evans, R., and Azaele, S. (2021a). Redundancy-selection trade-off in phenotype-structured populations. *Journal of Theoretical Biology*, 531:110884.

Miele, L., Evans, R., Cunniffe, N., and Bevacqua, D. (2021b). Control strategies for heterogeneous plant pathogens: evolutionary and agricultural consequences. *bioRxiv*.

Moran, P. A. P. (1958). Random processes in genetics. In *Mathematical proceedings of the cambridge philosophical society*, volume 54, pages 60–71. Cambridge University Press.

Murray, J. D. (2007). *Mathematical biology: I. An introduction*, volume 17. Springer Science & Business Media.

Nei, M. (2013). *Mutation-driven evolution*. OUP Oxford.

Norberg, U. M. and Rayner, J. M. (1987). Ecological morphology and flight in bats (mammalia; chiroptera): wing adaptations, flight performance, foraging strategy and echolocation. *Philosophical Transactions of the Royal Society of London. B, Biological Sciences*, 316(1179):335–427.

Orr, H. A. (2005). The genetic theory of adaptation: a brief history. *Nature Reviews Genetics*, 6(2):119–127.

Orr, H. A. (2006). The distribution of fitness effects among beneficial mutations in fisher's geometric model of adaptation. *Journal of theoretical biology*, 238(2):279–285.

Osmanovic, D., Kessler, D. A., Rabin, Y., and Soen, Y. (2018). Darwinian selection of host and bacteria supports emergence of lamarckian-like adaptation of the system as a whole. *Biology direct*, 13(1):1–13.

Pacciani-Mori, L., Giometto, A., Suweis, S., and Maritan, A. (2020). Dynamic metabolic adaptation can promote species coexistence in competitive communities. *PLoS computational biology*, 16(5):e1007896.

Page, K. M. and Nowak, M. A. (2002). Unifying evolutionary dynamics. *Journal of theoretical biology*, 219(1):93–98.

Park, J.-M., Munoz, E., and Deem, M. W. (2010). Quasispecies theory for finite populations. *Physical Review E*, 81(1):011902.

Parnell, S., Van Den Bosch, F., and Gilligan, C. (2006). Large-scale fungicide spray heterogeneity and the regional spread of resistant pathogen strains. *Phytopathology*, 96(5):549–555.

Patyka, V., Buletsa, N., Pasichnyk, L., Zhitkevich, N., Kalinichenko, A., Gnatiuk, T., and Butsenko, L. (2016). Specifics of pesticides effects on the phytopathogenic bacteria. *Ecological Chemistry and Engineering S*, 23(2):311–331.

Perrier, A., Barlet, X., Rengel, D., Prior, P., Poussier, S., Genin, S., and Guidot, A. (2019). Spontaneous mutations in a regulatory gene induce phenotypic heterogeneity and adaptation of ralstonia solanacearum to changing environments. *Environmental microbiology*, 21(8):3140–3152.

Pisco, A. O., Brock, A., Zhou, J., Moor, A., Mojtahedi, M., Jackson, D., and Huang, S. (2013). Non-darwinian dynamics in therapy-induced cancer drug resistance. *Nature communications*, 4(1):1–11.

Poelwijk, F. J., Kiviet, D. J., Weinreich, D. M., and Tans, S. J. (2007). Empirical fitness landscapes reveal accessible evolutionary paths. *Nature*, 445(7126):383.

Pontes, J. G. d. M., Fernandes, L. S., dos Santos, R. V., Tasic, L., and Fill, T. P. (2020). Virulence factors in the phytopathogen–host interactions: An overview. *Journal of Agricultural and Food Chemistry*, 68(29):7555–7570.

Porco, T. C., Lloyd-Smith, J. O., Gross, K. L., and Galvani, A. P. (2005). The effect of treatment on pathogen virulence. *Journal of Theoretical Biology*, 233(1):91–102.

Pretty, J., Benton, T. G., Bharucha, Z. P., Dicks, L. V., Flora, C. B., Godfray, H. C. J., Goulson, D., Hartley, S., Lampkin, N., Morris, C., Pierzynski, G., Prasad, P. V., Reganold, J., Rockström, J., Smith, P., Thorne, P., and Wratten, S. (2018). Global assessment of agricultural system redesign for sustainable intensification. *Nature Sustainability*, 1(8):441–446.

Pugliese, A. (2002). On the evolutionary coexistence of parasite strains. *Mathematical biosciences*, 177:355–375.

Raj, A. and Van Oudenaarden, A. (2008). Nature, nurture, or chance: stochastic gene expression and its consequences. *Cell*, 135(2):216–226.

Rigato, E. and Fusco, G. (2020). Effects of phenotypic robustness on adaptive evolutionary dynamics. *Evolutionary Biology*, 47(3):233–239.

Ristaino, J. B., Anderson, P. K., Bebber, D. P., Brauman, K. A., Cunniffe, N. J., Fedoroff, N. V., Finegold, C., Garrett, K. A., Gilligan, C. A., Jones, C. M., et al. (2021). The persistent threat of emerging plant disease pandemics to global food security. *Proceedings of the National Academy of Sciences*, 118(23).

Ruijgrok, M. and Ruijgrok, T. W. (2015). An effective replicator equation for games with a continuous strategy set. *Dynamic Games and Applications*, 5(2):157–179.

Russell, P. (2005). A century of fungicide evolution. *The Journal of Agricultural Science*, 143:11.

Saakian, D. B., Biebricher, C. K., and Hu, C.-K. (2009). Phase diagram for the eigen quasispecies theory with a truncated fitness landscape. *Physical Review E*, 79(4):041905.

Saakian, D. B., Deem, M. W., and Hu, C.-K. (2012). Finite population size effects in quasispecies models with single-peak fitness landscape. *EPL (Europhysics Letters)*, 98(1):18001.

Saakian, D. B. and Hu, C.-K. (2004). Solvable biological evolution model with a parallel mutation-selection scheme. *Physical Review E*, 69(4):046121.

Saakian, D. B. and Hu, C.-K. (2006). Exact solution of the eigen model with general fitness functions and degradation rates. *Proceedings of the National Academy of Sciences*, 103(13):4935–4939.

Sasaki, A. (1994). Evolution of antigen drift/switching: continuously evading pathogens. *Journal of Theoretical Biology*, 168(3):291–308.

Sasaki, A. and Haraguchi, Y. (2000). Antigenic drift of viruses within a host: a finite site model with demographic stochasticity. *Journal of Molecular Evolution*, 51(3):245–255.

Sato, K. and Kaneko, K. (2007). Evolution equation of phenotype distribution: General formulation and application to error catastrophe. *Physical Review E*, 75(6):061909.

Savary, S., Willocquet, L., Pethybridge, S. J., Esker, P., McRoberts, N., and Nelson,

A. (2019). The global burden of pathogens and pests on major food crops. *Nature Ecology and Evolution*, 3(3):430–439.

Schröter, L. and Dersch, P. (2019). Phenotypic diversification of microbial pathogens—cooperating and preparing for the future. *Journal of molecular biology*, 431(23):4645–4655.

Sella, G. and Hirsh, A. E. (2005). The application of statistical physics to evolutionary biology. *Proceedings of the National Academy of Sciences*, 102(27):9541–9546.

Shaw, M. (2000). Models of the effects of dose heterogeneity and escape on selection pressure for pesticide resistance. *Phytopathology*, 90(4):333–339.

Shi, R., Jiang, X., and Chen, L. (2009). A predator–prey model with disease in the prey and two impulses for integrated pest management. *Applied Mathematical Modelling*, 33(5):2248–2256.

Shoval, O., Sheftel, H., Shinar, G., Hart, Y., Ramote, O., Mayo, A., Dekel, E., Kavanagh, K., and Alon, U. (2012). Evolutionary trade-offs, pareto optimality, and the geometry of phenotype space. *Science*, 336(6085):1157–1160.

Smith, J. M. (1970). Natural selection and the concept of a protein space. *Nature*, 225(5232):563–564.

Steels, H., James, S., Roberts, I., and Stratford, M. (2000). Sorbic acid resistance: the inoculum effect. *Yeast*, 16(13):1173–1183.

Stockholm, D., Benchaouir, R., Picot, J., Rameau, P., Neildez, T. M. A., Landini, G., Laplace-Builhé, C., and Paldi, A. (2007). The origin of phenotypic heterogeneity in a clonal cell population in vitro. *PloS one*, 2(4):e394.

Traulsen, A., Claussen, J. C., and Hauert, C. (2005). Coevolutionary dynamics: from finite to infinite populations. *Physical review letters*, 95(23):238701.

Traulsen, A., Claussen, J. C., and Hauert, C. (2006). Coevolutionary dynamics in large, but finite populations. *Physical Review E*, 74(1):011901.

Tsimring, L. S., Levine, H., and Kessler, D. A. (1996). Rna virus evolution via a fitness-space model. *Physical review letters*, 76(23):4440.

Van den Berg, F., Paveley, N., and Van den Bosch, F. (2016). Dose and number of applications that maximize fungicide effective life exemplified by zymoseptoria tritici on wheat–a model analysis. *Plant pathology*, 65(8):1380–1389.

van den Bosch, F. and Gilligan, C. A. (2008). Models of fungicide resistance dynamics. *Annu. Rev. Phytopathol.*, 46:123–147.

Van Kampen, N. G. (1992). *Stochastic processes in physics and chemistry*, volume 1. Elsevier.

Van Nimwegen, E., Crutchfield, J. P., and Huynen, M. (1999). Neutral evolution of mutational robustness. *Proceedings of the National Academy of Sciences*, 96(17):9716–9720.

Waage, P. and Gulberg, C. M. (1986). Studies concerning affinity. *Journal of chemical education*, 63(12):1044.

Wagner, A. (1999). Redundant gene functions and natural selection. *Journal of evolutionary biology*, 12(1):1–16.

Wagner, A. (2005). Robustness, evolvability, and neutrality. *FEBS letters*, 579(8):1772–1778.

Wagner, A. (2008). Neutralism and selectionism: a network-based reconciliation. *Nature Reviews Genetics*, 9(12):965.

Wagner, A. (2011). *The origins of evolutionary innovations: a theory of transformative change in living systems*. OUP Oxford.

Wakano, J. Y., Funaki, T., and Yokoyama, S. (2017). Derivation of replicator–mutator equations from a model in population genetics. *Japan Journal of Industrial and Applied Mathematics*, 34(2):473–488.

Walter, A. and Lion, S. (2021). Epidemiological and evolutionary consequences of periodicity in treatment coverage. *Proceedings of the Royal Society B*, 288(1946):20203007.

Weiße, A. Y., Oyarzún, D. A., Danos, V., and Swain, P. S. (2015). Mechanistic links between cellular trade-offs, gene expression, and growth. *Proceedings of the National Academy of Sciences*, 112(9):E1038–E1047.

Wilke, C. O. (2005). Quasispecies theory in the context of population genetics. *BMC evolutionary biology*, 5(1):44.

Wilson, E. O. (1980). Caste and division of labor in leaf-cutter ants (hymenoptera: Formicidae: Atta). *Behavioral ecology and sociobiology*, 7(2):157–165.

Wright, S. (1931). Evolution in mendelian populations. *Genetics*, 16(2):97.

Wright, S. (1932). *The roles of mutation, inbreeding, crossbreeding, and selection in evolution*, volume 1. na.

Xue, B., Sartori, P., and Leibler, S. (2019). Environment-to-phenotype mapping and adaptation strategies in varying environments. *Proceedings of the National Academy of Sciences*, 116(28):13847–13855.

Yang, J., Tauschek, M., and Robins-Browne, R. M. (2011). Control of bacterial virulence by arac-like regulators that respond to chemical signals. *Trends in microbiology*, 19(3):128–135.

Zeng, Z.-B. and Cockerham, C. C. (1993). Mutation models and quantitative genetic variation. *Genetics*, 133(3):729–736.